

Poster Abstracts: New Methods

223. A Technique for Automated Registration of Cardiac T_2^* Images

Sandeep Gupta,¹ Daniel Herzka,² Garth Beache.³ ¹GE Medical Systems, 600 N. Wolfe Street, Baltimore, Maryland, United States; ²Johns Hopkins University, Medical Imaging Laboratory, Baltimore, Maryland, United States; ³University of Maryland at Baltimore, 22 South Greene Street, Baltimore, Maryland, United States

Introduction: Blood oxygenation level dependent (BOLD) MRI has recently been applied to the human heart as a means of assessing perfusion reserve, without the administration of extrinsic contrast agents [1–3]. In this technique, the change in the relaxation-time T_2^* under administration of a pharmacological stress agent such as dipyridamole is measured and can be shown to be proportional to changes in blood flow and O_2 delivery.

Purpose: In order to accurately measure T_2^* changes and quantify physiological parameters, it is important that the T_2^* parametric images under baseline and stress epochs be corrected for motion by spatial registration prior to analysis. Automatic registration of these images is hampered by the poor signal-to-noise ratio (SNR) typically characteristic of those images. In this work, we present a novel method for registering the relaxation-time images by using higher SNR extrapolated proton-density-weighted images. We compare this registration scheme with direct registration of T_2^* images.

Methods: Acquisition: A subset of the data reported in [3] was used for this study. Briefly, five healthy subjects were scanned on a Signa 1.5T GE system. A set of nine images with TE values between 2 and 26 ms was acquired in one breathhold using a gated, spoiled gradient-echo sequence. Key imaging parameters were: TR = 28 ms, flip angle = 30°, BW = ± 62.5 kHz, matrix 256 × 120, FOV = 40 cm by 40 cm, slice thickness = 10 mm. Baseline images were repeated approximately seven times to establish reproducibility. Dipyridamole was then administered peripherally (0.56 mg/kg total, over 4 min). Stress images were repeatedly acquired approximately every minute for twenty minutes. This constituted a T_2^* temporal dataset over baseline and stress epochs.

Analysis: The nine TE images were combined to derive T_2^* images using a pixel-wise linear fit to a logarithmic plot of the MRI

signal as a function of TE. Corresponding to each T_2^* image, we also calculated an extrapolated TE = 0 ms image. We denote this computed proton-density-weighted image as the A_0 image. The estimated A_0 value for each pixel was determined by taking the exponent of the y-intercept of a line fitted to the logarithm of the individual pixel values at each TE. All pixels with correlation coefficients (R) less than 0.95 were discarded to minimize artifacts.

Registration of the time-series was done using a fast, fully automated algorithm based on cross-correlation of geometric invariants [4]. The accuracy of the registration was quantified by measuring the motion of the anterior right-ventricular (RV) insertion point in each image of the registered T_2^* series. We compare the accuracy of directly registering the T_2^* images with that of first registering the post-processed A_0 images and then copying the result to the T_2^* images. For comparison purposes, we also report the results of registration using the acquired shortest TE value (TE_1) image. Finally, we measured the SNR in a representative T_2^* image, A_0 image, and TE_1 image for each subject and report the results.

Results: The methods were validated on five healthy subjects. Typical SNR of the underlying TE images used to generate T_2^* maps ranged from approximately 40, for the shortest echo-time, to 10, for the longest echo-time. The mean SNR (of the five subjects) of the estimated T_2^* images was 4, and of the synthesized A_0 images was 139. A comparison of motion reduction due to registration using T_2^* images, A_0 images, and TE_1 images is shown in Table 1 below.

For each subject, the mean motion of the RV insertion point, characterizing the motion of a given image, in the T_2^* time-series is reported in pixel units for the unregistered images and for each of the three registration schemes. The numbers in parenthesis denote the maximum (worst-case) motion in pixel units between image pairs. It can be seen that for all subjects, registration using the higher SNR A_0 images yields the best motion correction. In cases where motion in the unregistered images is large, this technique outperforms both the other methods of registration. TE_1 registration yields acceptable results in cases of small motion. T_2^* image registration is the least accurate because of the poor SNR and artifacts present in the maps.

Conclusion: In the present work, we have demonstrated that automatic registration of the higher SNR A_0 images leads to

Table 1

Comparison of Registration Methods

	Motion in Unreg. Images	Motion After A_0 reg.	Motion After TE_1 reg.	Motion After T_2^* reg.
Subj. 1	2 (6)	1 (2)	2 (2)	2 (3)
Subj. 2	1 (2)	0 (1)	0 (1)	1 (2)
Subj. 3	2 (3)	1 (2)	1 (2)	2 (3)
Subj. 4	3 (4)	1 (2)	2 (2)	2 (3)
Subj. 5	1 (1)	0 (1)	0 (1)	1 (1)

greater motion reduction than that resulting from directly registering the T_2^* images, or the TE_1 images. Thus, an approach to improved registration of T_2^* images which we have employed in our studies consists of first registering the synthesized A_0 dataset, and then using this as a template to register the associated T_2^* dataset. External standards will be required to determine whether these differences in registration affect the determination of derived physiological parameters.

Supported by KO1 HL03837.

References

1. Li D.B. et al., AJR, 172: (1), p 141–145, Jan 1999.
2. Wacker et al., MRM, 41:(4), p 686–695, Apr 1999.
3. Beache et al., Circ., 104:(1), p 1214–1217, Sep 2001.
4. Meiyappan et al., Proc. ISMRM, 1:37, 2000, Denver.

224. Submillimeter Coronary MR Imaging Using Prospective Variable-Density Adaptive Averaging

Marshall Sussman,¹ Graham Wright,¹ ¹Sunnybrook and Women's College Health Science Centre, University of Toronto, Research Building, S612, Toronto, Ontario, Canada

Introduction: High-resolution MR coronary imaging requires accurate compensation for cardiac and respiratory motion and distortion. Conventional compensation schemes can be adversely affected by a reliance on indirect measures of coronary motion (e.g. diaphragm position, ECG waveforms, etc.) as well as a complete neglect of anatomical distortion. In the variable-density (VD) adaptive averaging technique^{1,2}, high-resolution images are acquired with motion and distortion information provided directly and continuously from non-aliased, low-resolution real-time images of the coronary anatomy. Previously, this technique has been used to acquire medium-resolution (~ 1 mm) retrospectively-corrected coronary images. In this study, submillimeter prospectively-guided coronary images were acquired. Results were compared to conventional breath-hold spiral images.

Purpose: In the VD adaptive averaging technique, high-resolution images are generated from n_0 VD-spiral interleaves. The inner high-density part of the VD-spiral, in addition to contributing to the high-resolution image, can also be used to generate non-aliased, low-resolution images after every n_i

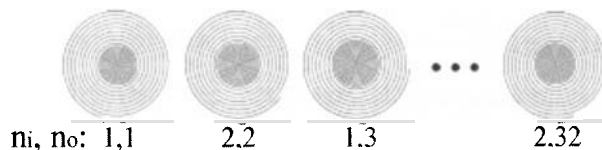


Figure 1. VD-spiral with $n_i=2$ and $n_0=32$. After 32 interleaves, a high resolution image is acquired. After every 2 interleaves, a low resolution image can be formed from the high-density inner spiral.

interleaves ($n_i < n_0$) (Fig. 1). If n_i is small, images can be generated in real time. From these images, periods of coronary motion and distortion quiescence can be identified directly. This is accomplished using the correlation coefficient (CC) template matching algorithm³. In this algorithm, CC values are calculated between each inner spiral image and a template obtained from a previously acquired image containing the coronary artery of interest. The larger the CC value, the greater the similarity between the image and template. This information is used (in real-time) to prospectively reacquire data with the most distortion (i.e. the lowest CC value). As the scan progresses, overall data quality improves since the relative distortion continually decreases. Data acquisition ceases when the CC values reach a steady state. Images are reconstructed after the removal of any displacement.

Methods: Images of coronary arteries were acquired using VD-spirals with $n_i = 4$ (2.9 mm), $n_0 = 20$ (0.78 mm) and 4 NEX. TR was 40 ms (\rightarrow inner spiral temporal resolution = 160 ms). Plethysmograph waveforms were monitored, but not used for cardiac triggering. For comparison, 16-interleaf cardiac-triggered breath-hold spiral images (0.78 mm) were also acquired.

Results: The motion compensation capabilities of the VD-technique can be observed by comparing a real-time inner to a full spiral image (Fig. 2). The full image, acquired over multiple cardiac and respiratory cycles, has significantly improved resolution without any obvious artifact relative to the “instantaneously” acquired inner spiral image. Despite the higher-resolution of the full spiral image, it's longer acquisition time provides a comparable SNR to the inner spiral image. A further demonstration of the technique's motion compensation capabilities is provided by comparing a VD- to a breath-hold spiral image (Figs. 3a, b). In the VD-image, a significant improvement in edge sharpness and vessel conspicuity is

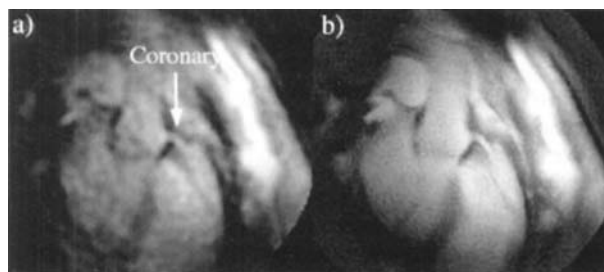


Figure 2. (a) Inner and (b) full spiral images of the coronary.

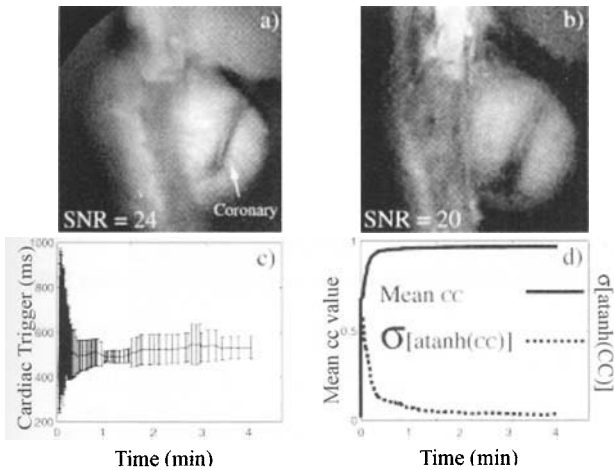


Figure 3. (a)VD- and (b) breath-hold spiral RCA images. (c) Mean cardiac trigger time and (d) mean and standard deviation of the CC values vs. scan time for the VD acquisition.

observed. In this case, the VD-technique is therefore better at identifying periods of distortion quiescence than a combination of cardiac triggering and breath-holding. The nature of the data selected by the CC algorithm can be inferred by analyzing the time between data acquisition and the cardiac trigger of each interleaf in the full image (Fig. 3c). For the majority of time towards steady state, the variability in trigger times among the VD-interleaves is $\pm 50\text{ms}$ —roughly the temporal resolution of the scan. This suggests that the approach to steady state involves fine-tuning the exact data acquisition time within the temporal limits of the scan. The acquisition time for the VD-scan was longer than the breath-hold scan (1 min/NEX vs. $\sim 20\text{s}$). SNR efficiency was also lower due to the much shorter TR of the VD-scan (40ms vs. 1 heartbeat). However, given the very gradual approach to steady state (Fig. 3d), it may be possible to decrease scan time significantly at the cost of only a small decrease in data quality.

Conclusion: The prospective VD adaptive averaging technique is capable of providing submillimeter coronary images. Due to the use of direct coronary visualization, its motion compensation capabilities may be superior to conventional triggering/breath-hold methods. The technique's SNR efficiency, which is presently somewhat low, may be improved with only minor modifications to the algorithm.

Support by the Heart and Stroke Foundation of Canada, Canadian Institutes of Health Research

References

1. Hardy, C.J. *et al.*, *MRM*, 2000, 44:940–946
2. Sussman, M.S. *et al.*, *ISMRM*, 2001, 175
3. Sussman, M.S. *et al.*, *ISMRM*, 1999, 1267

225. Combination of Breath-Holding and Free-Breathing Navigator-Gated 3D Coronary MRA

Michael Huber,¹ Markus Oelhafen,¹ Sebastian Kozerke,¹ Oliver Weber,¹ Peter Boesiger.¹ ¹University and ETH Zurich, Inst. of Biomedical Engineering, Zurich, Switzerland

Introduction: In coronary magnetic resonance angiography (MRA) three-dimensional acquisition techniques offer superior signal-to-noise-ratio (SNR), thin adjacent slices and the ability to post-process the data. As a consequence of the increased amount of data, the acquisition has to be split either into multiple breath-holds^{1,2} or it can be measured with navigator gating during free-breathing^{3,4}. The multiple breath-hold approach however requires patient collaboration and has the problem of reproducibility of the breath-hold level. On the other hand the free-breathing navigator-gated scan is prolonged due to the limited acceptance rate of the breathing positions. To reduce scan time, the gating window has to be enlarged. However, the ratio between profiles measured close to the ideal end-expiratory position and profiles acquired during larger diaphragmatic displacements decreases with increasing size of the navigator window.

Purpose: In the present work a free-breathing navigator-gated 3D coronary MRA is extended with the application of an initial

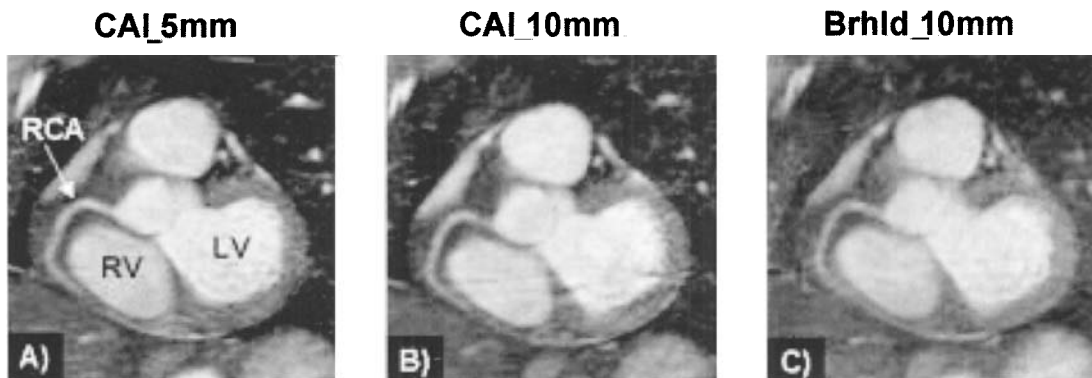


Figure 1. Reformatted RCA images, obtained in three scans in a healthy volunteer. A) conventional free-breathing navigator-gated, 5mm gating window B) conventional free-breathing navigator-gated, 10mm gating window C) single breath-hold extended free-breathing navigator-gated, 10mm gating window.

Table 1
Image Quality Parameters

	CAI_5mm	CAI_10mm	Brhld_10mm
SNR	13.2 ± 3.0	13.2 ± 2.6	16.7 ± 2.4
CNR	7.6 ± 2.3	6.9 ± 1.9	7.4 ± 1.2
Vessel sharpness (%)	54.6 ± 4.9	47.5 ± 4.6	46.1 ± 4.3

single breath-hold, prior to the free-breathing data acquisition phase. This may enable the acquisition of the most central k-space part during minimal diaphragmatic displacement.

Methods: In conventional coronary 3D scans the k-space data for each (kx,ky)-plane is acquired separately, i.e., kz is kept constant until an entire (kx,ky)-plane is acquired. Concept of our approach is the acquisition of the most relevant k-space information during an initial single breath-hold at the beginning of the scan. This necessitates that k-space is no longer filled plane by plane but moreover includes simultaneous variation of both ky and kz⁵ according to a predefined central profile read order.

Eight healthy adult subjects were examined on a commercial 1.5T Philips Gyroscan ACS-NT system equipped with PowerTrak 6000 gradients (21mT/m, 200msec rise time) and a five-element cardiac synergy coil. The central k-space acquisition scheme was implemented for a navigator-gated and prospectively corrected 3D TFE sequence with T2 preparation and fat suppression⁴. The FOV was 360mm × 270mm and 512 × 268 data points were sampled using partial Fourier sampling. 10 slices were acquired and interpolated to 20 slices of 1.5mm thickness using zero filling in k-space. TE was 2.1 ms, TR 7.6ms and a = 30°. For each volunteer three high-resolution free-breathing scans were performed with following additional parameters: A) A 5mm navigator window using conventional k-space acquisition (CAI_5mm). B) A 10mm navigator window using a conventional k-space acquisition order (CAI_10mm). C) A 10mm navigator window using the new proposed central k-space acquisition order combined with an initial breath-hold of 15 cardiac cycles (Brhld_10mm).

For an objective comparison of the resulting images, SNR, CNR and the vessel sharpness of the right coronary artery (RCA) were measured.

Results: An increase of SNR by 26% could be achieved with the single breath-hold extended free-breathing scan when compared to the conventionally acquired scans (Tab. 1). No difference however was found for the CNR values of the three methods applied. As expected, the vessel sharpness of the 5mm navigator gated acquisition was approximately 15% higher when compared with the 10mm navigator gated acquisitions. No difference of the vessel sharpness was observed between the scans with the increased 10mm navigator window.

Conclusion: The application of a single initial breath-hold at the beginning of free-breathing navigator-gated and corrected coronary MRA enables for the acquisition of relevant k-space data during minimal respiratory motion. Combined with a central 3D k-space filling order an increase of SNR could be achieved. Since the signal from the myocardial muscle was similarly enhanced as the signal from the arterial blood, no

difference in CNR was found. As expected, the enlarged gating window had a negative impact on the sharpness of the RCA. However, the presented method may be a valuable technique for contrast enhanced first-pass angiography. During the initial breath-hold period most important k-space information could be acquired at high T1-relaxation of the blood, while remaining k-space data could be measured during the subsequent post-bolus phase at free-breathing.

226. Identification of Patent Foramen Ovale Using MRI

David Bolon,¹ Zoran Lasic,¹ Robert Sommer,¹ Martin Leon,¹ Cindy Comeau,¹ Sylvain Milet,² Paul Licato,² Dusan Knezevic,¹ Vladimir Ilic,¹ Steven Wolff.¹ ¹*Lenox Hill Hospital, 100 E 77 St, New York, NY, USA;* ²*Advanced Cardiovascular Imaging, 62 e 88 st, New York, NY, USA*

Introduction: Blood clots traversing a patent foramen ovale (PFO) are an important cardiac source of arterial emboli. Identifying a PFO is potentially quite difficult because the amount of shunted blood is small (typically less than 1 ml), the shunt is transient, and the shunt must be evoked by physiologic maneuvers (e.g. Valsalva). The diagnosis is typically made by transesophageal echocardiography (TEE) by visualizing echo-contrast (agitated saline) pass from the right atrium (RA) to the left atrium (LA) through the PFO. Valsalva maneuver, timed to RA opacification, increases the sensitivity of TEE by causing transient elevation of RA pressure and increasing right-to-left shunting of contrast.

Purpose: To develop a less invasive protocol that uses MRI to assess for a PFO.

Methods: All subjects were imaged in accordance with IRB approval. Six subjects had known PFO documented by echocardiography and no evidence of right heart enlargement to suggest the presence of a significant left-to-right shunt. Each subject received an intravenous bolus of gadolinium contrast (Optimark: 10–20 ml at 3 ml/s).

Two different pulse sequences were investigated. The first sequence was an EPI sequence (FGRET) commonly used for perfusion imaging. A 90° notched saturation pulse was used for T1-weighting. Images were acquired without gating in order to attain the highest temporal resolution. Imaging parameters were: TR/TE = 6.9/1.3 ms; FOV = 36 × 36 cm; matrix 128 × 96, slice thickness = 10–20mm, and 1 NEX. With these parameters, two slice locations were acquired in an interleaved fashion at a rate of 4 frames/sec for each slice location. Patients were instructed to release Valsalva 5–7 seconds after the contrast injection started. This was the anticipated timing of contrast arrival in the right atrium.

The second pulse sequence was an ungated gradient echo sequence that used a nonselective inversion pulse for T1 weighting. Imaging parameters were: TR/TE/TI = 3.4/1.4/50 ms, FOV = 48 × 36 cm; matrix 64–96 × 96, slice thickness = 20 mm, and 0.5 NEX. Images from a single slice location were reconstructed in real-time at a rate of 4 frames/sec. When the operator visualized contrast in the right atrium, patients were instructed to release Valsalva.

To assess each sequence for its ability to detect signal from a PFO shunt and suppress signal from flowing blood, the PFO enhancement factor (PEF) was determined as follows:

PEF = (Peak LA Shunt Signal – Mean LA Signal pre-contrast)/Std. Dev. of LA Signal pre-contrast

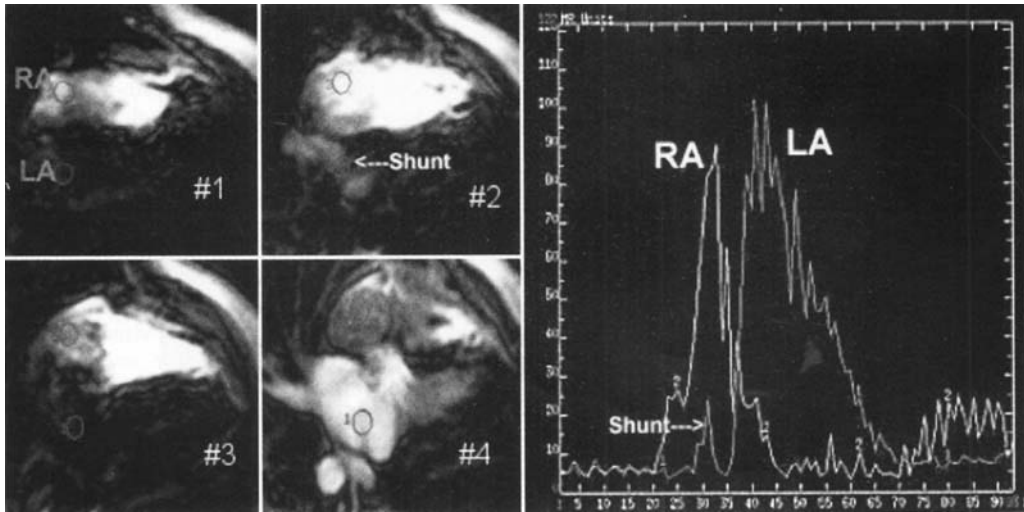


Figure 1.

A similar parameter that was also assessed was the left atrial enhancement factor (LAEF), which was determined as follows:

$$\text{LAEF} = (\text{Peak LA Signal post-contrast} - \text{Mean LA Signal pre-contrast}) / \text{Std. Dev. of LA Signal pre-contrast}.$$

An advantage of the LAEF is that it is not influenced by the size of the PFO.

Clinicians performing TEE often attempt multiple injections of contrast when seeking to identify a PFO, due to the necessity of good patient cooperation with the timing of the Valsalva to the arrival of contrast in the right atrium. Therefore, we also assessed the effectiveness of the pulse sequences with a second contrast injection, delivered 5–10 min. after the first.

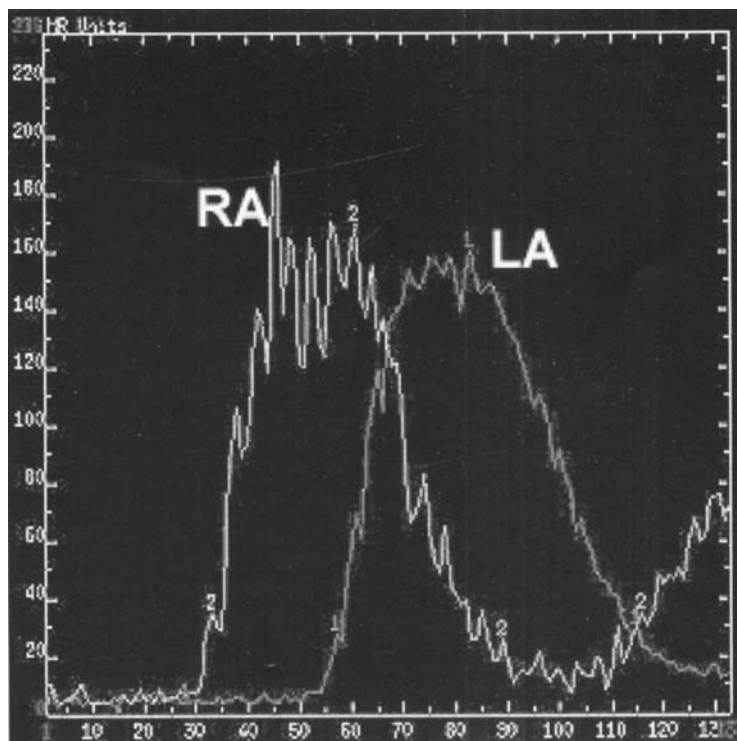


Figure 2.

Results: The FGRET sequence was successful in identifying a PFO in 2/4 patients. The real-time sequence identified PFO in 2/2 patients. Subjectively, the real-time sequence appears better for detecting PFOs. Objectively, it had 4–5 fold higher LAEF (1093 ± 528 vs. 256 ± 157) and PEF 264 ± 115 vs. 51 ± 30). The increased sensitivity of the real-time sequence persisted when a second injection was used: LAEF 590 ± 315 for real-time vs. 150 ± 47 for perfusion.

Figure 1 shows selected 4-chamber views using the real-time sequence: Image #1 shows contrast in the right atrium and right ventricle. Image #2 shows transient contrast in the left atrium. Image #3 shows the shunted contrast in the left atrium has dissipated. Image #4 shows contrast from the pulmonary veins entering the left atrium and left ventricle. The graph to the right shows atrial signal intensity as a function of time. The graph clearly shows transient early enhancement of the left atrium, which is not seen in a normal volunteer (Figure 2).

Conclusion: PFO can be detected with MRI. The real-time sequence appears superior to the FGRET sequence for detecting PFO. An added advantage of the real-time sequence is that more precise timing of Valsalva release can be utilized because the arrival of contrast in the right atrium can be directly visualized during image acquisition.

227. Quantitative Coronary Analysis and Visualization Based on Three Dimensional Coronary Magnetic Resonance Angiography

Alex Etienne,¹ Peter Boesiger,² Warren Manning,³ Eike Nagel,⁴ René Botnar,⁵ Matthias Stuber.⁵ ¹ETH Zurich, Chemin de la Tour Ronde 5, Saint-Légier, Vaud, Switzerland; ²University and ETH Zurich, Gloriastrasse 35, Zurich, Switzerland; ³Harvard University, Division of Cardiology, 406 Brookline Avenue, Boston, MA, United States; ⁴German Heart Institute Berlin, Augustenburger Platz 1, Berlin, Germany; ⁵Beth Israel Deaconess Medical Center, 330 Brookline Ave, Boston, Massachusetts, United States

Introduction: Current state-of-the-art magnetic resonance angiography (MRA) acquisition schemes enable the three-dimensional (3D) assessment of the coronary arterial tree.

Hereby, endogenous (T2Prep, MTC, dual-inversion) and exogenous (extracellular contrast agents, blood-pool agents) contrast enhancement mechanisms together with multiple motion suppression strategies (breath-holding, prospective and retrospective navigators, mid-diastolic and late-diastolic image acquisition etc.) are currently under investigation in patient and healthy subject studies. For an objective, quantitative comparison between such coronary MRA techniques, and to allow for visualization and quantitative definition of lumen narrowing disease, the availability of a comprehensive coronary MRA visualization and analysis package would be desirable.

Purpose: To develop a comprehensive coronary vessel analysis package which facilitates visualization of the coronary anatomy and which allows for an objective, quantitative analysis of coronary MRA data.

Methods: For the visualization of 3D coronary MRA data, the user manually identifies a series of points on the coronary tree. Hereby, three orthogonal views (in three different viewports) of the 3D data-set facilitate the identification of the major coronary segments. The user can freely navigate in the 3D data-set and specific points on the coronary anatomy are identified per interactive mouse-click. The user-defined points are subsequently considered as members of the coronary artery tree, and prescribe a locally deformed surface which fits all the user-defined coronary points. After triangulation of this locally deformed surface, a parallel projection leads to the final, planar, reformatted image. Hereby, a maximum intensity projection is performed and a thickness of the volume in which maximum intensity projection is performed can be defined by the user. For an objective comparison between different acquisition schemes, it is possible to store the user-selected data points and re-load them for another MR data-set acquired in the same subject. Upon completion of the definition of the coronary tree, length measurements can be performed on the reformatted, planar representation of the coronary anatomy. Hereby, the user-specified 3D data points are utilized for true 3D length assessment. To further facilitate objective quantitative image analysis, a previously described vessel tracking algorithm together with vessel diameter measurements and the determination of the vessel sharpness along the vessels are included (1). For local vessel sharpness definition and to determine the local

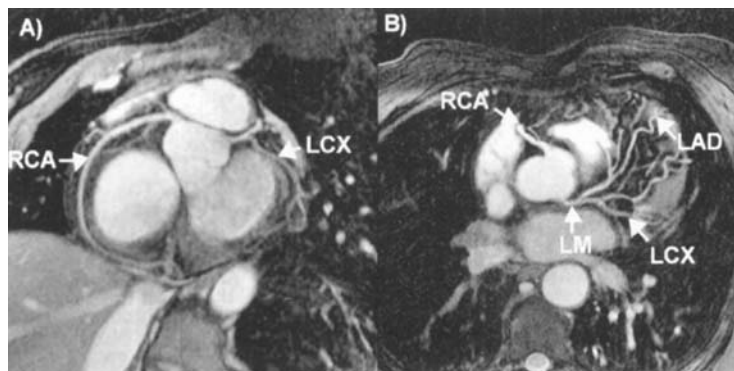


Figure 1. Reformatted 3D coronary MRA data of a right (A) and left (B) coronary arterial system.

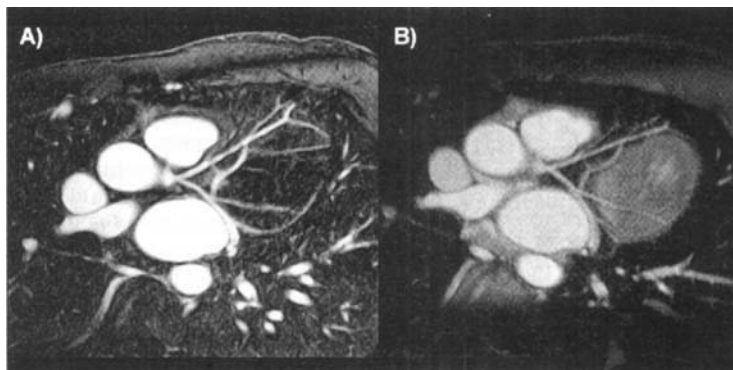


Figure 2. Reformatted left coronary system acquired with a blood-pool agent B-22956 (A) and a conventional T2Prep imaging technique (B).

vessel diameter, a Deriche image, based on a first order derivative of the reformatted image (2) is calculated by the software. Contrast-to-noise ratio (CNR) and signal-to-noise ratio (SNR) are assessed based on user-specified regions of interest (ROI) in the background of the image, in the myocardium, and in the blood-pool. To enable objective comparison between two scanning methods, these ROIs can be stored and re-loaded if needed. For further processing of the quantitative data including vessel diameter, vessel sharpness, vessel length, SNR and CNR, numerical values are written into an ASCII file. For visualization purposes, the reformatted images can be stored as a TIFF, JPEG or GIF format. The software was implemented on a commercial 1.4MHz Pentium 4 PC under Windows2000 and IDL 5.2 (Interactive Data Language, Research Systems Incorporated, Boulder, CO).

Results: The presented tool facilitates visualization of the coronary anatomy in a single image (Figures 1 & 2). Reformatted images obtained using a previously described 3D coronary MRA acquisition technique (3) are shown in Figure 1. A 14cm segment of a right coronary artery (RCA) is displayed together with the left coronary circumflex (LCX) (Figure 1A). A simultaneous visualization of multiple coronary segments of a left and right coronary arterial system is seen in Figure 1B, where a proximal portion of the RCA is displayed along with the left main (LM), the left anterior descending (LAD), the LCX and multiple branching vessels. Example reformatted coronary MRA obtained with a blood-pool agent (B-22956, Bracco Imaging SpA, Milan, Italy) are displayed (Figure 2A) together with a more conventional T2Prep acquisition (Figure 2B) acquired in the same subject. Numerical analysis performed for the LAD showed an average 2.6mm vessel diameter with T2Prep (vs. 2.7mm with contrast agent), a 11.5cm contiguous length of the LAD (vs. 11.7 with contrast agent), a vessel sharpness of 0.5 (vs. 0.6 with contrast agent) and a SNR/CNR of 32/19 (vs. 37/44 with contrast agent).

Conclusion: The present coronary analysis tool enables the visualization and the documentation of coronary MRA data while simultaneous display of multiple coronary vessels is feasible. It further facilitates quantitative coronary analysis and therefore appears to be well suited for objective, quantitative comparisons between different scanning techniques. The utility for quantitative coronary analysis and grading of stenosis

remains to be investigated in patients with x-ray defined coronary artery disease.

228. Infarct Imaging Using Free-Breathing Navigated Inversion Recovery

James Moon,¹ Jennifer Keegan,² Peter Gatehouse,¹ Christine Lorenz,³ Dudley Pennell.⁴ ¹Royal Brompton Hospital, Royal Brompton Hospital, London, England, United Kingdom; ²Royal Brompton Heart & Lung Hospital, Magnetic Resonance Unit, London, England, UK; ³Washington University in St. Louis, CMR Unit, London, England, United Kingdom; ⁴Royal Brompton and Harefield NHS Trust, Sydney Street, London, England, United Kingdom

Introduction: Segmented inversion-recovery (IR) after gadolinium results in high contrast images. The limits of image quality during breath-hold are defined by a number of factors. Sequence factors include the need to image as near as possible to zero crossing (null point) of normal myocardium, but a long read-out (typically 23 lines, TE 4 ms) puts the edges of k-space significantly off null; the effect of the imaging RF pulses on the contrast between infarct and normal myocardium and low SNR with smaller voxels. Patient factors may include poor breath-hold ability and arrhythmia.

Purpose: To develop a free-breathing, navigated IR sequence to aid imaging patients where conventional IR is unsatisfactory and potentially to improve on conventional image quality.

Methods: A free-breathing, navigator-gated segmented IR sequence was implemented on a Siemens Sonata system. The navigator consisted of orthogonal 90 and 180 RF pulses on the right hemi-diaphragm. The total time of the navigator was 90 ms, including a 30 ms gap before read-out. The segmented IR sequence used allows adjustment of TE, the read-out flip angle, segmentation and voxel size. 10 patients were studied; 4 with acute myocardial infarction, 2 post Hypertrophic Cardiomyopathy (HCM) septal ablation, 4 with fibrosis associated with HCM.

Results: Figure 1 shows breath-hold (a) and navigated (b) sample images in a patient with an acute MI and microvascular

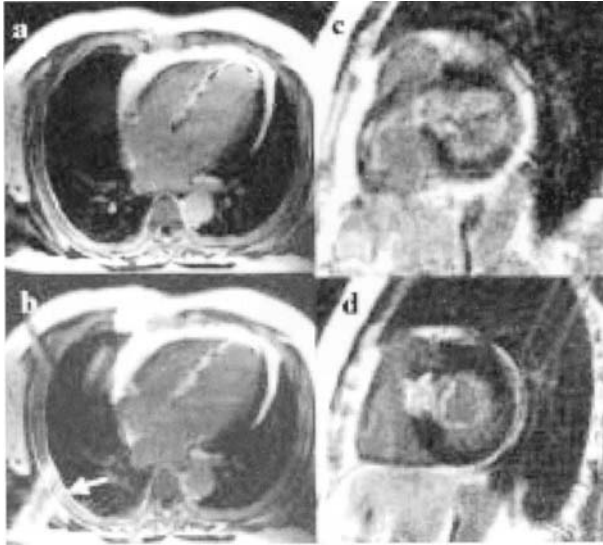


Figure 1.

obstruction in with equivalent image quality; (c) breath-hold and (d) navigated show improved image quality with the navigator. The navigator pulse artefact is arrowed. Using the same IR parameters, the navigated sequence image quality was the same as the breath-hold in 6 patients, worse in 3 patients and better in 1 patient. In this patient, poor breath-holds prevented scan interpretation without the navigated images. Scan efficiency (reflecting the number of accepted acquisitions) at a 6mm acceptance window was 44% (range 19–75%) so scan time was longer. Patients with poor quality navigated images tended to have greater diaphragmatic excursion (20mm vs 14.5mm, $p = 0.01$). In patients with good quality navigated images it was possible to change imaging parameters, reduce the number of segments from 23 to 9, increase the read-out flip angle from 20 to 23 and reduced pixel size. In 2 out of 7 patients, this resulted in improved image quality over the best non-navigated images.

Conclusion: Post gadolinium free-breathing navigated IR is practical for patients in whom breath-hold techniques are unsatisfactory. It may provide a way of obtaining higher quality images than conventional techniques in selected patients. Some patients had poor quality navigated images possibly related to large diaphragmatic excursions. This group may benefit from both pre and post read-out navigators or slice following methods.

229. Breath-Hold Signal Loss Sequence for Qualitative Assessment of Blood Flow Disturbances in Cardiovascular MR

Jennifer Keegan,¹ Peter Gatehouse,¹ Anna John,¹ Steven Collins,¹ David Firmin.¹ ¹Royal Brompton and Harefield NHS Trust, Magnetic Resonance Unit, London, England, UK

Introduction: In cardiovascular MR, flow compensated gradient echo sequences with echo times of around 15ms have been

shown to exhibit signal loss in areas of complex blood flow (1). Although not directly related to the severity of stenosis or to other pathology, the level of signal loss has proved to be a clinically useful indicator and can also aid in the positioning of further imaging planes for quantitative analysis with phase velocity mapping. Due to the requirement for a long echo time however, such a sequence cannot be segmented to allow breath-hold acquisition and studies typically take approximately 2 minutes to acquire with respiratory motion artefact being a frequent problem.

Purpose: The purpose of this research is to develop a segmented gradient echo sequence which results in a degree of signal loss similar to that obtained with a conventional sequence whilst allowing the entire acquisition to be performed in the duration of a single breath-hold.

Methods: This work was carried out on a Siemens Sonata scanner equipped with gradients having a peak gradient strength of 40mT/m and a peak slew rate of 200mT/m/ms. Two sequences were developed, based on a simple segmented gradient echo sequence with increased flow sensitivity and view-sharing, as shown in Figures 1. In the first (a), velocity sensitivity was introduced with the addition of a bi-polar gradient in both the slice-select and read directions. In phantom and initial patient studies, the velocity sensitivity in both directions was adjusted to give a similar extent and degree of signal loss as a conventional TE14 sequence. In the second (b), the gradient waveforms in the slice-select and read directions were modified to give an acceleration sensitivity, whilst maintaining velocity compensation. This involved the addition of extra gradient lobes between the slice selection and signal readout. The phase shifts due to acceleration in both directions were equal to those introduced by the conventional sequence. The TEs of the sequences developed in (a) and (b) were 6.9 ms and 8.2 ms respectively. Breath-hold acquisitions with 7 views

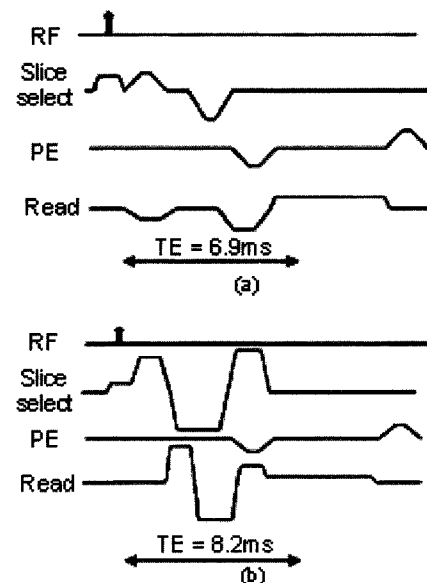


Figure 1. Velocity sensitised (a) and acceleration sensitised (b) gradient echo sequences.

per segment and view-sharing enabled the acquisition of cine data with effective temporal resolutions of 45 and 50 ms over 18 cardiac cycles.

Results: Figure 2 shows the results of using these sequences in a subject with aortic stenosis and regurgitation. Figure 2(a) shows a single cine frame from a conventional sequence acquired over approximately 2 minutes showing signal loss at the valve plane which extends into the left ventricle. Respiratory motion artefact is also present and the image is considerably degraded, this being particularly apparent at the level of diaphragm edge. Figures 2(b) and (c) show the corresponding cine frames from the velocity and acceleration sensitised breath-hold sequences shown in Figures 1(a) and (b) respectively, both showing a similar degree and extent of signal loss as the TE14 sequence. The image quality in Figure 2(b) however, is considerably degraded by artefacts from constant velocity blood which smear out in the phase encode direction. In comparison, the acceleration sensitised acquisition shown in Figure 2(c), where constant velocity material is rephased at the centre of the echo readout, is of high quality and devoid of both respiratory and blood flow artefacts. It is thought that variations in blood flow velocities from beat to beat can result in phase variations and associated artefacts when using the velocity sensitised sequence whereas the high acceleration and other high orders of motion are only present in the region of highly complex flow where the related phase shifts tend to result in signal cancellation.

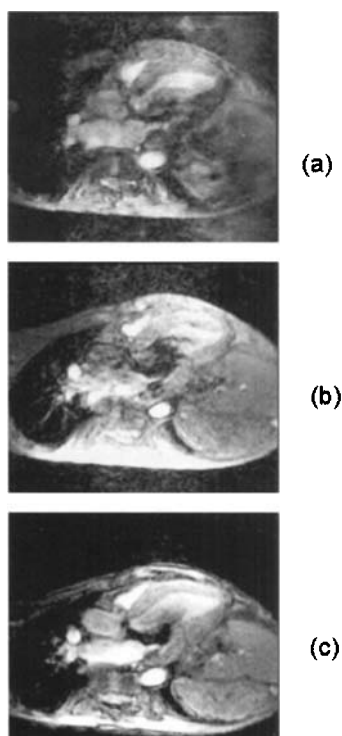


Figure 2. Single frames from (a) a conventional sequence, (b) the breath-hold velocity sensitised sequence and (c) the breath-hold acceleration sensitised sequence

Conclusion: We have developed a segmented sequence which is able to generate similar degrees of signal loss to a conventional gradient echo sequence. By comparison, the acquisition duration is considerably reduced and breath-hold imaging is feasible, removing respiratory motion artefact. Although the most obvious approach to generating signal loss is to add velocity sensitivity to a previously compensated sequence, as in Figure 1(a), we have shown that artefact from flowing blood degrades the image (Figure 2(b)). Signal loss is instead best generated by using the acceleration sensitive sequence shown in Figure 1(b) where both stationary and constant velocity blood signal are rephased.

230. Black-Blood Dual Contrast Fast Spin Echo of the Heart with Stir Preparation

Agus Priatna,¹ Dee Wu.¹ ¹Marconi Medical System, 595 Miner Road, Cleveland, Ohio, United States

Introduction: The use of black-blood imaging for cardiac applications has increased in recent years [1,2,3]. The main advantage of the black-blood imaging is that it provides excellent blood signal nulling for reducing flow artifacts in tissue boundaries. Simonetti et al used black-blood preparation with fast spin echo (FSE) sequences combined with short tau inversion recovery (STIR) for imaging of the heart [2]. In that study [2], diseased tissues were characterized based on fat suppressed T2 weighted images of the heart. In disease states, a lesion which may contain fat deposits in myocardium was differentiated from healthy tissue with STIR preparation. In addition to T2 weighted imaging, characterization studies were also performed using T1-weighted fast spin echo imaging [4]. T1-weighted and T2-weighted imaging combined with fat suppression are useful for imaging of the heart.

Purpose: A sequence that provides both black-blood T1 and T2 weighted imaging was proposed using a dual contrast fast spin echo in a single acquisition [5,6]. The black-blood dual contrast FSE sequences have provided excellent T1 and T2 weighted imaging of the heart, aorta, and the vasculatures of the neck [5,6]. In addition to providing black-blood T1 and T2 weighted images of the heart, the technique described here utilizes a STIR preparation for fat suppression. Thus, it provides black-blood dual contrast images in a single acquisition plus superb fat suppression. Both T1 and T2 weighted images are acquired at the same phase of the cardiac cycle, thus minimizing misregistration.

Methods: Black-blood STIR preparation was implemented with dual-contrast FSE sequences on 1.5T Eclipse whole body scanner system (Marconi Medical Systems, Inc., Cleveland, Ohio) with a gradient system of 27 mT/m with a slew rate of 72 T/m/s. The black-blood STIR preparation consisted of three adiabatic inversion recovery (IR) pulses. A non-selective adiabatic inversion pulse was followed immediately by a selective inversion pulse to provide black-blood suppression. The third selective RF pulse was used for fat suppression. The inversion time from the first inversion pulse to the imaging acquisition was set to 625 msec to null the blood, and the inversion time of the third IR pulse to the acquisition was 150 msec to suppress the fat signal.

The dual-contrast fast spin echo sequence used a split echo train lengths (ETL). A total of 16 ETL was used for the sequence. The first group of echoes (8 ETL) formed the T1-weighted image of which the first echo signal was arranged to the center of k-space. The second group of ETL (8 ETL) formed the T2-weighted image of which the middle echo signal (ETL/2) was placed to the center of k-space. The inter-echo spacing was 6.5 msec. The first echo time was 6.5 msec for T1-weighted imaging and the second echo time was 58.5 msec for T2-weighted imaging.

Images of the heart of a normal volunteer were obtained with ECG triggered black-blood STIR dual-contrast FSE sequence each within a short breathold period. For comparisons, regular black-blood dual contrast FSE without STIR preparation was also performed on the same subject. The acquisition was acquired every other R-R interval and a breathold was performed during inspiration. Other imaging parameters are: matrix size = 128 × 256, thickness = 10 mm, NSA = 1, bandwidth = 62.5 kHz, FOV = 30 cm. A rectangular field of view was applied to shorten the scan time.

Results: Figure 1A and 1B show the black-blood T1 and T2 weighted images, respectively, of the short axis of the heart obtained with black-blood dual contrast FSE without STIR preparation. Figure 1C shows the black-blood STIR T1-weighted image and Figure 1D is the corresponding T2-weighted image. The blood is completely darkened on all T1 and T2 weighted images. Also the blood-tissue boundaries are clear and no blood flow artifacts are observed. Notice that with STIR preparation, the myocardial fat is completely suppressed as shown on the bottom images.

Conclusion: As seen in the images, black-blood STIR dual contrast FSE sequence provides excellent T1 and T2 weighted images of the heart. The technique suppresses the blood flow artifacts as well as the fat. Good fat suppression is critical for studies such as for characterizing myocardial lesion that may contain fat deposit. As seen in the figures,

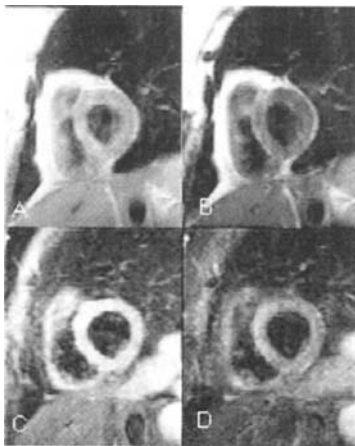


Figure 1. [A] and [B] are T1 and T2 weighted black-blood FSE, respectively acquired in a single acquisition. [C] and [D] are T1 and T2 weighted images, respectively, with STIR preparation.

the image pairs are taken at the same location and at the same phase of the cardiac cycle, minimizing misregistration. The images are also free from artifacts caused by the cardiac and respiratory motion.

In conclusion, fat suppressed black-blood T1 and T2 weighted fast spin echo imaging of the heart can be performed using STIR preparation pulse in a single acquisition and within a breathold period.

231. Interactive Cardiac Localization with Single-Shot Black-Blood Field Echo Sequence

Agus Priatna,¹ Derrick Green,¹ Dee Wu.¹ ¹Marconi Medical Systems, 595 Miner Road, Cleveland, Ohio, United States

Introduction: Interactive localization for cardiac applications has now been used in clinical environment [1,2]. Interactive interface allows fast localization of the cardiac anatomy. Most commonly, the imaging techniques used for interactive localization utilize a "bright blood" technique such as field echo and spiral or echo planar imaging sequences [1,2,3]. These sequences provide fast acquisitions, however, the images produced by bright blood technique suffer from blood flow artifacts that may cause difficulty visualizing small structures such as heart valves.

Previously, black-blood imaging technique has been used for non-interactive cardiac localization as the technique produces less flow artifacts and provide good contrast between ventricular space and heart tissues [4] and thus provides a good alternative for cardiac piloting. Though previously, black-blood interactive has been demonstrated using presaturation pulses[5], we show the effective utility of using double inversion technique for the improved visualization which results in better localization of the cardiac anatomy.

Purpose: We present the utility of using a double inversion single shot imaging as an interactive pilot. Thus permitting more accurate and faster positioning to the desired anatomy. The black-blood technique avoids the need of temporal information phases that is sometime used in bright blood technique. This technique also suppresses flow artifacts.

Methods: Black-blood preparation was implemented with a single-shot rf-spoiled field echo sequence on 1.0T Polaris whole body scanner system (Marconi Medical Systems, Inc., Cleveland, Ohio) with a gradient system of 27 mT/m with a slew rate of 72 T/m/s. The black-blood preparation consisted of two adiabatic inversion recovery (IR) pulses. A non-selective adiabatic inversion pulse was followed immediately by a selective inversion pulse to provide black-blood suppression. The inversion time from the first inversion pulse to the imaging acquisition was set to 625 msec for nulling the blood.

An rf-spoiled field echo sequence was created with all of the phase encoding views collected all within a single-shot excitation. The acquisition was ECG triggered using a gating interval of three. This allows the the magnetization to fully recover before each imaging excitation. The sample

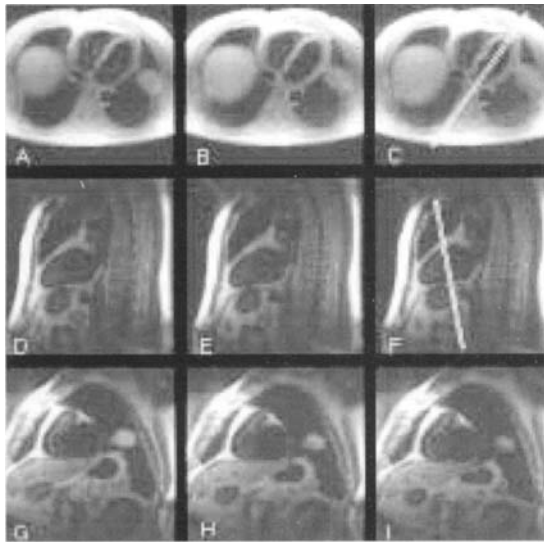


Figure 1. Successive acquisitions using black-blood single shot field echo sequence with interactive interface. Top row shows the tranverse slices. Middle row shows the two chamber views and the bottom row shows the short axis series.

parameters were used in a volunteer: heart rate = 850 msec: TE = 2.0 msec, matrix size = 112×256 , thickness = 10 mm, NSA = 1, bandwidth = 50 kHz, FOV = 35 cm.

Results: Figure 1. shows a series of the heart images during localization obtained with the black-blood single-shot field echo sequence. These images (from A to I) are obtained successively one after another. The top row shows a series of tranverse slice views. On C, the slice orientation is interactively placed to produce the two chamber views as shown in the middle row. On F, the orientation is then placed to produce the short axis views as shown at the bottom row. Notice that the blood still appear black on successive acquisitions. The contrast and the anatomy appear significantly improved over bright blood with no flow artifacts and artifacts from cardiac or respiratory motion.

Conclusion: As seen in the images that black-blood single-shot field echo sequence can be used interactively and produced high quality of black-blood images. The myocardium is clearly depicted as seen from the top row images. Many applications that benefit from this localization technique include heart valves or coronary artery localizations.

In conclusion, a black-blood, single-shot, rf-spoiled field echo sequence was developed for use of interactive piloting. This technique avoids the need of temporal information phases sometimes used in bright blood piloting. The technique also shows better prescription of the desired planes for subtle structures. The reduction of artifacts associated with bright blood technique is also observed. Finally, this technique allows an easy, fast, and interactive environment that is very practical for cardiac clinical applications.

232. Assessment of Segmental Wall Motion Using Interactive Real-Time Magnetic Resonance Imaging: Comparison with 2D Echocardiography and Breath-Hold TrueFISP

Harald P. Kühl,¹ Arno Bücker,¹ Alexander Wall,¹ Elmar Spüntrup,¹ Rolf W. Günther,¹ Peter Hanrath.¹

¹University Hospital Aachen, Pauwelstrasse 30, Aachen, Germany

Introduction: Cardiac MRI is limited by the need for repeated breath-holds and ECG triggering. Real-time cardiac MRI obviates the need to perform breath-holds which may be especially valuable in patients with severe cardiopulmonary disease. Furthermore, real-time cardiac MRI obviates the need for ECG triggering which may improve image quality in patients with arrhythmia such as atrial fibrillation. However, real-time cardiac MRI using gradient-echo techniques has showed only moderate image quality especially in the long-axis views of the heart. The recent introduction of MRI sequences with steady state precession has resulted in a dramatic improvement of image quality which was most pronounced in long-axis views of the left ventricle. The combination of these sequences with real-time cardiac MRI imaging may therefore be a valuable alternative to echocardiography for the assessment of regional wall motion in patients with poor acoustic echo window.

Purpose: The purpose of the study was to compare an interactive real-time MRI technique to 2D echocardiography for the assessment of segmental endocardial visibility and segmental wall motion.

Methods: For real-time cardiac MRI we used a radial trueFisp sequence (RADIAL, TE/TR 1.3/2.9 ms, matrix 128/256). 2D echocardiography was performed using second harmonic imaging (ECHO). An ECG-triggered, breathhold trueFisp sequence (BH-TF, TE/TR 1.8/3.6ms, matrix 256 × 256) was used as reference standard for wall motion assessment. MRI was performed on a 1.5 T scanner (ACS-NT, Philips, Best, The Netherlands). An interactive user interface allowed on-the-fly free plane definition during real-time scanning. With all modalities standard views including a mid-ventricular short-axis view and 3 long-axis views were acquired. Segmental endocardial visibility (0 = poor to 2 = good) and regional wall motion (0 = not evaluable to 4 dyskinesia) were scored according to the 16 segment model proposed by the ASE for all techniques. 23 non-selected patients referred for routine echocardiography were included.

Results: Two patients had atrial fibrillation. Out of 368 matched segments acquired with all three modalities poor visibility was present in 20.7% of segments with ECHO, 1.4% with RADIAL ($p < 0.001$ vs. ECHO) and 0.4% with BH-TF ($p < 0.001$ vs. Echo and $p = ns$ vs. RADIAL). Mean visibility score was significantly lower with ECHO (1.32 ± 0.8) as compared to RADIAL and BH-TF (1.95 ± 0.2 and 1.93 ± 0.3 ; $p < 0.001$ vs. ECHO). Mean wall motion score was not different between the modalities although there was a trend towards higher scores with ECHO.

Conclusion: Image quality using RADIAL is comparable to standard BH-TF and superior to ECHO for the visualization of segmental wall motion in this group of unselected patients. RADIAL may be a valuable alternative to echocardiography for the assessment of regional function in patients with limited

acoustic window. Moreover RADIAL may allow scanning of patients with severe cardiopulmonary disease incapable of breath-holding and patients with arrhythmias such as atrial fibrillation.

233. Black Blood Fiesta in Clinical Practice

David Stanley,¹ James Glockner,² Jason Polzin.³ ¹GE Medical Systems, 1601 Lavaque Road, Proctor, Minnesota, United States; ²Mayo Clinic, Department of Radiology, Rochester, Minnesota, United States; ³GE Medical Systems, P. O. Box 414, W875, Milwaukee, Wisconsin, United States

Introduction: Black Blood imaging is often useful for evaluation of cardiac and vascular morphology, and a variety of techniques have been described in the literature. Conventional spin echo sequences are robust and widely available, but are relatively long and frequently degraded by artifacts. Double inversion fast spin echo sequences offer excellent resolution and signal to noise ratio (SNR) but require breath holds of 10–20 seconds for each slice. Single shot fast spin echo sequences with blood suppression inversion pulses are much faster and generally yield diagnostic images, but can suffer from excessive blurring due to the long echo train length. We present results from a single-shot black blood steady-state free precession sequence (black blood fiesta) which may serve as a useful alternative to some of the sequences noted above. Images can be acquired in less than 1 second, and multiple excitations can be averaged to improve SNR in patients with reasonable breath hold capacity and adequate gating.

Purpose: To describe initial clinical applications of the black blood fiesta sequence and compare results with a standard black blood sequence (double IR fast spin echo).

Methods: The black blood fiesta sequence employs a non-selective RF blood suppression pulse followed by a slice-selective refocusing pulse. An image can be obtained in either 1 or 2 R–R intervals, and multiple acquisition can be averaged if necessary. Ten patients scheduled for cardiac or thoracic MRI and requiring black blood images of the heart or aorta were included in the study. Black blood images were obtained using double IR fast spin echo and black blood fiesta sequences with identical orientation, slice thickness and field of view. The two sets of images were then compared. Myocardial SNR was measured, and a qualitative scale was used to rate image quality and blood suppression. Finally, images were classified as acceptable, unacceptable, or indeterminate for reaching a clinical diagnosis.

Results: Double IR FSE images had a higher SNR and were qualitatively superior in comparison to black blood fiesta images. Exceptions occur in patients with poor breath hold capacity, where black blood fiesta images were of acceptable quality even when acquired without breath holding. Blood suppression was similar for both sequences, with problems generally occurring when image orientation included in-plane rather than through-plane flow. Black blood fiesta images were nearly always considered acceptable for reaching a clinical diagnosis.

Conclusion: Double IR fast spin echo produced superior images in most patients, but a significant cost in imaging time and breath-hold length. There are many patients who clearly benefit from a sequence that can produce acceptable images without breath holding.

234. Assessment of a Method to Generate Myocardial Contours for Left Ventricle Analysis Without User Input

Mark Crowe,¹ Marie-Pierre Jolly,² John Vargas,³ Orlando Simonetti.⁴ ¹Vanderbilt University, P.O. Box 1006-B, Nashville, Tennessee, United States; ²Siemens Corporate Research, Imaging and Visualization Department, Princeton, NJ, United States; ³Northwestern University, 303 E Chicago, Chicago, Illinois, United States; ⁴Siemens Medical Systems, Ontario Center East Tower, Chicago, IL, United States

Introduction: To analyze left ventricular volume and mass from short-axis, cine images quickly and accurately, a method for generating endocardial and epicardial contours is needed that requires minimal user input, yet produces reliable results. The volume and mass measurements obtained from an automatic image segmentation method were compared to hand-drawn contours.

Purpose: This study determines whether the automatic method produces sufficiently accurate results.

Methods: Short-axis cine images covering the heart from base to apex were obtained in twenty-two patients that underwent a MR myocardial viability/function exam using a 1.5-T Siemens Magnetom Sonata. The short-axis, cine images were acquired using a breath-hold, TrueFISP sequence. The Argus software package (Siemens, Iselin, NJ) was used for generation of all automatic and hand-drawn contours, as well as the calculation of cardiac volume and mass parameters.

Since only the end-diastolic (ED) and end-systolic (ES) phase contours are necessary to calculate end-diastolic volume (EDV), end-systolic volume (ESV), ejection fraction (EF), stroke volume (SV), and myocardial mass, only ED and ES images were used in the analysis. "Gold standard" myocardial borders were established by hand-drawing endo- and epicardial borders on the ED and ES images. An experienced user

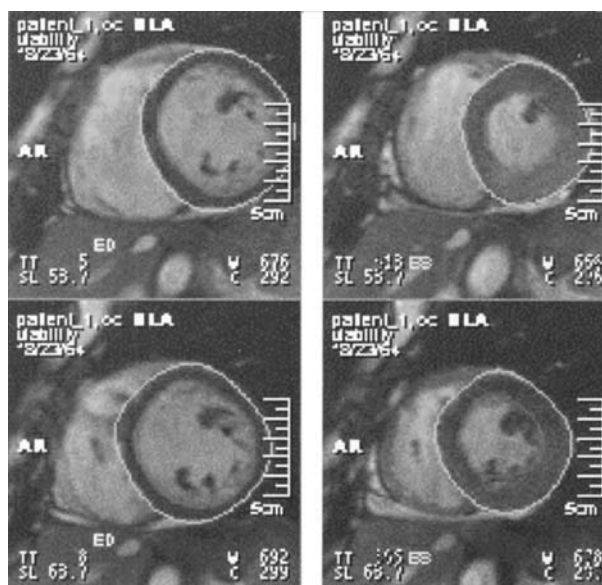


Figure 1. ED and ES Contours from Automatic Method.

Table 1
Accuracy of the Automatic Method

	Base Units	%
EDV (ml)	-6.5 ± 12.11	-4.15 ± 8.2
ESV (ml)	-3.48 ± 7.14	-4.2 ± 10.1
SV (ml)	-2.09 ± 9.14	-0.99 ± 13.3
EF (%)	0.68 ± 3.92	2.4 ± 10.1
Mass (g)	13.24 ± 10.2	9.6 ± 8.3

reviewed the contours and made any necessary corrections. A fully automatic contour generation method was then used to produce contours on the ED and ES images. This method uses a combination of image processing techniques such as region segmentation, active contours, and shape matching. It is described in details in [1]. The only user inputs provided to the automatic segmentation method were the identification of ED and ES phases out of the full cine series, and cropping the images closely around the heart, as shown in Figure 1.

Using the gold standard results for comparison, the average difference and standard deviation were calculated in base units and as a percentage. The results of the method under review were analyzed by a paired t-test and regression analysis.

Results: The automatic method slightly underestimated the endocardial contours. As a result, the EDV and ESV measurements for each patient were less than the gold standard measurements. Table 1 shows that the EDV was underestimated by an average 6.5 ± 12.11 ml (4.15 ± 8.2 %) and the ESV was underestimated by an average 3.48 ± 7.14 ml (4.2 ± 10.1 %). Regions that contain papillary muscles or a mixture of wall/blood pool appeared to be the primary cause of error in endocardial border determination.

The automatic method overestimated the mass by an average of 13.24 ± 10.2 grams (9.6 ± 8.3 %). This overestimation was also primarily due to the underestimation of the endocardial contour area. The size of the overestimation also suggests that on average the epicardial contour is slightly overestimated.

Conclusion: The fully automatic method of myocardial boundary definition requires no user contour input. This method calculated ventricular volume within 5% and mass within 10% of hand-drawn "Gold-standard" contours. Further studies are required to determine if this accuracy is maintained in a wider population of patients.

235. Adapting Steady State Free Precession MR Imaging for Myocardial Tagging

Jjm Zwanenburg,¹ Jt Marcus,¹ Jpa Kuijjer,¹ Ac Van Rossum,¹ Rm Heethaar.¹ ¹VU University Medical Center, PO Box 7057, Amsterdam, Noord-Holland, Netherlands

Introduction: The steady state free precession (SSFP) imaging sequence has two important advantages: it is fast and it has a

good signal to noise ratio (SNR). Therefore, it would be profitable to combine SSFP with myocardial tagging. Compared to a conventional spoiled gradient echo (SGE) tagging sequence, a SSFP tagging sequence would allow for either a higher time resolution of the tagged cine or for a shorter acquisition time at identical SNR in the myocardium. Two points must be considered in combining SSFP with tagging. First, the steady state must be preserved while a tagging pattern need to be applied at every ECG-R wave. Second, the SNR of the myocardium is not optimal for tagging in usual SSFP sequences, because these are optimized for high contrast between blood and myocardium.

Purpose: It is the purpose of this work to adapt the SSFP sequence such that the steady state is preserved while a tagging pattern is applied, and that the SNR of the myocardium is optimal.

Methods: MR imaging was performed on a 1.5 T Siemens Sonata whole body scanner, with a 4-element phased-array coil configuration. After each ECG-R wave, the tag modulation was applied with two non-selective RF pulses separated by field gradients in the frequency encoding direction, yielding a sinusoidal modulation of tissue magnetization [1]. The two tagging pulses each had a flip angle of 55° .

Adapted SSFP sequence: We used the method described by Scheffler et al. [2] to combine the SSFP with magnetization preparation. An $\alpha/2$ flip-back pulse stores the steady state transverse magnetization as longitudinal magnetization. After application of the tagging block, the longitudinal magnetization is excited by an $\alpha/2$ pulse to continue the SSFP acquisition.

Taking into account the T_1 and T_2 values of the myocardium, we calculated the optimal flip angle for maximum signal in the myocardium, and thus for maximum amplitude of the tagging pattern. Besides, the bandwidth (BW) was calculated for which the SSFP was expected to have the same SNR as our standard spoiled gradient echo (SGE) sequence.

We measured tagged mid ventricular short axis cines with a series of six SSFP sequences on two volunteers. In this series, the BW varied from 343 Hz/pixel to 930 Hz/pixel. Accordingly,

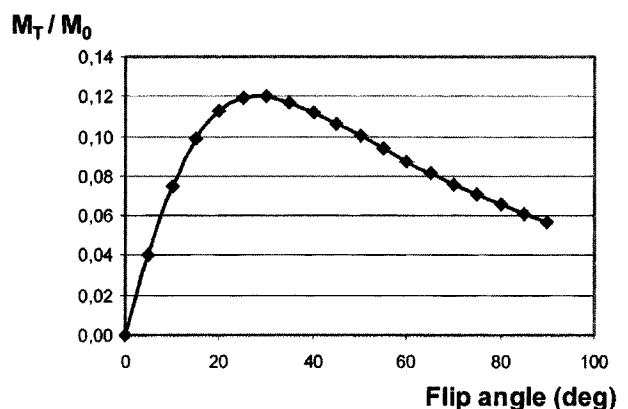


Figure 1. Measure for the theoretical SSFP signal amplitude in the myocardium as function of the flip angle. The figure shows the amount of transversal magnetization M_T relative to the initial longitudinal magnetization M_0 .

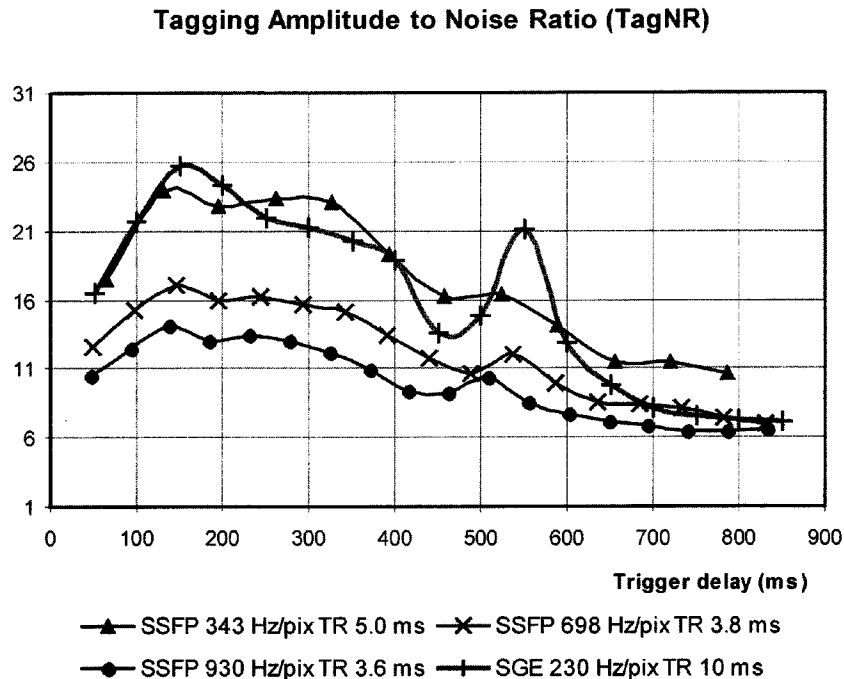


Figure 2. The TagNR during the heart cycle for three SSFP acquisitions and the reference SGE acquisition.

the TR varied from 5.0 ms to 3.6 ms. Other parameters for the SSFP were: $\alpha = 20^\circ$, FOV 300×300 mm, slice thickness 5 mm, 256×79 matrix, and 13 k_y /beat.

SGE reference sequence: Imaging parameters of our reference SGE sequence were: $\alpha = 15^\circ$, TR 10 ms, BW 230 Hz/pixel, FOV 300×300 mm, slice thickness 5 mm, 256×80 matrix, and 5 k_y /beat.

To compare between the SSFP tagging and the reference SGE tagging, we defined the tagging amplitude to noise ratio (TagNR). The TagNR is defined as the intensity of the myocardium in the harmonic magnitude image [3] divided by the background-noise standard deviation of that image.

Results: Figure 1 shows the theoretical SSFP signal amplitude in the myocardium as function of the flip angle (T_1 800 ms, T_2 50 ms for the myocardium). The maximum signal is obtained with a flip angle close to $\alpha = 30^\circ$. Experiments showed that a lower flip angle improves the tag persistence considerably, while the TagNR is only slightly reduced. We found $\alpha = 20^\circ$ to be a good compromise.

For the first volunteer, figure 2 compares the TagNR for three different BWs with that for the SGE. The SSFP sequence with BW 343 Hz/pixel yielded a TagNR quite comparable with the SGE sequence throughout the cardiac cycle. In the second volunteer, the TagNR of the 343 Hz/pixel SSFP acquisition was at least equal to the TagNR of the SGE acquisition throughout the cardiac cycle.

Discussion: From theory, the SSFP sequences were expected to yield an even better TagNR in comparison with the SGE, than we observed. In our human SSFP images, however, artifacts due to fast flowing blood may have some

negative effect on the TagNR, while it still compares well with the TagNR in SGE images.

Conclusion: We have shown that with $\alpha = 20^\circ$, and BW 343 Hz/pixel, the SSFP tagging yields the same TagNR as the SGE tagging, while the SSFP image acquisition is two times as fast as the SGE acquisition.

Acknowledgement

This work was supported by the Netherlands Heart Foundation, grant 2000.220.

236. 3D True-FISP Imaging of the Coronary Arteries: Improved Contrast with T2-Preparation

Steven Shea,¹ Vibhas Deshpande,¹ Yiucho Chung,² John Finn,¹ Debiao Li.¹ ¹Northwestern University, Department of Radiology, Chicago, Illinois, United States; ²Siemens Medical Solutions, Research and Development, Chicago, IL, United States

Introduction: Recently, coronary artery imaging using segmented True-FISP has become feasible, providing excellent SNR and increased CNR when compared to FLASH techniques (1). However, myocardium suppression may be insufficient because the magnetization is in transience to steady-state. Previous research in coronary artery imaging using FLASH has shown that a T2-preparation scheme can effectively suppress the myocardial signal (2, 3). This is due to the fact that the T2 of myocardium is considerably less than that of arterial blood.

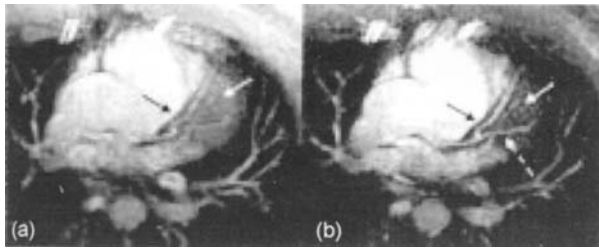


Figure 1. MIP images of the LAD. (a) has been acquired without T2-preparation while (b) has been acquired with a T2-preparation duration of 40 ms. Myocardial suppression is clearly superior with T2-preparation (solid arrows), resulting in better delineation of the LAD. Note that the diagonal branch (dashed arrow) is clearly defined in (b).

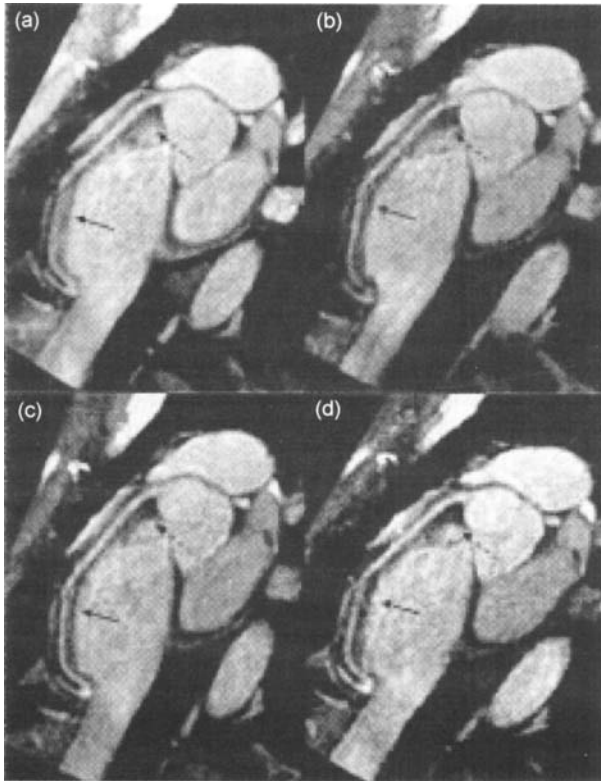


Figure 2. MIP images of the RCA with (a) no T2-preparation, (b) 24 ms T2-preparation, (c) 40 ms T2-preparation, and (d) 60 ms T2-preparation. Note that the mid-segment of the RCA (solid arrow) is better delineated in (c) as compared to the other images. Also, the myocardial signal at the proximal portion of the RCA (dashed arrow) was much better suppressed in the (c) and (d) compared to (a).

Table 1

SNR/CNR Measurements for Different T2-Preparations

	none	24 ms	40 ms	60 ms
SNR	9.0 ± 2.7	8.1 ± 2.9	7.6 ± 2.8	6.3 ± 2.6
CNR	3.1 ± 1.3	3.7 ± 1.4	4.2 ± 1.7	3.5 ± 1.9

T2-preparation can also benefit True-FISP imaging of the coronary arteries.

Purpose: The purpose of this work was to evaluate a T2-prepared, ECG-triggered, fat-saturated, segmented 3D True-FISP sequence for coronary artery imaging within a single breath-hold. T2-preparation was used to enhance visualization of the distal portions of the coronary arteries as well as improve overall delineation of the arteries.

Methods: Seven volunteers were imaged with a segmented 3D True-FISP sequence with no T2-preparation and with T2-preparation durations of 24 ms, 40 ms, and 60 ms on a Siemens 1.5T Sonata scanner with a high performance gradient system. The T2-preparation scheme implemented was the one previously described by Brittain et al. (2). The parameters for each scan were as follows: TR/TE = 3.1/1.3 ms, flip angle = 70°, readout bandwidth = 980 Hz/pixel, number of phase-encode lines acquired per heartbeat = 41, and in-plane resolution = 1.3 × 1.0 mm². Asymmetric sampling was employed to reduce TR with the echo center occurring at the 64th point in a 256-point readout period. A slab thickness of 18 mm was used with a total of 6 partitions that were sinc-interpolated to 12. Phase-encoding lines were acquired centrally, and partition-encoding steps were linear. The entire scan was completed in 24 cardiac cycles during a breath-hold on inspiration. Measurements were made between the different sets of images to analyze SNR and CNR. For image comparison, maximum intensity projections (MIP's) were performed using standard Siemens software.

Results: Comparisons of images of the left anterior descending (LAD) and right (RCA) coronary arteries acquired with and without T2-preparation (Figs. 1–2) show that a T2-preparation time of 40 ms provided the best myocardial suppression and the best contrast between the coronary arteries and surrounding myocardium. Results of SNR and CNR measurements are shown

Table 2

Resulting p-Values from CNR Comparisons with Different T2-Preparation Times. Values in Bold Indicate Significant Differences (p < 0.05)

	none	24 ms	40 ms	60 ms
none	—	0.02	0.002	0.3
24 ms	0.02	—	0.04	0.53
40 ms	0.002	0.04	—	0.01
60 ms	0.3	0.53	0.01	—

in Table 1. As was expected, SNR was less in all T2-preparation images compared to those without T2-preparation. However, CNR significantly increased for T2-preparation times of 24 and 40 ms compared to no T2-preparation (Table 2). Also, CNR was significantly greater for a T2-preparation duration of 40 ms than that of 24 ms. Finally, the CNR for images with a T2-preparation time of 40 ms were significantly greater than those with a T2-preparation time of 60 ms.

Conclusion: 3D True-FISP imaging of the coronary arteries with T2-preparation provides better myocardial suppression and coronary delineation compared to True-FISP imaging without preparation. A 40 ms T2-preparation duration was found to be the optimal time for True-FISP.

References

1. Deshpande VS et al. MRM 2001; 46:494–502.
2. Brittain JH et al. MRM 1995; 33:689–96.
3. Botnar RM et al. Circ 1999; 99:3139–48.

237. Contrast Enhanced 3D Free-Breathing Coronary MRA Using the Blood-Pool Agent B-22956 (Gadocoletic Acid)

Matthias Stuber,¹ Michael Huber,² Eike Nagel,³ Ingo Paetsch,³ Axel Bornstedt,³ Bernhard Schnackenburg,³ Peter Boesiger,² Anna La Noce,⁴ Friedrich Cavagna,⁴ Eckart Fleck.³ ¹Beth Israel Deaconess Medical Center, Cardiovascular Division, Boston, MA, United States; ²University and ETH Zurich, Gloriastrasse 35, Zurich, Switzerland; ³German Heart Institute Berlin, Augustenburger Platz 1, Berlin, Germany; ⁴Bracco Spa, Imaging Department, Milan, Italy

Introduction: For coronary magnetic resonance angiography (MRA), contrast enhancement between the coronary blood-pool and the surrounding tissue is of crucial importance. For 3D coronary MRA, the in-flow contrast is generally reduced, thereby necessitating the use of alternative contrast enhancement mechanisms. Non-exogenous bright-blood contrast

enhancement techniques have been successfully applied and include the T2Prep (1), magnetization transfer prepulses (MTC) (2), fat saturation and the dual-inversion pre-pulse for black-blood visualization of the coronary arterial lumen (3). For exogenous contrast enhancement of the coronary lumen, extracellular contrast agents may not be ideal for prolonged free-breathing 3D coronary MRA, since they quickly extravasate into the extracellular space. Therefore, blood-pool agents which remain intravascular for a prolonged period of time appear desirable. In the present study, a free-breathing navigator gated and corrected 3D inversion-recovery sequence was implemented with intravenous injection of the blood-pool agent B-22956 (Bracco Imaging SpA, Milan, Italy). The results were compared to non-contrast agent enhanced T2Prep coronary MRA obtained in the same subjects.

Purpose: To investigate the potential of the new blood-pool agent B-22956 for free-breathing navigator gated and corrected 3D coronary MRA.

Methods: For contrast enhanced coronary MRA, an inversion-recovery (TI = 180 ms) 3D navigator gated (5 mm gating window) and corrected segmented k-space gradient echo imaging sequence (TR = 7 ms, TE = 2.1 ms, 70 ms acquisition window, 512matrix, 360 mm FOV) was used (Figure 1). A 3D volume of 3 cm thickness consisting of ten adjacent 3 mm slices was acquired. To facilitate right hemidiaphragmatic navigator performance in the presence of a non-selective inversion pre-pulse, a 2D selective diaphragmatic pencil beam 180° NAV-RESTORE (3) was implemented to re-invert liver magnetization for subsequent navigator lung-liver interface detection. Prior to the contrast enhanced coronary MRA data acquisition, a baseline T2Prep scan of the same volume targeted coronary anatomy was acquired. Hereby, only the inversion pre-pulse and the NAV-RESTORE were replaced by a T2Prep (TE = 50 ms) for endogenous contrast enhancement. All other sequence elements and timing remained unchanged. Both endogenous and exogenous contrast enhanced scans were acquired using vector ECG triggering and diastolic image acquisition. Both techniques were implemented on a commercial 1.5T Philips Gyroscan ACS NT system. Six healthy adult

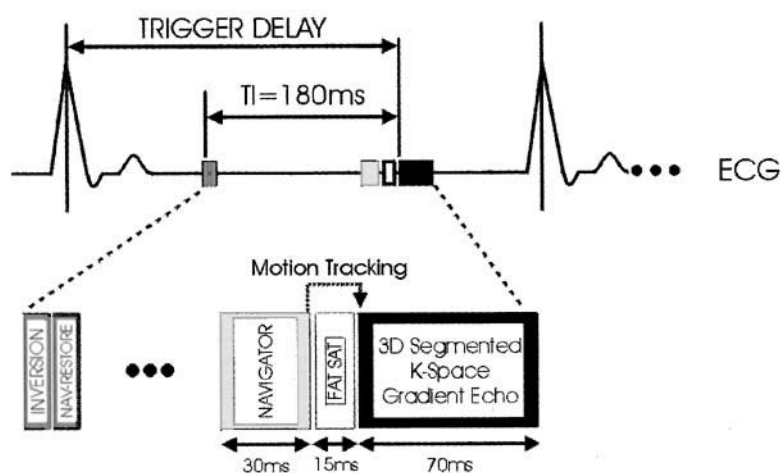


Figure 1. Imaging sequence for free-breathing blood-pool agent enhanced 3D coronary MRA

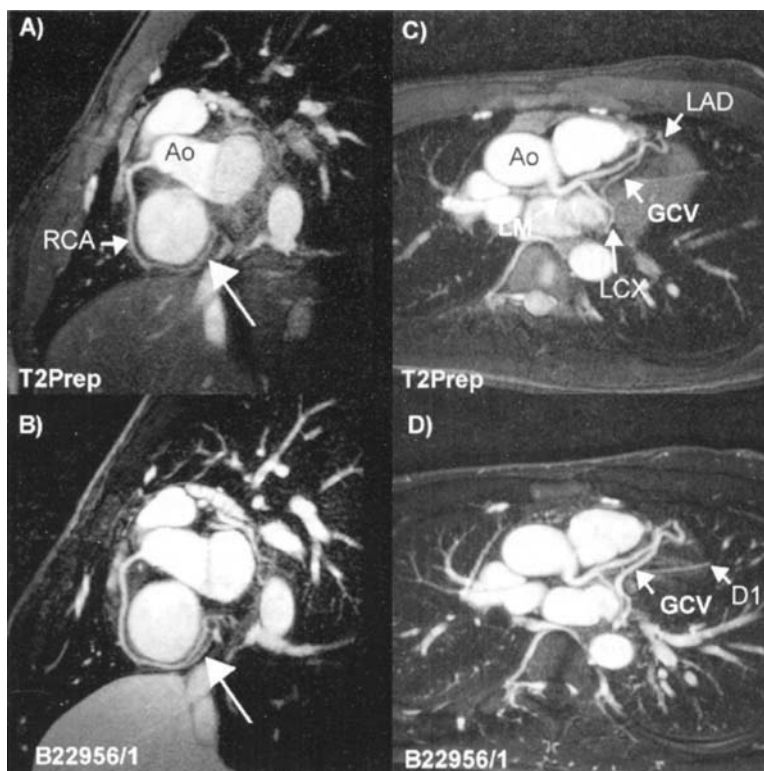


Figure 2. T2Prep (A & C) and B-22956 contrast enhanced (B & D) coronary MRA

subjects were investigated and a 0.075 mmol/kg bodyweight dose of the blood-pool agent B-22956 was administered intravenously. The molecular structure of this agent features a polyaminocarboxylate Gd complex linked to a deoxycholic acid moiety by means of a flexible spacer. Blood-pool agent enhanced coronary MRA always followed the T2Prep scans and data collection started 5 minutes post injection. For quantitative comparisons, signal-to-noise (SNR) and contrast-to-noise (CNR) were assessed for both, the T2Prep and the blood-pool agent enhanced scans and multiplanar reformatting was performed.

Results: In Figure 2, a right coronary artery (RCA) acquired with a T2Prep (A) and with the intravascular contrast agent (B) is shown. An enhanced contrast with an improved detail visibility (solid arrow) can be observed post contrast. A T2Prep acquisition of a left coronary arterial system showing the left main (LM), the left anterior descending (LAD), and the left coronary circumflex (LCX) is displayed in Figure 2C together with a signal attenuated great cardiac vein (GCV). The corresponding acquisition post contrast is displayed in Figure 2D, in which the same coronary anatomy with enhanced visual contrast and vessel definition is seen along with a signal enhanced GCV and a first order diagonal branch (D1). On the coronary MRA acquired post injection, a 30% improvement in SNR was found when compared to the T2Prep images (41 ± 5 B-22956 vs. 31 ± 6 T2Prep; $p < 0.05$). Consistent with the increased SNR, a 100% CNR enhancement (35 ± 5 B-22956

vs. 17 ± 5 T2Prep; $p < 0.05$) was found in the images acquired with the blood-pool agent.

Conclusion: By the combination of the blood-pool agent B-22956 and navigator gated and corrected inversion-recovery 3D coronary MRA data acquisition, high-quality coronary MRA can be acquired with high contrast during free breathing. While venous enhancement is more prominent on the contrast enhanced images, the use of B-22956 leads to a significantly enhanced SNR, CNR when compared to the more conventional T2Prep approach. The present methodology remains to be tested in studies of patients with coronary pathology.

238. Estimation of Perfusion and Blood Volume from Contrast Kinetics

Leon Axel,¹ James Eric McCloud.¹ ¹University of Pennsylvania, Department of Radiology, Philadelphia, Pennsylvania, United States

Introduction: Rapid sequence imaging of enhancement after the injection of a bolus of contrast agent provides information about regional perfusion of tissue such as the myocardium. Inclusion in the images of a large arterial blood-filled structure upstream, such as the left ventricular cavity, offers the possibility of correcting for the effects of the input function. However, most such analyses use overly simplified approaches,

Table 1*Low Flow State*

	Known Value	Estimate \pm sd	Model \pm sd
Delay (s)	1.6	3.06 \pm 0.97	1.76 \pm 0.74
Flow (ml/g/min)	0.5	0.53 \pm 0.09	0.48 \pm 0.13
Plasma vol (ml/ml)	0.07	0.10 \pm 0.03	0.09 \pm 0.05

such as the slopes of the enhancement curves, while a full deconvolution approach may be complicated and unstable.

Purpose: Assuming the intensity data has already been converted to contrast concentrations, we describe a method for estimating the perfusion from the tissue and input concentration curves. We further describe a method for estimating the tissue transit time from these curves, which then permits calculating the blood (or plasma) volume. These values can either be used by themselves or as initial values for an iterative approach to further deconvolution of the curves.

Methods: Assuming a linear response of the tissue to a contrast bolus, we model the observed tissue response as the convolution of the input function with two impulse responses, the arterial transfer function between the input observation site and the tissue (characterised by a delay time), and the tissue residue function (characterized by a transit time). The delay time can be estimated from the difference in times of departure of the curves from the baseline. For times short compared to the transit time, the rising portion of the tissue curve will be given by the integral of the input curve, corrected for the delay time and scaled by the perfusion flow; comparing this integral with the observed curve allows us to estimate the perfusion as their relative scaling factor. We can estimate the first moment of the tissue residue function by the difference of the peak times of the curves, minus the delay time; the tissue transit time will be approximately twice this value. This can be used to estimate the blood volume, as the product of the perfusion and the transit time; extravascular exchange before the peak of the curve will tend to make this somewhat of an overestimate.

This approach was used to estimate the delay time, perfusion and plasma volume for a series of simulated (based on representative real data) dynamic contrast enhancement studies at a range of flow states. These values were also used as the

Table 2*Normal Flow State*

	Known Value	Estimate \pm sd	Model \pm
Delay (s)	1.6	2.85 \pm 0.66	2.06 \pm 0.64
Flow (ml/g/min)	1	0.82 \pm 0.09	1.11 \pm 0.50
Plasma vol (ml/ml)	0.07	0.12 \pm 0.04	0.09 \pm 0.05

Table 3*High Flow State*

	Known Value	Estimate \pm sd	Model \pm sd
Delay (s)	1.6	2.42 \pm 0.45	1.46 \pm 0.56
Flow (ml/g/min)	3	1.39 \pm 0.09	2.00 \pm 1.05
Plasma vol (ml/ml)	0.07	0.13 \pm 0.05	0.12 \pm 0.04

initial values for a fuller deconvolution analysis using a model-based approach.

Results: The results of 300 Monte Carlo simulations performed as described above are summarized in the Tables. The approximate perfusion values derived were close to the final values from the full analysis (within about 20%) for low and normal range flows, although the values for high flows tended to be underestimated; the blood volume values were less reliable (about 70% too high).

Conclusion: This relatively simple approach to estimating absolute perfusion and blood volume values from dynamic contrast enhancement provides useful results directly, particularly for perfusion; these can also be used as initial values for further analysis by other methods.

239. Simultaneous Determination of Myocardial Function and Assessment Of Fractional Distribution Volume by Slice-Following CSPAMM Tagging

Oliver Weber,¹ Maythem Saeed,¹ Gabriele Krombach,¹ Alastair Martin,¹ Charles Higgins.¹ ¹*Department of Radiology, University of California at San Francisco, San Francisco, CA, USA*

Introduction: The complementary use of functional (such as global and local contractility, wall motion and thickening, and ventricular rotation) and viability (such as fractional distribution volume; fDV) parameters provides valuable information regarding the treatment of coronary artery disease. Recent progress in tagging evaluation (such as HARP [1]) has re-awakened interest in myocardial tagging for accurate determination of ventricular function. Assessment of fDV, calculated from T1 values in tissue and the blood pool before and after gadolinium chelate injection, has been shown to be useful for grading the severity of myocardial injury [2].

We present an approach allowing determination of both functional and relative viability parameters from a single tagging experiment.

Purpose: To demonstrate the feasibility of simultaneous determination of myocardial function and assessment of relative fDV values using complementary spatial modulation of magnetization (CSPAMM) [3].

Methods: CSPAMM is a subtraction method, based on two images acquired with periodically modulated z-magnetization prepared in opposite directions. T1 sensitivity is usually reduced by the application of an optimized pulse angle scheme [4]. For the current application, however, constant excitation

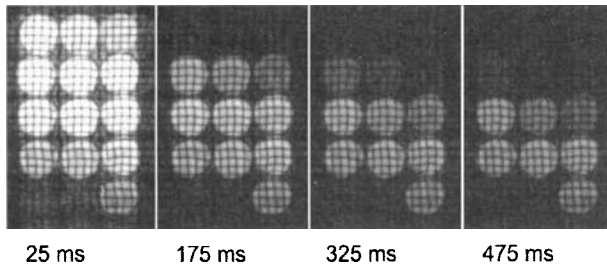


Figure 1. Images acquired at different time points after the tagging preparation pulses. The bottles contain water and different concentrations of Gd-DTPA-BMA, resulting in T1 values between 11.5 ms (top right) to 2727 ms (bottom right).

angles were deliberately used to generate a strong dependence on T1. True T1 values were calculated from the apparent T1* according to the theory deduced by Look and Locker [5]. The utilized implementation of CSPAMM included a slice following feature [4], thus ensuring that the same slice of the heart was imaged throughout the heart cycle despite the long-axis contraction.

MRI: All experiments were performed on a 1.5T Philips Gyroscan Intera I/T Cardiovascular system. Two sets of turbo-field echo planar CSPAMM images with orthogonal tag line orientations were acquired in a single measurement. Imaging parameters were as follows: TR = 14.9 ms, TE = 3.1 ms, flip angle 10°, matrix size 128, field of view 20 cm, slice thickness 8 mm, tag line distance 8 mm, TFE factor 2, EPI factor 3, temporal resolution 29.9 ms/heart phase. In a total acquisition time of 26 heartbeats, 16–25 heart phases were acquired.

Phantom experiments: In 13 plastic bottles, distilled water was doped with different concentrations of Gd-DTPA-BMA (Omniscan, Nycomed Amersham, UK), resulting in T1 values in the range 11.5–2727 ms, as determined by spectroscopic methods. Imaging was performed using a birdcage head-coil.

Animal experiments: Three adult beagle dogs were used in the current investigation. All procedures were performed in accordance with the NIH Guide for Care and Use of Laboratory Animals and with the approval of the local Committee on Animal Research. Anesthesia was initiated with 30 mg/kg sodium pentobarbital i.v. Additional injections were administered as required. The animals were intubated and artificially ventilated with room air. Heart rate and oxygen saturation were continuously monitored. A catheter placed in the left cephalic vein was used for administration of the contrast medium. After baseline measurements, Gd-DTBP-BMA was administered as a bolus followed by constant contrast agent infusion (4% of the bolus per minute) to achieve equilibrium concentrations of 0.03 mmol/kg, 0.1 mmol/kg, and 0.3 mmol/kg, which was assumed to be reached after 15 minutes. Fifteen minutes elapsed between each dose to ensure the washout of the contrast medium. Imaging was performed in short axis orientation during a single breathhold before contrast agent administration, as well as at each level of Gd-concentration, using two elliptic receiver coils.

Results: Phantom experiments: In the phantom measurements, increasing T1 values resulted in a slower signal decay (Fig. 1) with a monotonous relation. The apparent flip angle to be used in the Look-Locker correction formula [5], as determined by a least square fit of the measured T1 values to the known T1 values, was determined to be 21.0°, thus approximately twice as large as the actual flip angle.

Animal experiments: The in situ studies confirmed the faster tag fading with higher contrast agent concentration (Fig. 2). At the lowest Gd-DTPA-BMA dose, tag persistence was granted throughout systole until mid-diastole. Medium contrast agent dose restricted reliable tagging evaluation to the entire systole and early diastole, whereas at the highest dose, tag fading limited tag line assessment to early systole.

Absolute fDV values were not accessible from the tagging images alone due to inherent signal loss in the blood pool of the slice followed images. When using T1 values of blood determined in separate T1 measurements, fDV was over-

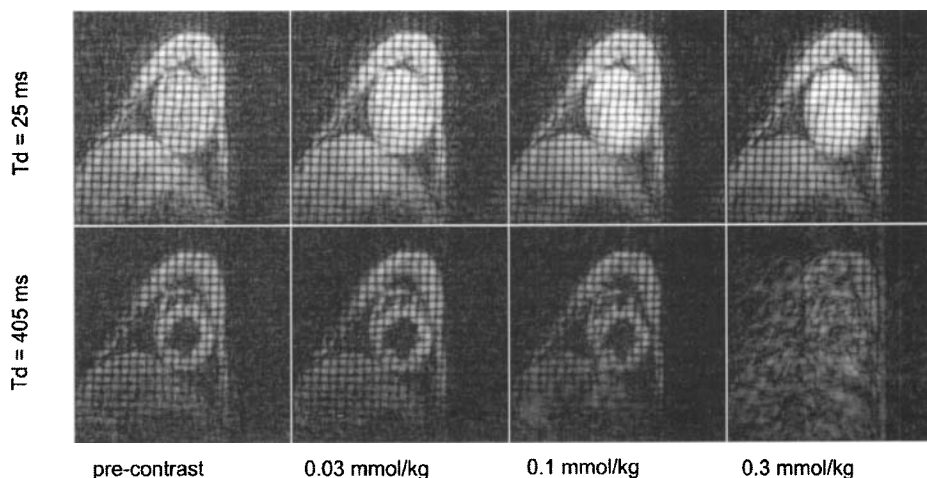


Figure 2. In vivo tagging images, acquired pre-contrast and at three different contrast agent doses. An early phase, acquired shortly after the R-wave, and a phase acquired in early diastole are shown.

estimated at the dose of 0.03 mmol/kg, but in the expected range of approximately 0.2 for the higher doses.

Conclusion: These in vitro and in vivo experiments demonstrate the feasibility of simultaneous assessment of myocardial function and determination of relative fractional distribution volumes by slice followed CSPAMM tagging. Absolute fDV values may be obtained with a separate T1 measurement of the blood. Further studies are needed to explore the mechanisms involved in CSPAMM tagging with MR contrast media.

240. Intracellular Myocardial Sodium MRI

Jan Van Emous,¹ Cees Van Echteld.² ¹Interuniversity Cardiology Institute of the Netherlands, CardioNMR Laboratory, Room G02.523, Utrecht Netherlands; ²University Medical Center Utrecht, CardioNMR Laboratory, Room G02.523, Utrecht Netherlands

Introduction: Using ²³Na MRS we¹ and others² have demonstrated that intracellular Na⁺ (Na_i⁺) starts to rise within minutes after the onset of myocardial ischemia due to inhibition of the Na⁺/K⁺ ATPase and continued influx. We have also

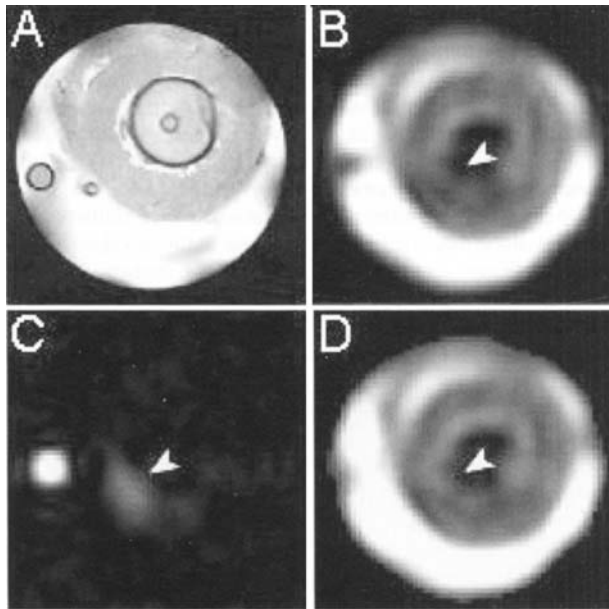


Figure 1. Fig 1 A shows a gated, short axis ¹H 2D gradient echo image (256 × 256, FOV 20 × 20 mm, nominal voxel size 15 nl, total imaging time 52 s) of an isolated rat heart. Figs. 1B–D are short axis ²³Na 2D k-space filtered chemical shift images (16 × 16, FOV 20 × 20 mm, nominal voxel size 7.8 μl, total imaging time 15 min) of an isolated shift reagent perfused rat heart during LAD ligation; B: extracellular-, C: intracellular- and D: total Na⁺. Arrows point to the region affected by LAD-ligation. The reference signal in image C is from a glass capillary containing 0.9% NaCl.

demonstrated that upon timely reperfusion [Na_i⁺] decreases due to immediate resumption of Na⁺/K⁺ ATPase activity³. These observations make [Na_i⁺] a very attractive marker for the detection of ischemia, Na⁺/K⁺ ATPase activity, and viability. At present, the radioactive tracer ²⁰¹Tl gives still one of the most clinically reliable estimates of myocardial viability. It has also been firmly established that ²⁰¹Tl is transported into viable cells through the Na⁺/K⁺ ATPase. ²³Na MRI would therefore seem to be an attractive alternative clinical method to determine myocardial viability. The potential of this approach has been demonstrated in rabbit and dog hearts, showing increased ²³Na MR image intensity in non-viable myocardium⁴. Even ²³Na MR images of human volunteers^{5,6} and patients with subacute and chronic myocardial infarction⁷ have been published. However, all these ²³Na MR images concern images of total myocardial Na⁺. Depending on the severity and duration of the ischemic insult, information on Na_i⁺ may be crucial. For example, if coronary flow to the affected tissue is completely absent an increase of Na_i⁺ will occur while no change of total Na⁺ is expected.

Purpose: In this preliminary investigation we have studied the prospects of intracellular myocardial Na⁺ imaging.

Methods: Isolated hearts of male Wistar rats were perfused with a modified Krebs-Henseleit solution at 37°C and 76 mmHg while stimulated at 300 beats min⁻¹. Cardiac contractility was monitored using a left intraventricular latex balloon. A custom made device was sutured to a number of hearts, to enable ligation of the left anterior descending coronary artery (LAD) from outside the NMR-magnet. Hearts were submerged in normothermic effluent throughout the experiments. Following instrumentation, hearts were lowered into a 9.4 T vertical bore magnet interfaced to a Bruker AVANCE 400 spectrometer equipped with a 1000 mT/m micro-imaging accessory. Gated short and long axis ¹H 2D gradient echo images (256 × 256, FOV 20 × 20 mm, slice thickness 2.5 mm, TE/TR 7/200 ms) were acquired using a 20 mm birdcage-coil tuned to 400.15 MHz, to serve as an anatomical reference. Thereafter, the ¹H coil was replaced by a 20 mm birdcage tuned to the ²³Na resonance frequency (105.85 MHz) to acquire short axis ²³Na 2D gradient echo images (32 × 32, FOV 20 × 20 mm, slice thickness 3 mm, nominal voxel size 1.2 μl, TE/TR 1.9/50 ms, total imaging time: 15'). To separate the intra- and extracellular Na⁺ resonance, 3.5 mM of the ²³Na NMR shift reagent TmDOTP5- was included in the perfusate (free [Ca²⁺] 0.85 mM). ²³Na imaging of intra- and extracellular Na⁺ was performed by 2D chemical shift imaging (CSI) using a (512 or 256) × 16 × 16 matrix size and a 5000 Hz spectral width (slice thickness 5 mm, nominal voxel size 7.8 μl, TR 60.5 or 35 ms, total imaging time: 15' or 8'). To improve S/N and to reduce Gibbs ringing k-space filtering with Hanning windows was applied. Image resolution was improved prior to presentation by zero-filling in the spatial domain and Gaussian filtering in the spectroscopic domain.

Results: In comparison to the anatomical ¹H reference images, S/N and resolution of the total Na⁺ gradient echo images is poor, although the left and right ventricular wall are clearly discernable. In the ²³Na CSI images Na_i⁺ could be visualized under basal conditions but only using k-space filtering. During 60' of ischemia Na_i⁺ image intensity steadily increased and during 60' of reperfusion Na_i⁺ image intensity increased even further, most likely the result of additional Na⁺

influx and the occurrence of contracture. In the extracellular Na^+ images a concomitant decrease in image intensity can be observed. As can be seen in Fig. 1, following ligation of the LAD, hyperintensity in the affected region is clearly visible at the unshifted intracellular resonance frequency, indicating an increase of Na_i^+ in the ischemic tissue. Note that virtually no changes in the extracellular and total Na^+ images can be seen. Hearts which underwent a 2 h period of low (4%) flow ischemia also showed a steady increase of Na_i^+ image intensity. The extracardiac resonance showed a frequency shift, most likely due to acidic wash-out. During a subsequent 60' period of reperfusion partial recovery of Na_i^+ could be observed.

Conclusion: These data demonstrate that intracellular ^{23}Na CSI imaging can be used to delineate ischemic tissue in the isolated perfused rat heart in a reasonable amount of time. Intracellular Na^+ imaging is superior to total Na^+ imaging in identifying the affected zone under zero flow circumstances. However, in order to visualize Na_i^+ under basal conditions, S/N of the ^{23}Na CSI still needs to be improved, which we currently try to achieve by k-space filtered acquisition and improved coil and sequence design.

241. Localized Imaging of the Aortic Vessel Wall

Rene M Botnar,¹ W Yong Kim,² Kraig V Kissinger,¹ Warren J Manning.¹ ¹Beth Israel Deaconess Medical Center, 330 Brookline Ave, Boston, Massachusetts, United States; ²Institute of Experimental Clinical Research, Brendstrupgaardsvej, Aarhus, Denmark

Introduction: Artherosclerosis is a systemic disease of the vessel wall and multiple vascular territories. Post mortem autopsy and transesophageal echo (TEE) studies have shown that thoracic aortic atherosclerosis is common among patients with stroke (1,2) and coronary artery disease (CAD) (3). Thus,

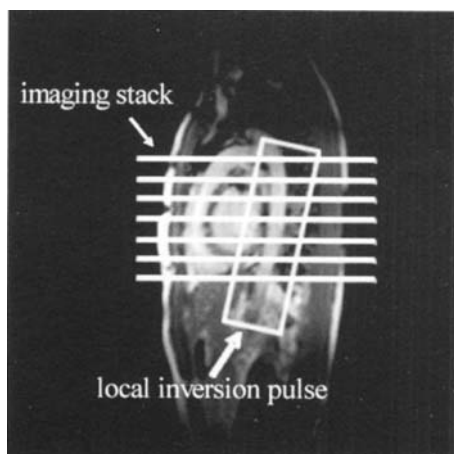


Figure 1. Sagittal slice of the thorax. A pencil beam shaped local inversion prepulse was placed along the thoracic aorta to selectively re-invert spins in the vicinity of the aortic vessel wall.

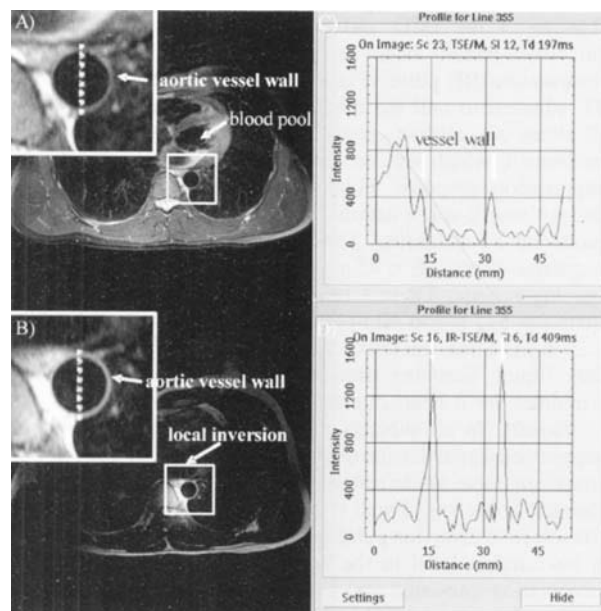


Figure 2. Transverse slices of the thoracic aorta acquired with a conventional TSE (A) and a local inversion TSE (B) technique. The magnified images (A,B) and profiles (C,D) drawn across the aorta demonstrate a better delineation of the aortic vessel wall using the local inversion prepulse (B,D).

early detection of subclinical aortic arteriosclerosis may allow for therapeutic intervention to prevent later cardiac and neurologic events. Non-invasive magnetic resonance imaging (MRI) has been shown to have great potential to assess vessel wall thickness and plaque composition and a good correlation between TEE and MRI could be demonstrated for thoracic aortic plaque imaging (4). Furthermore aortic plaque measurements using MRI showed a good reproducibility regarding plaque area and plaque burden (5). However, a potential obstacle to high-resolution aortic vessel wall imaging are artifacts from respiratory motion and non sufficiently suppressed signal from vascular blood.

Purpose: To develop a localized imaging technique that allows for selective imaging of the aortic vessel wall while suppressing signal from the chest wall and the vascular blood pools thereby reducing the artifact level in the region of interest.

Methods: A local inversion multi-slice fast spin echo (TSE) technique was implemented on a commercial Philips Gyroscan ACS-NT MR scanner equipped with PowerTrak 6000 gradients (23 mT/m/ms, 220 μs rise time), a cardiac synergy coil, and an advanced cardiac software package (INCA2). For cardiac synchronization, 4 electrodes were placed on the left hemi thorax and R-wave detection was performed using a vector ECG algorithm. To minimize signal outside of the abdominal aorta and to restore signal only in the immediate vicinity of the aortic vessel wall, a local inversion pre-pulse was implemented. First, a non-selective 180° inversion RF pulse is applied directly after the

R-wave of the ECG and immediately followed by a 2D selective pencil beam shaped (60 mm diameter) 180° re-inversion RF pulse (Figure 1). After the inversion delay TI, adjusted to null the magnetization of blood, a multislice (2 slices per cardiac cycle) T2 weighted TSE readout was performed, which was preceded by a frequency selective fat suppression prepulse. Four signal averages were acquired and a linear k-space acquisition scheme was used to achieve moderate T2 weighting. The parameters of the TSE imaging sequence were TE = 45 ms, echo train length = 14, echo spacing = 6 ms, TR = 3 heart beats, FOV = 330 mm, scan matrix = 512 × 256 (in-plane spatial resolution = 0.64 × 1.29 mm). Slice thickness was 5 mm and interslice spacing was 10 mm. Scanning time for 12 slices was approximately 6 minutes for a heart rate of 60 bpm.

Results: In all subjects the local inversion pulse reliably suppressed signal outside of the area defined by the 2D selective inversion pulse, while restoring the signal in the vicinity of the thoracic aortic vessel wall (Figure 2b). The performance of the 2D selective inversion pulse resulted in high dynamic range and a low artifact level in the area of interest (Figure 2b). This observation translated into good definition of the aortic vessel wall as shown in a profile across the aortic vessel wall (Figure 2d). On the conventional TSE images acquired without the novel prepulse, the aortic vessel wall is less well delineated (Figure 2a), which is translated into reduced intensity peaks, which represent the aortic vessel wall (Figure 2c).

Conclusion: We successfully implement and demonstrate the use of a localized inversion technique for multislice aortic vessel wall imaging. The novel technique allows for the acquisition of images with a very small apparent FOV, thereby increasing the dynamic range and reducing the artifact level in the region of interest. This improvement resulted in a better delineation of the aortic vessel wall, which may allow more accurate detection of subclinical aortic atherosclerosis.

242. Automatic Detection of Endo- and Epicardial Contours in Short-Axis Cardiac MR Data Using 3D Active Appearance Models

Boudewijn Lelieveldt,¹ Steven Mitchell,² Johan Bosch,¹ Rob Van Der Geest,¹ Milan Sonka,² Johan Reiber.¹ ¹Leiden University Medical Center, Radiology, Div. of Image Processing, Leiden, Netherlands; ²University of Iowa, dept. of Electrical and Computer Engineering, Iowa City, Iowa, USA

Introduction: To quantitatively evaluate global and regional Left Ventricular (LV) function from short-axis cardiac MR images, the contours of the LV endocardium (ENDO) and epicardium (EPI) need to be traced in the images. In clinical studies this is mainly performed manually, which is time-consuming and sensitive to inter- and intra-observer variations.

Purpose: To develop and validate a robust, automated contour detection technique for tracing the ENDO and EPI contours in short-axis cardiac MR studies.

Methods: Methods: previously, we presented a powerful contour detection technique for the endo- and epicardium in single slice short-axis cardiac MR images based on 2D Active Appearance Models (AAMs). An AAM describes the image appearance and the shape of an object from a set of examples as

a statistical model. Its application so far however, was limited to 2D images. In this work we extended the AAM method to 3D in order to robustly detect endo- and epicardial contours in multi-slice, multi phase image sets. We extended the AAM technique to 3D in two manners:

1: We developed an Active Appearance Motion Model (AAMM). In the AAMM, the heart's shape and appearance is modeled for 16 timeframes of the cardiac cycle. The AAMM can be applied to fully automated contour detection in an MR time sequence by minimizing the difference between the model and an image sequence, where the model is constrained to "statistically plausible" image sequences. This ensures a time-continuous segmentation of a complete image sequence.

2: We developed a fully 3D Active Appearance Model (3D AAM). In the 3D AAM, the 3D shape and image appearance of the LV are modeled in an intrinsically 3D manner. The 3D AAM can be applied to detect the 3D contours (surfaces) of the endo- and epicardium by fully automatically fitting the 3D model to the short-axis volume in a single phase, where the shape and image appearance of the segmentation is restricted within statistically trained limits.

We evaluated the AAMM and the 3D AAM in two validation studies:

1: To evaluate the AAMM method, cardiac MR studies were collected from 15 normal subjects and 10 myocardial infarction patients. Three mid-ventricular slices were available for the performed validation studies. LV ENDO and EPI contours were traced by an expert. Validation was performed using a leave-one-subject-out approach. Border positioning errors were calculated for all borders. Four clinically important measures were calculated: LV ENDO area, LV EPI area, LV myocardial mass, and LV ejection fraction (EF). LV myocardial mass and EF were determined volumetrically from only three adjacent slices.

2: The 3D AAM method was evaluated on cardiac MR studies from 18 patients and 38 normal subjects. LV ENDO and EPI contours were expert traced in ED for the complete LV. Validation and training was performed using a leave-one-subject-out approach. The 3D AAM allows the evaluation of volume measures for the entire LV, therefore endocardial volume and LV wall mass were computed for the whole LV and compared to the manually defined independent standard.

Results: 2D + time AAMM: The results of the AAMM validation study show a high robustness of the fully automated AAMM approach. In two, highly pathological cases of severe post-infarct LV dilation, the automated detection failed. In all 15 normal and in 8 out of 10 patient cases, the automatically detected contours demonstrated clinically acceptable accuracy, both in border positioning errors and in EF, LV mass and slice-based ENDO and EPI area measures. Mean signed ENDO and EPI border positioning errors were 0.12 ± 0.91 mm and 0.46 ± 0.97 mm, respectively, showing minimal border detection bias. Mean unsigned positioning errors were 0.63 ± 0.65 mm and 0.77 ± 0.74 mm, respectively, showing small absolute differences from the independent standard. Mean signed and unsigned ED LV mass errors were -0.5 ± 4.5 g and 3.6 ± 2.6 g. Mean signed and unsigned EF errors were small: $-1.2 \pm 8.2\%$ and $6.8 \pm 4.5\%$, respectively. **3D AAM:** Figure 1 (on next page) shows an example of 3D AAM detected LV ENDO and EPI contours. The 3D AAM method showed acceptable contours in 53 out of 56 cases. In

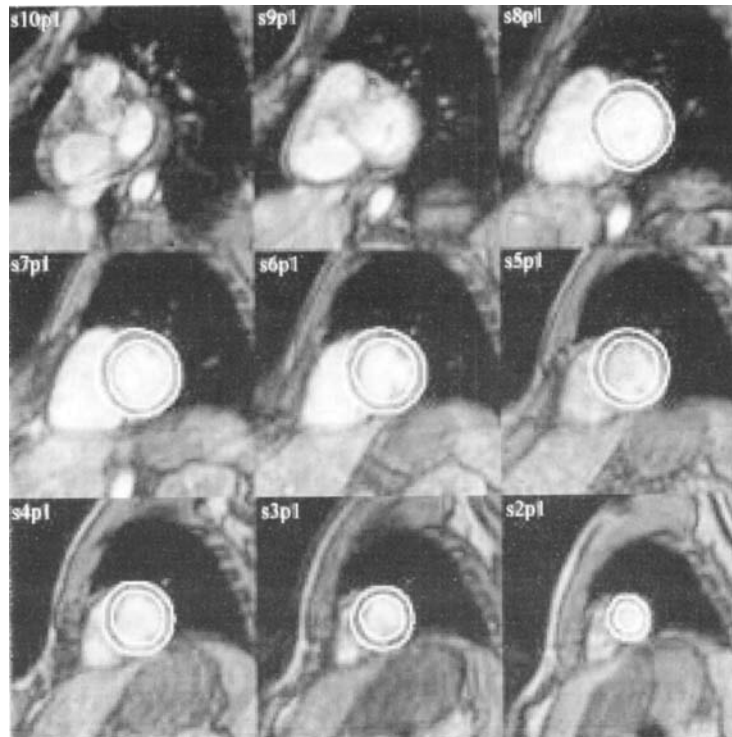


Figure 1.

three cases, the matching did not converge to an acceptable solution, and these cases were excluded from further quantitative analysis. Global functional parameters such as endocardial volume and myocardial mass correlated well: $Y = 0.86X + 11.3$ ($r = 0.97$) for automated (Y) versus manual LV ENDO volume (X) and $Q = 0.76 V + 22.2$ ($r = 0.88$) for automated (Q) versus manual (V) LV wall mass. The contours of the apex were slightly less accurately detected than the mid-ventricular contours, most likely due to the fact that the apex only asserts a small influence in the minimization criterion.

Both the 3D AAM and the 2D + time AAMM showed a robust behavior in routinely acquired clinical image data. For the AAMM, in all 15 normal and in 8 out of 10 patient cases, the fully automatically detected contours demonstrated clinically acceptable accuracy, both in border positioning errors and in EF, LV mass and slice-based ENDO and EPI area measures.

The 3D AAM detected correct contours in 53 out of 56 image sets, where the 3D AAM LV volume and myocardial wall mass correlated well. Both the 3D AAM and the AAMM produced contours that excluded papillary muscles and epicardial fat. However, the 3D AAM border positioning errors in the apical region were in some cases clinically unacceptable. Further development to improve 3D AAM border localization in the apex is ongoing. Moreover, integration of both approaches into a truly 4D AAM (3D + time) is a topic of current research.

Conclusion: Both AAMM's and 3D AAM's have demonstrated to be robust contour detection methods for ENDO- and

EPI contours, and show great potential to reduce analysis time for routine cardiac MR examinations.

243. Interventional MRI: Inversion-Recovery Prepared Flash for Real-Time Catheter Tracking and MR Angiography

Jordin Green,¹ Reed Omary,¹ Yiu-Cho Chung,² Syam Vasireddy,¹ Richard Tang,¹ Yongzhong Li,¹ Paul Finn,¹ Debiao Li.¹ ¹Northwestern University, 448 E. Ontario St., Chicago, Illinois, United States; ²Siemens Medical Solutions, 448 E. Ontario St., Chicago, Illinois, United States

Introduction: In the past several years there has been a new focus on interventional MRI. Interventional MRI does not require exposure to ionizing radiation or to a toxic contrast agent. It could also be used to provide accurate soft tissue information in a patient who has already been catheterized.

Catheter visualization is of key importance in any interventional setting. Various methods have been developed in order to detect a catheter *in vivo*. Recently, Omary et al. introduced a passive monitoring approach for catheter visualization using a gadolinium (Gd)-filled sheath (1). Since the T1 of the solution inside the catheter is greatly reduced by the presence of Gd, the catheter can be detected in a T1 weighted sequence. The use of a 2D projection imaging technique allows for tracking of the catheter with a high

temporal resolution while keeping all relevant anatomy in-plane. However, when using a thick-slice projection, it becomes very important to obtain a high level of background suppression to ensure there is adequate contrast between vessel and background.

Purpose: The purpose of this study is to demonstrate the feasibility of using inversion-recovery (IR)-prepared FLASH (fast low-angle shot) for catheter tracking and MR angiography (MRA) and to compare it to a conventional technique in vivo in a porcine model.

Methods: Animal preparation was as follows: Pigs ($n = 3$) had an 8 F catheter introduced into the aorta via the femoral artery using an X-Ray angiography suite. The catheter was placed at a location upstream from the renal arteries. The subject was then placed in the MR scanner and the catheter was filled with 4% diluted Gd using an automatic injector. Images of the catheter were taken using the IR-prepared sequence and a conventional spoiled gradient echo sequence. Renal angiography was performed with each sequence by separate injections of 15 mL of 4% diluted Gd over 3 s using an automatic injection system.

The imaging protocol for the IR-prepared sequence was as follows: A 180° IR pulse was played out, followed by a delay time (TI), followed by a standard spoiled gradient-echo acquisition scheme. Three acquisitions were used to form an image. Imaging parameters were TR/TE/flip angle = 2.4 ms/1.2 ms/ 25° , FOV = 215 mm \times 300 mm, matrix = 123 \times 256, 41 lines/segment, TI = 50 ms. Each image was taken with slice thickness = 50 mm and slice thickness = 100 mm. Temporal resolution was 2 frames/s.

The conventional sequence was a single-shot, high flip angle spoiled gradient echo sequence. TR/TE/flip angle = 5.3 ms/2.6 ms/ 90° . Other parameters were the same as the IR-prepared sequence. Temporal resolution was 1.3 frames/s. A longer TR and lower temporal resolution was required in order



Figure 1. Catheter image taken using IR-FLASH. The catheter is located in the descending aorta of a pig. All surrounding tissue is suppressed, with the exception of the bowel (broken arrow), which is bright due to short T1 components in the pig's diet. 2. Identical subject using conventional FLASH. Poor suppression obscures large sections of the catheter at several locations (solid arrows). 3. Renal artery image taken using IR-FLASH sequence after injection of 4% Gd from a catheter located slightly upstream from the renal arteries in the descending aorta. The catheter is visible at the edge of the field of view (solid arrow). The same imaging protocol was used for catheter tracking and renal MRA.

to meet the Specific Absorption Ratio requirements built-in to the scanner.

The ratio of catheter-to-background signal ratio was used to evaluate catheter visualization.

Results: In all images acquired with IR-FLASH, background signal was well suppressed and the catheter was well depicted without the use of post-processing. A sample image of the catheter taken using IR-FLASH is given in Figure 1. The catheter:background signal ratio was measured to be 2.7 ± 0.2 . For comparison, Figure 2 is an image of the same subject using conventional FLASH. The catheter:background signal ratio was 1.4 ± 0.3 . The increase in this ratio using the prepared sequence is statistically significant ($p < .001$).

For the renal angiogram, the aorta and proximal renal arteries are all clearly visible. An image taken during the injection is given as Figure 3. More distal portions of the renals were not visible since the catheter was located in the aorta during injection. Mean vessel signal:background signal for the renal angiogram was found to be 2.02.

Conclusion: We have demonstrated that it is feasible to view a catheter and perform an angiogram with high temporal resolution (2 frames/s) using an IR-prepared FLASH technique for background suppression. The angiogram was performed using only 6 mL of Gd, allowing for multiple contrast injections during a single session. Additionally, the prepared sequence can be used for both catheter tracking and angiograms. This technique could be useful in future attempts to develop cardiac interventions using MRI.

References

1. Omary RA et. al. *JVIR* 2000; 11: 1079–1085.

244. Delayed Contrast-Enhanced MRI Using a 3D Inversion-Recovery (IR) Sequence Allows Rapid Evaluation of Myocardial Viability Within One Breath-Hold

Harald P. Kühl,¹ Theano Papavasiliu,¹ Aernout M. Beek,¹ Marc B.M. Hofman,¹ Albert C. Van Rossum,¹ ¹VU University Medical Center, De Boelelaan 1117, Amsterdam, The Netherlands

Introduction: Delayed contrast-enhanced magnetic resonance imaging has been shown to allow assessment of myocardial

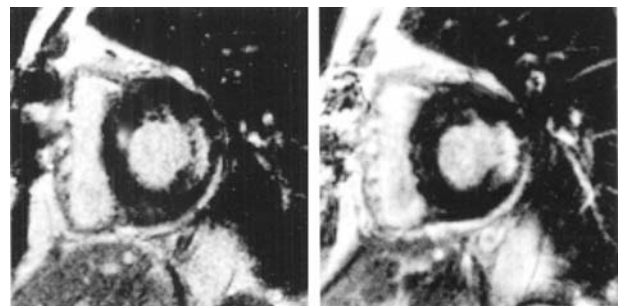


Figure 1.

viability in patient with ischemic heart disease. The current approach requires multiple breath-holds to generate a set of images covering the left ventricle which is time-consuming and may introduce misregistration of slices. We evaluated a novel approach using a 3D sequence which allows complete data acquisition within one single breath-hold.

Purpose: To assess the value of a novel 3D IR sequence (data acquisition in one single breath-hold) in comparison to a standard 2D IR sequence (data acquisition in multiple breath-holds) for the detection and assessment of the transmural extent of hyperenhancement in patients with chronic coronary artery disease.

Methods: 10 patients (62 ± 12 years, 3 females) underwent contrast-enhanced MRI on a 1.5T MR scanner (Sonata, Siemens, Erlangen, Germany) for viability assessment 15 minutes after 0.2 mmol/kg Gadolinium-DTPA. For the standard approach we used a 2D segmented IR gradient-echo sequence (25 segments, TR/TE 9.6/4.4, FA 25°, TI 250–300 ms, matrix 208×256 , resolution $1.5-1.7 \times 1.3 \times 5$ mm) with data acquisition every other heartbeat. For the 3D approach we used a segmented IR gradient-echo sequence (77 segments, TR/TE 2.8/1.1, FA 25°, TI 200–230 ms, matrix $256 \times 208 \times 12$, resolution 1.4×1.4 mm, slice thickness 8.3 mm reconstructed to 5 mm) with data acquisition every heart beat. Double oblique short-axis views covering the left ventricle from base to apex were acquired with identical orientation and position using both sequences. In corresponding images we assessed total myocardial area and contrast-enhanced area for both techniques and calculated the signal to noise ratio (SNR) for enhanced myocardium as well as contrast to noise ratios (CNR) for enhanced vs. non-enhanced myocardium and blood. Observer agreement for the presence and the transmural extent (transmural vs. non-transmural) of hyperenhancement was evaluated in a total of 670 single segments in a randomized, blinded fashion.

Results: Imaging was successful in all patients. Myocardial areas and contrast-enhanced areas were not different between the 2D and 3D sequence (14.6 ± 5.4 cm² vs. 14.6 ± 5.4 cm² and 2.6 ± 1.7 cm² vs. 2.7 ± 1.8 cm²; $p = \text{ns}$). SNR and CNR were 300 to 450% larger for the 3D sequence compared to the 2D sequence. Agreement between two observers was 96% for the presence of hyperenhancement (Kappa = 0.92) and 90% for the transmural extent of hyperenhancement (Kappa = 0.83). However, the 3D images were more blurred allowing less detection of structural details. The figure shows corresponding short-axis views acquired with the 2D (left) and the 3D (right) IR-sequence. The information regarding the location and transmural extent of the hyperenhancement area is comparable in the two images. However less structural details can be appreciated in the image acquired with the 3D sequence (right).

Conclusion: Detection of myocardial hyperenhancement using a segmented 3D IR sequence is feasible in one single breath-hold and accurate compared to the standard 2D sequence. The improved SNR and CNR facilitate recognition of the hyperenhancement area and balance for blurred image quality. This fast sequence should be used for rapid screening for the presence of myocardial hyperenhancement. Acquisition of selected images using the 2D sequence can be added for accurate quantification of the transmural extent of hyperenhancement.

245. Evaluation of Reproducibility of Breath-Hold and Navigator Gated MR Techniques for Intracoronary Volume Flow Quantification

Willemijn Bedaux,¹ Mark Hofman,² Cees Visser,² Albert Van Rossum,³ ¹VU University Medical Center, De Boelelaan 1117, Amsterdam, Netherlands; ²VU Medical Center, P.O. Box 7057, Amsterdam, Netherlands; ³University Hospital Vrije Universiteit, Amsterdam, The Netherlands

Introduction: Magnetic Resonance (MR) techniques are available to measure coronary artery blood flow noninvasively. Comparison to invasive Doppler ultrasound measurements showed significant variability [1], questioning the reproducibility of the MR and ultrasound technique.

Purpose: The aim of this study was to assess the reproducibility of both the breath-hold and navigator based respiratory gated MR techniques.

Methods: MR imaging was performed in 12 healthy volunteers at a 1.5 Tesla whole body MR system (Vision, Siemens, Germany). A single breath-hold flow velocity mapping technique [2] and navigator based retrospective respiratory gated technique [3] (imaging parameters between brackets) were applied with an imaging plane perpendicular to the proximal left anterior descending artery. Imaging parameters included an acquisition window in the cardiac cycle of 105 (62) ms, a flip angle of 300, spatial resolution $1.0 \times 1.0 \times 6$ ($1.0 \times 1.4 \times 6$) mm³, an echo time of 5 (5.8) ms and a scan duration of 26 heart beats (7 minutes). A fat saturation pre-pulse was applied for each cardiac phase resulting in a temporal resolution of 125 (82) ms, the encoding velocity was set to 40 cm/s. For the gated acquisition 4–8 fold oversampling was applied depending on the size of the heart and respiratory rhythm of the subject. The breath-hold sequence was performed at inspiration as well as at expiration. The whole scan protocol was repeated in a second session after the subject was repositioned in the scanner. Heart rate and systemic arterial pressure were monitored and recorded during the whole imaging procedure. Mean values were compared using the paired t-test, and standard deviations were compared using the F-test.

Results: The mean volume flow in breath-holding at inspiration, at expiration and during regular breathing, were respectively 35 ± 11 ml/min, 29 ± 14 ml/min and 40 ± 17 ml/min, difference not significant. The reproducibility of these techniques were 9.0, 8.4 and 9.0 ml/min as expressed in the standard deviation (SD), which is not significantly different. Comparing the volume flow measurements and hemodynamic variables during the first and second session after repositioning the volunteer, no significant differences were found. Flow measurements in breath-holding at inspiration were also repeated within a single session showing a significant better reproducibility (SD 5 ml/min), which is in the same order of magnitude as the intra- and inter-observer variability (SD 6.6 and 4.8 ml/min, respectively).

Conclusion: This study shows no significant difference in reproducibility between the navigator and single breath-hold technique in the intracoronary volume flow quantification although the navigator technique allows a somewhat higher temporal and spatial resolution. Single breath-hold flow velocity mapping is a good alternative in the assessment of noninvasive coronary volume flow and flow reserve and its short acquisition

duration is of great advantage in stress measurements. Using these data an estimation of the reproducibility for a flow reserve measurement (the ratio of two measurements in one session) can be calculated in the order of 20%.

246. Free-Breathing Gadolinium-Enhanced MR Imaging of Myocardial Dysfunction

James W Goldfarb,¹ Meir Shinnar,¹ ¹University of Medicine and Dentistry of New Jersey; Robert Wood Johnson Hospital, Department of Medicine, New Brunswick, NJ, USA

Introduction: Recent studies have shown that reversible myocardial dysfunction can be identified using gadolinium-enhanced MR imaging. Images of the myocardium are made minutes after contrast agent administration and non-viable tissue is identified as hyperenhancing regions. Images have been acquired during suspended respiration to reduce or eliminate artifacts from motion of the heart during the normal respiratory cycle. Free-breathing acquisitions have been recently used to image the coronary arteries. The position of the diaphragm is monitored throughout the imaging acquisition and is used to gate and correct k-space data. Though coronary artery and myocardial viability pulse sequences differ significantly, the same "navigator" imaging strategy can be used.

Motivation: Since many patients may not tolerate short or repeated breath-holds, the use of a free-breathing acquisition may reduce artifacts due to poor breath-holding. In breath-hold acquisitions, time is wasted during breath-hold instructions, hyperventilation and resting. Navigator images may be consecutively acquired reducing total scan time and patient cooperation. Lastly, the removal of breath-hold duration constraints will allow the option of acquiring higher resolution 2D images or 3D image acquisitions which have the advantage of thinner contiguous slices and processing with multi-planar

reformation, maximum intensity projection and 3D rendering software.

Purpose: To develop and test two- and three- dimensional free-breathing methods for imaging of gadolinium-enhanced myocardial dysfunction.

Methods: 15 patients with known coronary artery disease participated in this study. Each patient was placed supine in a 1.5T clinical scanner (Philips Integra, Best, Netherlands). A gadolinium-based contrast agent was administered intravenously at a dose of 0.2 mmol per kilogram of body weight. Imaging commenced 10 minutes after contrast agent administration.

A segmented inversion recovery gradient-echo sequence was used TR/TE = 7.5/3.8 msec; FA = 15; k-space data was acquired in diastole. Breath-hold images were acquired at end-expiration; The duration of the inversion time (TI) was chosen to null the signal intensity of normal myocardium after contrast agent administration.

A vertical 2D selective real-time navigator for gating and motion tracking was applied at the dome of the right hemidiaphragm. The gating window was 10 mm and a correction factor of 0.6 was used to relate the position of the diaphragm to the position of the heart.

Images were consecutively collected using 2D breath-hold, 2D free-breathing and 3D free-breathing acquisitions.

Results: Magnetic resonance studies were completed in all participants without complications. An excellent agreement between breath-hold and free-breathing acquisitions was found.

Conclusion: Imaging of dysfunctional myocardium can be performed without breath-holding. The use of "navigator" techniques makes three-dimensional imaging of myocardial dysfunction possible in a reasonable period of time. Imaging during free-breathing is advantageous due to the reduced amount of patient cooperation required in this patient population.

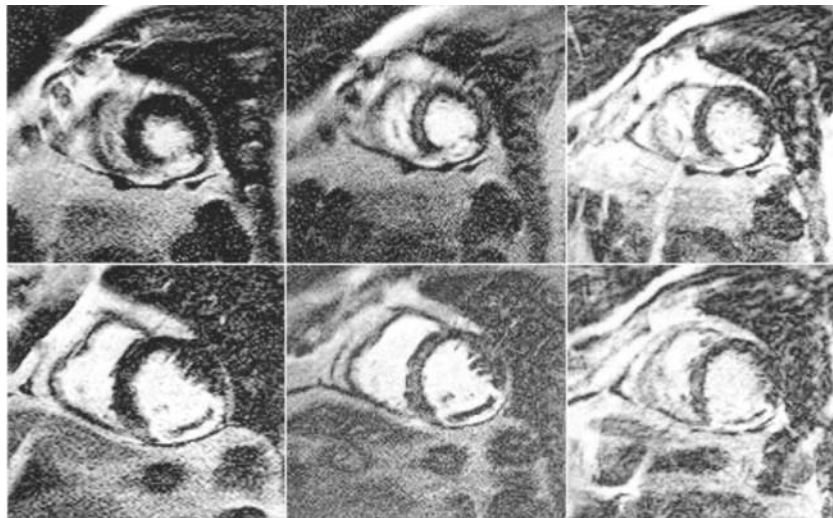


Figure 1. Example from one patient from two different short axis slices. Column 1: Breath-hold, Column 2: 2D free-breathing; Column 3: 3D free-breathing

247. Cardiac MR Clinical Basics: Full Functional Exam in “Five Plus One” Minutes

Mp Watkins,¹ Ta Williams,¹ Sa Wickline,¹ Sd Caruthers.²
¹Cardiovascular MR Laboratories at Washington University in St. Louis, Campus Box 8063 660 South Euclid Ave., St. Louis, MO, USA; ²Philips Medical Systems, Veenpluis 4-6, Best, Netherlands

Introduction: Cardiovascular MR imaging has become a recognized diagnostic technique for evaluating cardiovascular function. Previously, cardiac MR has been used for imaging of congenital diseases, tumors, and in patients unable to be imaged diagnostically with other modalities. Until recently the speed of technique and reconstruction have limited MR use. With the development of faster image acquisition and reconstruction schemes, cardiac MR can now be utilized as a non-invasive and robust screening modality of cardiovascular function in only one minute of planning plus five minutes of scanning. The “Five plus One” exam will enable additional scan time for further cardiovascular MR Imaging while minimizing the duration of the study.

Purpose: To develop a non-invasive rapid and robust diagnostic screening tool for cardiovascular function with magnetic resonance imaging.

Methods: To obtain a rapid diagnostic cardiac MR study for cardiovascular function several steps must be completed. We have developed this cardiovascular MR study by imaging 9 volunteers, both male and female, with a five-element cardiac

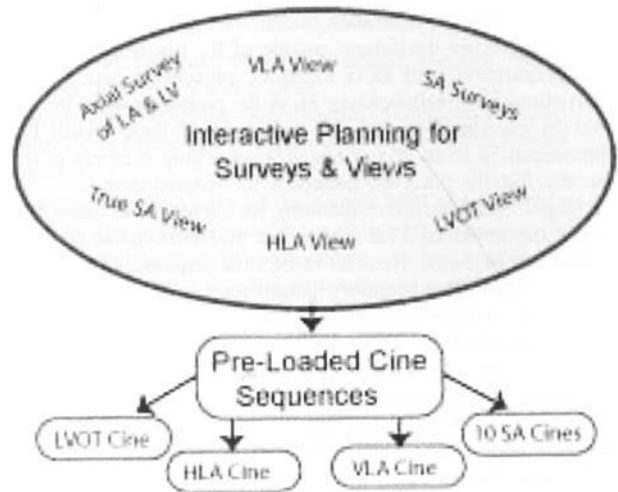


Figure 1. Five Plus One Approach.

synergy coil, on a clinical 1.5T scanner (Philips NT Intera Release 8, Best, The Netherlands), with a systematic approach shown in Figure 1. The sequences used were based on a steady-state gradient echo (bFFE) technique. For image localization, realtime interactive bFFE was used. Basic functional cine sequences were acquired as breath hold bFFE.

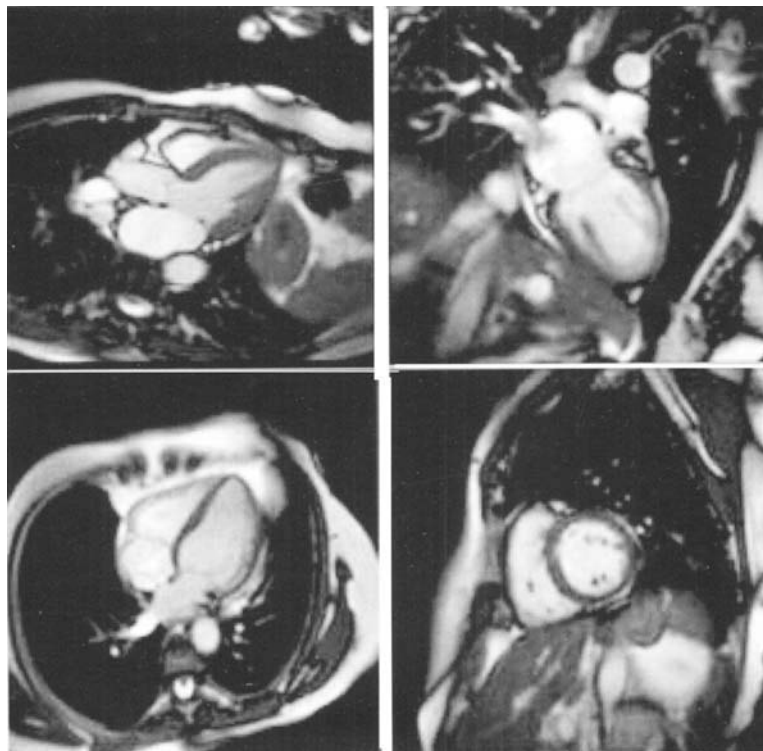


Figure 2. Functional Cine Images- LVOT,VLA,HLA,SA.

Step 1: Patient preparation outside of the magnet. The first step is to prepare the patient outside of the magnet, including skin preparation, and ECG electrode placement, and verbal instructions for breath holding. Have the patient practice breath hold by breathing in and out then holding their breath for approximately 15 to 20 seconds. This coaching is essential for success. Finally, place the patient in the magnet bore.

Step 2: Use interactive planning for surveys and views. To begin, the balanced FFE interactive sequence must be pre-loaded and prepared. Next all bFFE cine sequences should be pre-loaded and the geometry parameter set to reference the appropriate cine views of (HLA, LVOT, VLA, and SA) to be defined interactively. The interactive sequence is started and multiple images for surveying the cine views are acquired in two breath holds approximately 15 to 20 seconds each. The first view acquired is an axial survey to demonstrate the left ventricle and atrium. Then a VLA view is position from the axial, then a SA survey is positioned from the VLA during one breath hold. Next from the SA survey a LVOT and a HLA view are positioned, then a true SA view angled from the HLA within one breath hold. During each breath hold, images for each of the specified views are obtained and their geometries are stored in the respective geometry parameter. Then the sequence is stopped.

Step 3: Pre-loaded cine sequences are begun to complete the study. The next step, cine sequences are started and a series of breath holds begin. Single slice cine images with at least 20 heart phases are obtained of the horizontal long axis (HLA), left ventricular outflow tract (LVOT), and vertical long axis (VLA). Multiple slice cine images (10) with at least 15 heart phases are obtained in the short axis (SA) of both ventricles. The average breath holds, dependent on heart rate, were between 10–15 seconds.

Results: The studies were well tolerated by all 9 volunteers with an average age of 44 years. The final three studies gave the best overall functional images which are comparable to conventional cardiac studies. The most significant decrease in time came from the interactive planning portion trimmed from the first volunteer to the last volunteer by 1 minute 30 seconds.

Conclusion: The use of a systematic study protocol decreases patient time in the scanner making a rapid screening of cardiovascular function possible. With the present technology of balanced fast field echo (bFFE), an interactive tool for surveys, and realtime reconstruction, a full functional study can be completed in six minutes total. Assuming a fixed examination length, this five plus one functional study will allow additional scan time for coronary imaging, flow studies of valves, stress testing, or other types of cardiovascular MR imaging.

248. Saving Time with Sensitivity Encoding in Cardiac Function Assessment

Sebastian Flacke,¹ Christoph Axmann,¹ Mathias Hackenbroch,¹ Ulrich Hofer,¹ Hans H Schild,¹ Torsten Sommer.¹ ¹University of Bonn, Sigmund Freud Strasse 25, Bonn, NRW, Germany

Introduction: The accuracy of the MRI determination of left ventricular mass and ejection fraction is highly dependent on

the contrast between blood and myocardium. With the Introduction: of coherent steady state gradient echo sequences (TrueFISP, Fiesta or balanced-FFE) excellent image contrast is provided even in patients with reduced left ventricular function as contrast is independent of flow and signal of myocardium and blood is proportional to T1/T2 for short repetition times [1]. If such contrast schemes are combined with parallel data acquisition, such as sensitivity encoding, where the sensitivity of surface coils is used to reduce the number of phase encoding steps, a further reduction of imaging time can be achieved. However, this increase in imaging speed is combined with a reduced signal-to-noise ratio [2].

Purpose: To investigate whether the scan duration of b-FFE sequences in the assessment of cardiac function can be reduced using SENSitivity Encoding (SENSE) without loss of diagnostic information.

Methods: Ten healthy volunteers and ten patients with ischemic cardiomyopathy were imaged at 1.5T (Intera Release 8, Philips Medical Systems, Best, The Netherlands) using a five element phased array surface coil. Standard breathhold b-FFE acquisitions were compared to parallel data acquisitions using sensitivity encoding (SENSE). Parallel imaging was used to reduce the number of breathholds keeping all other sequence parameters identical for both sequences. In healthy volunteers and patients a 12 breathhold b-FFE sequence (TR/TE/FA 3.5 ms/1.75 ms/60°, matrix 192 × 256, FOV 380mm, breathhold duration 12s) was compared to its 6 breathhold b-FFE-SENSE counterpart (breathhold duration 13s). Slice thickness was varied between 8 and 10mm to assure complete heart coverage. 18 heart phases were acquired yielding a temporal resolution of less than 50ms for all acquisitions. Data were analyzed by manually tracing the endo- and epicardial borders. End-systolic and enddiastolic volumes, ejection fraction and myocardial mass were calculated based on the Simpson rule using the software MASS (Medis, Leiden, The Netherlands). Image quality was assessed using contrast-to-noise (CNR) and signal-to-noise (SNR) measurements. Signal intensity was measured in the myocardial septum to avoid contribution from epicardial fat and in the mid ventricular cavity for the blood signal. Signal-to-noise was expressed as signal intensity of a region of interest divided by the standard deviation of the measured signal and contrast-to-noise was calculated as the signal difference divided by the average of the standard deviations of both signals. SNR, CNR and calculated ventricular mass and volume were compared between techniques using a paired sampled student's t-test.

Results: Image quality was sufficiently good for all acquisitions to allow tracing of endo- and epicardial borders despite a signal drop of the parallel acquisition technique for blood (29.7%) and myocardium (23.2%). We observed a greater signal drop and an increased standard deviation of the measured signal in the left ventricular blood pool than in the myocardium. This resulted in a drop of CNR of 37% ($p < .001$) for the parallel data acquisition scheme compared to the standard acquisition. In 7 of 20 examinations we observed small reconstruction artifacts in the b-FFE-SENSE images as a result of incomplete unfolding of the images (Figure 1a and 1b).

However, these image artifacts did not affect the tracing of cardiac borders. There was excellent agreement between



Figure 1.

standard b-FFE and b-FFE-SENSE for the calculation of endsystolic volume ($p = .17$), enddiastolic volume ($p = .81$), ejection fraction ($p = .44$) and left ventricular mass ($p = .28$).

Conclusion: The intrinsic high contrast-to-noise of the b-FFE images is sufficient to allow precise delineation of endo- and epicardial borders after parallel data acquisition, despite the decreased SNR and CNR. Sensitivity encoding can reduce scan duration without loss of diagnostic information and thus the total number of breathholds. If fewer breathholds are needed patient compliance may be increased even in comprehensive cardiac studies where more than fifty breathholds are often required.

249. Black Blood Myocardial Tagging in Mice

Frederick H. Epstein,¹ Wesley D. Gilson,¹ Zequan Yang,¹ Brent A. French,¹ Stuart S. Berr.¹

¹University of Virginia, Departments of Radiology and Biomedical Engineering, Charlottesville, Virginia, United States

Introduction: Over the past three years MRI has emerged as an accurate non-invasive imaging modality for measuring cardiac structure and function in vivo in transgenic and knockout mice. We and others have recently demonstrated myocardial tagging in mice (1, 2). In our work in particular, tagging is used to measure regional intramyocardial function in the setting of ischemia/reperfusion. At baseline and especially after myocardial infarction (MI), where ejection fraction (EF) is reduced, detection of the endocardial border can be difficult due to poor contrast between myocardium and the blood pool on these gradient-echo based images.

Purpose: The purpose of this study was to improve myocardium-blood contrast in tagged images acquired from normal and infarcted mice. We hypothesized that the double inversion recovery technique (3,4), which is commonly used to null the blood signal at a single cardiac phase in human imaging, could be used to null the blood signal during all of systole in mice because the total systolic time in mice is typically less than 90 ms.

Methods: MR imaging was performed on a 4.7T scanner (Varian, Inc., Palo Alto, CA) using a custom-made birdcage radio frequency coil (RF Design Consulting, Newberry, FL). C57BL/6 mice were imaged before and 1–2 days after MI. Our standard tagging sequence used a 6-lobe SPAMM radio frequency (RF) pulse applied immediately after the ECG trigger and a multi-slice FLASH acquisition. The FLASH acquisition used TR = 2 heart beats, TE = 5.5 ms, field of view = 25.6 × 25.6 mm², matrix size = 192 (readout) × 96 (phase encode), slice thickness = 1 mm (no inter-slice gap),

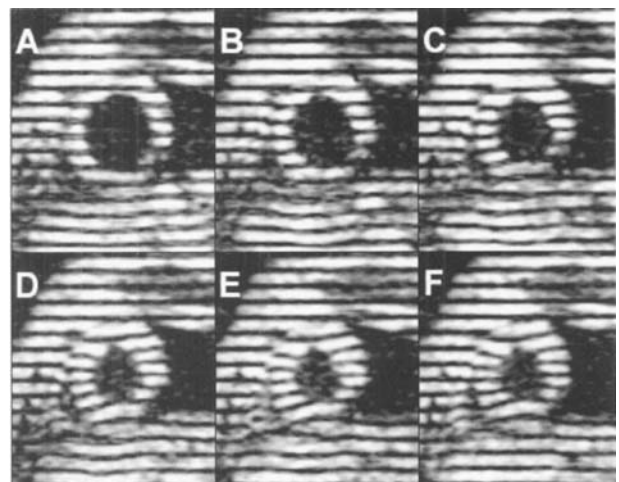


Figure 1. Black-blood myocardial tagging in a normal mouse. Six cardiac phases, from end-diastole (A) to end-systole (F), are shown for a single short-axis slice.

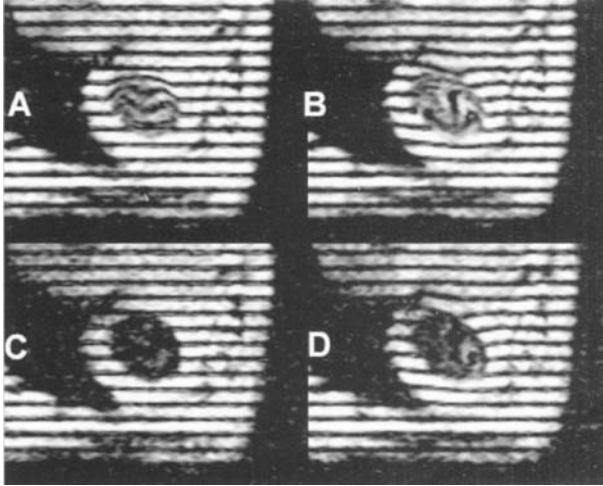


Figure 2. Conventional (A, B) and black-blood (C, D) myocardial tagging in a post-infarct mouse. End-diastolic images are shown in (A) and (C), and end-systolic images are shown in (B) and (D).

and flip angle = 30° . Additionally, the tag pulse flip angle was 180° and the tag separation was 0.7 mm. Also, as respiratory gating was not employed, 6 signal averages were used to reduce respiratory motion artifact and increase the signal-to-noise ratio. Six slices were acquired per scan, and slice positions were shifted in 6 different scans, resulting in the acquisition of 6 different cardiac phases throughout systole for all 6 slice locations.

In our modified sequence, a double inversion recovery module was applied every second heart beat immediately following the ECG trigger. In this configuration, SPAMM RF pulses were applied on odd heart beats and double inversion recovery pulses were applied on even heart beats. The double inversion recovery module used a non-selective square 180° pulse with duration = 250 microseconds followed by a slice selective sinc 180° pulse with duration = 2.5 ms. The slice selective 180° pulse was centered at the middle of the imaging volume and had a thickness of 9 mm. A gradient spoiler pulse was applied in the slice select direction following the 180° pulses.

Results: Example short-axis black-blood images from a normal mouse are shown in Fig. 1. In this example, multiple cardiac phases from end-diastole to end-systole are shown for a single slice location. Excellent blood signal suppression is seen in all phases. Example images after MI are shown in Fig. 2. In this case, end-diastolic and end-systolic conventional images are shown in (A) and (B), respectively, and end-diastolic and end-systolic blood-suppressed images are shown in (C) and (D), respectively. Fig. 2 demonstrates good blood suppression throughout systole even with low EF secondary to MI. For all post-MI mice, use of the double inversion recovery pulses resulted in a 50% suppression of the LV blood signal compared to conventional scanning, and the amount of suppression was independent of cardiac phase for 6 phases covering systole (typically 90 ms).

Conclusion: The double inversion recovery technique can be used to suppress the blood signal throughout systole in FLASH images acquired from normal and infarcted mice. Our initial experience using this technique suggests that it will improve the accuracy of detecting the endocardial border in myocardial tagging studies undertaken in mice.

250. The Importance of K-Space Trajectory in Echo-Planar Myocardial Tagging

Daniel Kim,¹ Michael Salerno,¹ Frederick Epstein,¹ ¹University of Virginia, Departments of Radiology and Biomedical Engineering, Charlottesville, Virginia, United States

Introduction: Myocardial tagging is an established method for imaging regional intramyocardial function, and may be useful for dobutamine MRI stress testing. To decrease breathhold duration or achieve real-time imaging with tagging, hybrid fast gradient-echo/echo-planar imaging (FGRE-EPI) can be used [1,2]. Within this setting, the specific k-space trajectory employed by the EPI readout can substantially modulate image artifacts. In the heart, primary sources of artifact include blood flow and magnetic field inhomogeneity (off-resonance effects). In general, trajectories that are insensitive to flow are sensitive to off-resonance effects, and vice versa.

Purpose: The aim of this study was to use computer simulations to compare different EPI and spiral trajectories for tagged cardiac imaging.

Methods: We assessed the properties of different echo-planar and spiral trajectories by utilizing the k-space formalism [3], which elegantly describes flow artifacts and off-resonance effects as functions of time-varying gradients. This formalism is described by the inverse MRI signal equation as,

$$s(x, y, u, v, f) = \iiint \iiint S(k_x, k_y) e^{i2\pi(k_x x + k_y y + k_u u + k_v v + k_f f)} dk_x dk_y dk_u dk_v dk_f \quad (1)$$

where the spatial parameters are x = readout direction and y = phase-encode (PE) direction, the velocity parameters are u = velocity in the readout direction and v = velocity in the PE direction, and f = off-resonance frequency. The k-space parameters are,

$$k_x = \gamma \int G_x(\tau) d\tau \quad (2)$$

$$k_y = \gamma \int G_y(\tau) d\tau \quad (3)$$

$$k_u = \gamma \int \tau G_x(\tau) d\tau \quad (4)$$

$$k_v = \gamma \int \tau G_y(\tau) d\tau \quad (5)$$

$$k_f = t \quad (6)$$

where the components of velocity k-space, k_u and k_v , depict flow properties in the readout and PE directions, respectively,

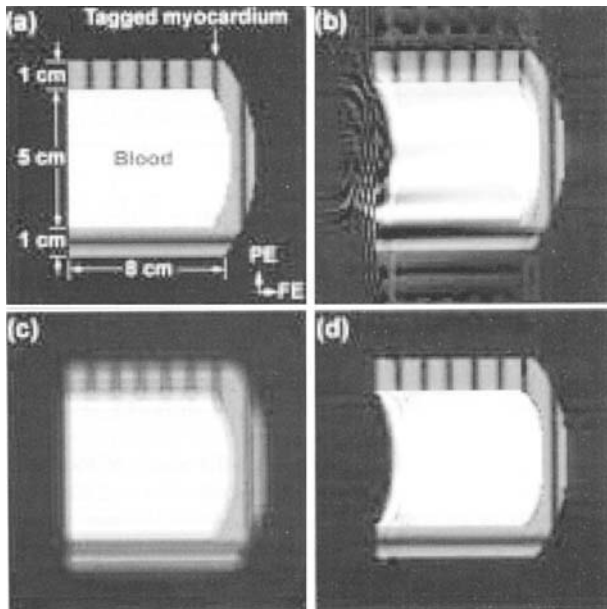


Figure 1. Simulated long-axis images. (a) ideal, (b) conventional FGRE-EPI, (c) interleaved spiral, and (d) FGRE-EPI employing flyback and GMS.

and the off-resonance k-space, k_f , describes the off-resonance properties. A mathematical model representing a section of the long-axis view of the heart (Fig. 1(a)), which includes flowing blood and off-resonance myocardial walls with tags, was used as an object for evaluating the artifacts arising from different trajectories. The simulated blood had a spatial in-plane distribution that was parabolic along the lateral axis and linear along the long axis. The tag thickness and spacing were 2.7173 and 10 pixels, respectively. Our simulation was performed using MATLAB (The Mathworks, MA). For each pixel in the heart model, the ideal k-space representation, $S(k_x, k_y)$ of Eq. 1, was generated via the 2D FFT, given its position and intensity. Next, given $S(k_x, k_y)$, $u(x, y)$, $v(x, y)$, $f(x, y)$, and the gradient waveforms corresponding to the k-space trajectory, Eqs. 2–6 are used to compute k_x , k_y , k_u , k_v , and k_f . Next, Eq. 1 is used to compute the resulting non-ideal sub-image for each pixel, which contains artifacts. This algorithm is repeated for all pixels, and the aggregate image is computed by a complex sum of the sub-images from all pixels. Finally, the magnitude image is displayed. Three trajectories were evaluated: conventional bottom-up (BU) FGRE-EPI, BU FGRE-EPI using optimized flyback gradients in the readout direction [4], and interleaved spiral. The gradient performance was specified as a full strength of 40 mT/m with a slew rate of 200 T/m/s. The peak blood velocity used was 2 m/s. The tagged myocardium was assumed to be 100 Hz off-resonance. The imaging parameters included echo train length = 4, field of view (FOV) = 0.32 m, readout period = 8.2 ms, number of readout points = 256, number of phase encode lines = 140, and receive bandwidth = 488.28

Hz/pixel. All FGRE-EPI sequences were partial Fourier acquisitions and used the finite impulse response method for reconstruction [5]. For the spiral protocol, readout time and sampling bandwidth were selected to achieve approximately the same SNR as FGRE-EPI acquisitions. Spiral pulse sequence parameters used included number of interleaves = 32 and readout period = 8.2 ms. A standard gridding algorithm was used to reconstruct the spiral images.

Results: Fig. 1 shows the simulation results for (a) ideal, (b) BU FGRE-EPI, (c) interleaved spiral, and (d) BU FGRE-EPI employing flyback. The BU FGRE-EPI sequence has good off-resonance properties as evidenced by good edge definition, but flow caused ghosting artifact, flow voids, and interference with tags. In the spiral image, flow artifacts were nearly suppressed, but myocardial tags were significantly blurred due to the poor off-resonance response. Blurring in spiral sequence may potentially be reduced using time-dependent field map corrections. The BU FGRE-EPI trajectory employing flyback suppressed most of the flow artifacts and preserved edge definition. Additionally, because in FGRE-EPI the readout gradients are different than the PE gradients, the effects of flow in the readout and PE directions must be assessed independently. Our simulation showed that applying gradient moment smoothing (GMS) [6] to all echo-planar trajectories suppressed artifacts due to flow along the PE direction (data not shown).

Conclusion: Our simulations show that k-space trajectory plays an important role in determining artifacts in FGRE-EPI myocardial tagging. To date, many of the properties demonstrated by our simulation have also been demonstrated experimentally (data not shown). While conventional FGRE-EPI is sensitive to flow artifacts and interleaved spiral is sensitive to off-resonance-induced blurring, the FGRE-EPI sequence that employs flyback and GMS may be simultaneously insensitive to both flow and off-resonance effects. Furthermore, by optimizing the flyback gradients, the imaging time increases only 23–36%. Our study suggests that hybrid FGRE-EPI sequences employing flyback and GMS may lead to improved image quality in short breathhold and real-time myocardial tagging.

251. Watershed Segmentation for Dual RF Flip Angle TrueFISP Images

P Horkaew,¹ Rd Merrifield,¹ J Keegan,¹ Dn Firmin,¹ Gz Yang.¹
¹Imperial College of Science, Technology and Medicine,
 University of London, Huxley Building, London, Greater
 London, United Kingdom

Introduction: In cardiac imaging, accurate delineation of anatomical boundaries is essential for the quantification of cardiac mass, volume and function. Whilst the fully automatic segmentation of medical images has been reported as a difficult task, semi-automatic techniques have enjoyed a greater degree of success in the past few years. With the recent advancement in imaging hardware and sequence design, there is substantial improvements in both image quality and resolution, allowing robust image segmentation techniques to be deployed clinically. This paper presents an interactive technique for the

Table 1

Percentage Error compared between semi-automatic method and manual delineation

	0	1	2	3	4	5	6	7	8	9
Average	1.39	0.37	2.31	5.11	-1.28	2.47	5.79	5.39	4.92	5.27
Std.	14.19	17.16	21.62	28.28	22.95	29.74	27.84	29.07	33.44	28.20
Max.	7.77	8.94	9.14	12.43	9.47	15.09	17.21	14.16	14.06	11.77
Min.	-5.01	-5.30	-4.94	-5.09	-10.82	-14.99	-5.86	-4.83	-6.89	-1.72

segmentation and temporal tracking of myocardial structure in dual RF flip angle TrueFISP images [1].

Methods: The proposed algorithm is based on a mathematical morphology segmentation framework. The approach requires a manual deposition of several initial seed points within the region of interest, i.e., the myocardial ring, on one image frame of the cine sequence. After anisotropic filtering [3], an immersion-based Watershed Transform [2], was applied and a Region Adjacency Graph (RAG) was then constructed. From the manually defined seed points, the regional sub-graphs were merged according to the local intensity mean and variance. For the remaining phases of the cine sequence, the partitioning for the myocardium in the previous time frame was projected onto the current frame and a new RAG was subsequently constructed. Region merging was then applied according to the centroids of overlapping regions with similar intensity distributions. After this, the user had the option of correcting the missing or over-segmented regions. For assessing the effectiveness of the proposed algorithm, we limited the number of mouse clicks during manual correction to be 4 for each image frame. The resultant segmentation results were then compared to that of full manual segmentation in terms of percentage errors.

The images were acquired using a Siemens Sonata 1.5T scanner (40 mT/m, 200 mT/m/ms) using a phased array coil with two anterior and two posterior coils. A dual flip angle (20/60) cine TrueFISP sequence (TE = 1.5 ms, TR = 3 ms, Slt = 8 mm) was used to acquire a mid-ventricular short axis view of the heart within a single breath hold. A total of 10 normal subjects were recruited for this study with consent. All images were analysed offline on a PIII 750 NT workstation.

Results: A total of 154 images were analysed and the corresponding result in terms of percentage errors for each subject is shown in the above table. With the proposed technique, the total segmentation time including manual correction for all cine phases of each subject is less than 1 minute, whereas a complete manual segmentation would take about 4 minutes for each subject.

Conclusion: In conclusion, the improvement in image quality offered by dual flip angle TrueFISP imaging sequence allows an easy way of performing interactive segmentation of the myocardium. It has been shown that by using the proposed method, the amount of user interaction is minimal, demonstrating its value for routine clinical use.

252. Comprehensive 45 Minutes MRI Study of Regional Ventricular Function, Myocardial Perfusion and Coronary Anatomy in Patients with Ischemic Heart Disease

Martha Morelos,¹ Anna Maria Sironi,¹ Alessandro Pingitore,¹ Massimo Lombardi.¹ ¹National Research Council, Via Moruzzi 1, Pisa, Italy

Introduction: Ventricular function, myocardial perfusion and coronary anatomy are main determinants of clinical outcome in ischemic patients. MRI have been shown to be an effective methodology to efficiently address each of these aspect.

Purpose: The aim of this study was to verify the feasibility of a comprehensive evaluation of ischemic heart disease within the same MRI examination, using the new generation of cardiovascular dedicated MRI systems. A CVi 1.5T magnet (GE-Milwaukee-USA) implemented with ultra-fast EKG-triggered sequences and phased-array receiving coil was used to evaluate patients (pts) with known or suspected ischemic heart disease.

Methods: Myocardial function was evaluated by FIESTA multislice sequence which allows to obtain cine multiphase images of the heart within 7–10 sec. Myocardial perfusion was assessed by a FGR/ET sequence capable to obtain up to 10 slices of the heart in short axis within two consecutive heart beats. Myocardial enhancement during the first pass of an i.v. Bolus of contrast agent (0.05 mmol/kg, gadodiamide - Nycomed-Norway) was considered indicative of perfusion. The coronary arteries were imaged using a multiphase (up to 10 phases within 14–20 seconds) SPGR sequence with spiral filling of the K-space (16 arms, 3096 points/matrix) (effective resolution 1mm). Scan plans were optimized by using a GRE real-time interactive sequence allowing to obtain an image every 227 msec.

Results: Results: 21 pts (18 male, age 58 ± 11 yy) were enrolled into the study. In each patient the image quality was such to allow a detailed evaluation of regional function and perfusion for the whole myocardium according to a 16 segment model. 66/336 myocardial segments resulted asynergic while 45/336 resulted hypo-perfused or non perfused. Left main and the proximal part of coronary arteries were always visualized (LAD 5.8 ± 0.6 cm), Cx (4.8 ± 0.4 cm), RCA (10.9 ± 10 cm). Seventeen patients underwent also invasive Rx angiography. No significant difference was found between MRI and Rx

coronary findings ($p = ns$). The mean scan time was 42 ± 11 min.

Conclusion: Conclusion: this study shows that a comprehensive evaluation of ischemic heart disease by MRI is consistently feasible with a reduced scan time.

253. A Study of the Motion and Deformation of the Heart Due to Respiration

Kate Mcleish,¹ David Atkinson,¹ Reza Razavi,¹ Jane Blackall,¹ Stephen Keevil,¹ Derek Hill.¹ ¹King's College, Guy's Hospital, London, United Kingdom

Introduction: The motion of the heart during the cardiac cycle has been effectively overcome by ECG gating triggered by the R-wave. Respiratory gating can be used in a similar way but leads to a large increase in scan time. Navigator echoes partly address the motion problem but as yet are not efficient enough for routine clinical use and generally only correct for motion in the foot-head direction. Breathhold acquisitions are a popular way of freezing motion with fast scan times. This is satisfactory for relatively fit patients but as yet large volumes or high resolution scans can not be covered without considerable image artifact. Continuous scanning would be desirable if the motion problem can be overcome.

Purpose: The purpose of this study is to quantify the motion of the heart due to respiration so that more accurate motion compensation methods can be employed. Current studies are restricted to affine registration on a number of manually selected landmarks. In this work, an intensity-based rigid registration algorithm is used on volume data, covering the whole heart, acquired at inhale and exhale positions on 5 volunteers and 5 patients. In addition, data were acquired at a number of intermediate positions (between 4 and 7) on 3 of the volunteers; the results of non-rigid registrations were used to build a subject-specific statistical model that allows easy visualisation of respiratory heart motion, including deformation.

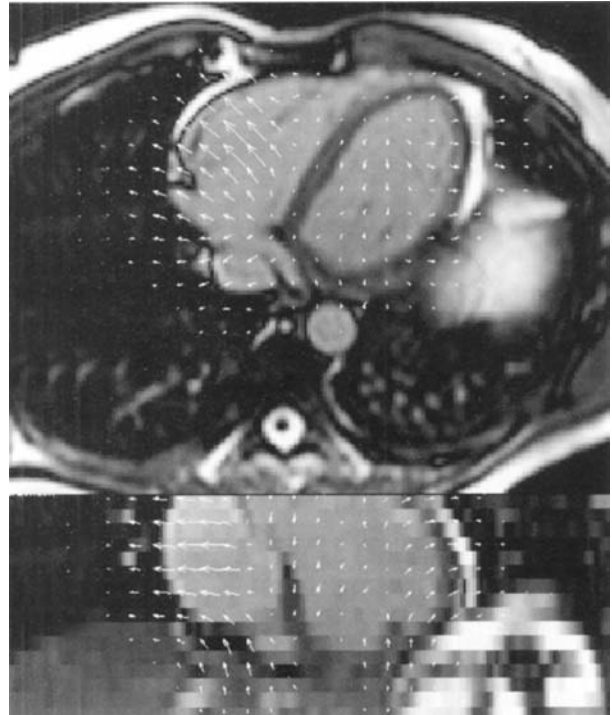


Figure 2. The deformation field produced for one of the registration results for volunteer 5. A transverse and coronal image are shown; the arrows indicate an expansion as the heart moves from maximum exhale to an inhale position.

Methods: Experiments were performed on a Philips Gyroscan Intera 8.1 scanner at 1.5 tesla. 3D, steady state free precession volume images were acquired in the transverse plane. The following parameters were used for volunteer scans, and those in parentheses for patient scans. The volume covered

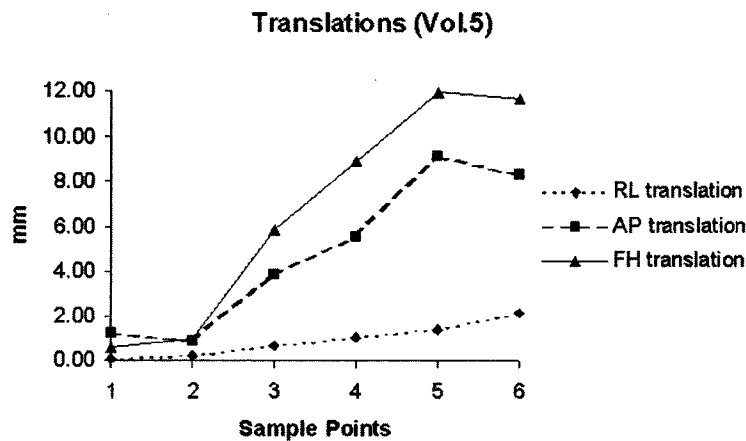


Figure 1. Translation results for volunteer 5, mm.

Table 1

FH trans.	AP trans.	RL trans.	FH rotat.	AP rotat.	RL rotat.
Vol. 1 9.1	8.9	2.3	-1.8	1.1	0.6
Vol. 2 17.2	7.0	6.0	-4.3	3.6	-2.3
Vol. 3 21.4	2.4	2.6	2.0	0.8	-2.0
Vol. 4 17.6	5.6	3.0	0.1	2.5	-1.9
Vol. 5 11.6	8.3	2.1	1.8	5.3	1.2
Pat. 1 18.7	7.3	1.5	-1.1	5.2	3.1
Pat. 2 11.4	1.2	0.2	-2.2	0.7	0.2
Pat. 3 7.1	2.1	-1.0	1.6	2.7	-0.9
Pat 4 3.8	1.0	1.1	0	1.3	-0.5
Pat. 5 7.2	4.5	0.2	1.3	1.3	-2.5

a 350*245 (350*333)mm² FOV with 25 slices of 6mm thickness, a 128*102 (192*94) k-space matrix was interpolated to 256*256. TR = 2.5(4)ms, TE = 1.2(2)ms, flip angle = 30 (50)°. Patient data were acquired using SENSE and there are two heart phases instead of the one diastolic phase collected from the volunteers. For the rigid registrations, the exhale volume is segmented and used as a target to which the inhale volume is registered. The result is three translations and three rotations. With the extra volunteer data the additional images are registered to the target using both rigid and non-rigid registration. This provides a deformation field that was superimposed on the images and also further analyzed as follows. An outer surface of the heart was generated from the segmented exhale volume and the deformation field was used to map this heart surface to the correct positions in the respiratory cycle. Principle component analysis on the surface landmarks allowed a statistical model to be produced.

Results: Table 1 shows the rigid registration results for all subjects. Translations are in mm and rotations in degrees. Positive numbers indicate movement toward the foot (FH), anterior (AP) and right (RL). Figure 1 shows a plot of the three orthogonal translations for volunteer 5, sample point 6 is at maximum inhale.

254. Coronary Artery Imaging with a Reduced Field-of-View

Steven Shea,¹ Andrew Larson,¹ Jordin Green,¹ Vibhas Deshpande,¹ John Finn,¹ Debiao Li.¹ ¹Northwestern University, Department of Radiology, Chicago, Illinois, United States

Introduction: The current technique for coronary artery imaging is an ECG-gated, segmented data acquisition acquired in mid-diastole. However, an average of 85% of the cardiac cycle is not used for imaging with this technique. Imaging efficiency could significantly be improved if some of this imaging time could be utilized.

Purpose: The purpose of this work was to test the feasibility of a reduced field-of-view (FOV) method (1-3) to increase the imaging efficiency of coronary artery imaging scan by a factor of two. Data acquired in earlier portions of the cardiac cycle were used to correct for FOV aliasing.

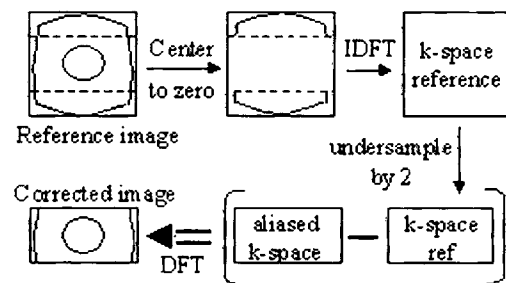


Figure 1. Diagram of correction method.

Methods: In coronary artery imaging, the FOV is larger than the imaging area of interest to prevent FOV wrap from the thoracic wall. If the aliasing artifact can be removed, the FOV can be made smaller and therefore decrease imaging time. During the cardiac cycle, one can assume that the outer half of the FOV (thoracic wall) is stationary during a breath-hold. The dynamic portion is located in the heart in the center half of the FOV. By employing a technique similar to one presented by Frederickson and Pelc (2), a reference image acquired earlier in the cardiac cycle at a full FOV can be used to remove aliasing artifact from an undersampled-FOV image acquired during mid-diastole.

A segmented, constant rf True-FISP (4) sequence was used for imaging so that signal levels would be constant across the cardiac cycle (steady-state). Segmented coronary k-space data was acquired in mid-diastole with a FOV reduced by a factor of two. Segmented reference k-space data was acquired with a full FOV (twice the number of phase-encode lines) during the cardiac cycle prior to coronary data acquisition. To remove FOV wrap from the coronary k-space data, first the center half of the reconstructed reference image was set to zero (Fig. 1). This image was then inverse discrete fourier transformed (IDFT) and the resulting k-space was undersampled by two. The k-space was subtracted from the aliased coronary k-space and then discrete fourier transformed (DFT) to form the corrected image.

Five dogs were imaged with a 2D segmented True-FISP sequence with the following parameters: TR/TE = 4.2/2.1 ms;

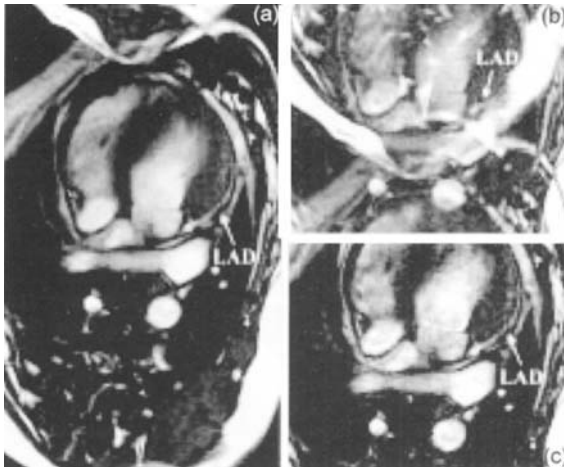


Figure 2. Images of the LAD (arrow) with (a) true image at full FOV, (b) uncorrected reduced FOV image, and (c) corrected reduced FOV image. Note that the imaging time in (c) is half of that in (a).

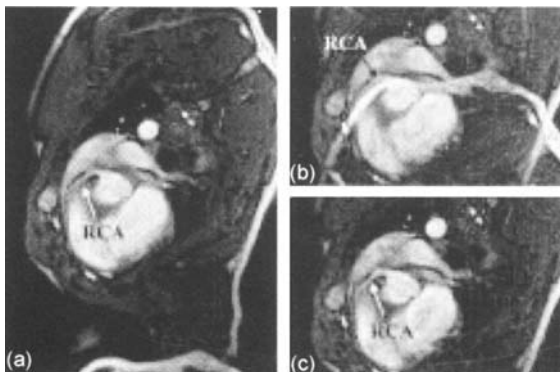


Figure 3. Images of the RCA (arrow) with (a) true image at full FOV, (b) uncorrected reduced FOV image, and (c) corrected reduced FOV image. Note that the imaging time in (c) is half of that in (a).

flip angle = 60°; readout bandwidth = 558 Hz/pixel; slice thickness = 4.0 mm; square FOV = 200–240 mm; in-plane resolution = 0.8–0.9 mm²; and 1–3 averages. Depending on animal heart-rate, 9–17 phase-encode lines were collected for reduced FOV coronary imaging. 18–34 lines were collected for the reference image. A second scan acquired with 9–17 phase-encode lines and a full FOV (and twice the imaging time) was used as a ‘true’ image for comparison with the corrected image.

Results: Figures 2 and 3 show results from two of the animal studies. In both cases, the FOV wrap was removed completely in the corrected image. Comparing the corrected images to the ‘true’ images, SNR is lower in the corrected images due to the smaller number of lines collected and the subtraction to form the correction image. However, coronary artery sharpness was similar in both images.

Conclusion: The reduced FOV method has increased time efficiency for coronary imaging by a factor of two. Aliasing artifact was not present in any of the corrected images. In order to apply this technique in humans, a method of fat-saturation will have to be added to the imaging sequence. However, because of the increased time efficiency, spatial resolution can be doubled for coronary artery imaging within a single breath-hold.

References

1. Hu X, Parrish TB. *MRM* 1994; 31:691–694.
2. Frederickson JO, Pelc NJ. *MRM* 1996; 35:621–625.
3. Madore B, Glover GH, Pelc NJ. *MRM* 1999; 42:813–828.
4. Carr JC, Simonetti O, et al. *Radiology* 2001; 219:828–834.

255. A Comparison of Right Ventricular Volume Measurement Between Segmented K-Space Gradient-Echo and Steady-State Free Precession Magnetic Resonance Imaging

Khaled Alfakih,¹ Holger Thiele,² Sven Plein,¹ Gavin Bainbridge,¹ John Ridgway,¹ Mohan Sivanathan.¹ ¹Leeds General Infirmary, B Floor, Clarendon wing, Leeds, W. Yorkshire, United Kingdom, ²University of Leipzig, Russenstr. 19, Leipzig, Sachsen, Germany

Introduction: Magnetic resonance imaging (MRI) is the most accurate imaging method for the evaluation of left ventricular (LV) and right ventricular (RV) volumes. Both segmented k-space turbo gradient-echo (TGE) and steady-state free precession (SSFP) imaging sequences are used for measurements of LV volumes. Comparative studies for assessing the LV volumes in patients using the two sequences have shown significant differences between them. They also showed lower intra and interobserver variabilities for SSFP. This was attributed to improved border delineation and better blood/myocardial contrast in SSFP imaging.

In TGE, contrast depends on blood flow through the imaging plane and slow flowing blood near the endocardial border leads to poor signal. In SSFP imaging, contrast is dependent on the T1/T2 ratio of tissues and is largely independent of blood flow through the imaging plane. In the RV trabeculations are more pronounced and the flow of blood is slower than in the LV. Also the acquisition is in the short axis where flow is not perpendicular to the imaging plane. This may accentuate the poor signal in TGE. Therefore SSFP acquisition should be particularly useful for imaging of the RV.

Purpose: To date RV volumes have not been compared between TGE and SSFP.

Methods: We studied 31 subjects, 21 normal volunteers and 10 patients with heart failure. Informed consent was obtained from all subjects and the local ethics committee approved the study.

The studies were performed on a 1.5-Tesla Philips Intera CV MRI system (Philips Medical Systems, Best, The Netherlands) using a five-element cardiac phased-array coil with electrocardiogram-gating and breath-holding. Survey scans were followed by breath-hold cine sequences in the axial, two-

Table 1

	RV EDV	RV ESV	RV SV	RV EF	LV SV
TGE mean \pm sd	144 \pm 34	58 \pm 24.7	86 \pm 17.7	61 \pm 8.9	92.3 \pm 21
SSFP \pm sd	155 \pm 35	68 \pm 24.5	87 \pm 17.5	57 \pm 7.6	91.6 \pm 22
Bias	11.1	9.8	1.2	-3.6	-0.7
%difference	7.4	15.6	1.4	6.1	0.8
Limits of Agreement	-17.4 to 39.5	-9.7 to 29.3	-24.7 to 27.2	-15.0 to 7.9	-21.2 to 19.8
r	0.91	0.92	0.72	0.76	0.88
P-value	0.0002	0.0001	0.61	0.002	0.71

chamber, and four-chamber planes to allow planning of the short axis orientation. Two multislice data sets covering the heart in 10–14 short axis slices were acquired using: 1) a TGE sequence (TR = 8.8 msec, TE = 5.2 msec, flip angle = 35°, 6-mm slice thickness, 4-mm interslice gap with one slice per breath-hold). 2) an SSFP sequence (TR = 3.34, TE = 1.67 msec, flip angle = 55°, slice thickness = 6 mm, 4-mm interslice gap with two slices per breath-hold).

Image analysis was performed off-line using commercially available MASS analysis software (Medis, the Netherlands). The endocardial contours were traced manually at end diastole and at end systole on all 31 subjects for both the LV and the RV by two experienced observers. One observer repeated the measurements for 10 randomly selected datasets after 2 weeks. The first phase of each slice was defined as end-diastole. End-systole was defined as the phase with the smallest total LV and RV volume. LV and RV end diastolic volume (EDV) and end systolic volumes (ESV) were computed using Simpson's rule. Stroke volume (SV) and ejection fraction (EF) were calculated.

The mean and standard deviation were calculated for all parameters. The agreement between the TGE and SSFP as well as interobserver variability on all 31 subjects and intraobserver variability on 10 subjects were calculated using Bland and Altman's method.

Results: There were significant differences with the SSFP sequence values being larger for the RV EDV, RV ESV and smaller for RV EF (see table above).

For the 21 normal volunteers The mean absolute difference between LV and RV stroke volume for TGE was 5.8 ml \pm 12.9 ($r^2 = 0.72$) and for SSFP was 4.6 ml \pm 6.9 ($r^2 = 0.92$).

Inter and intraobserver variability were lower for the SSFP than the TGE sequence. Interobserver variability for TGE EDV was -6.2 ± 18.5 , TGE EF% was 1.7 ± 7.0 , while interobserver variability for SSFP EDV was -10.1 ± 11.6 , SSFP EF% was 2.1 ± 4.5 . The intraobserver variability for TGE EDV was -6.1 ± 14.8 , TGE EF% was 1.2 ± 4.7 while intraobserver variability for SSFP EDV was -2.0 ± 6.3 , SSFP EF% was -1.1 ± 2.9 .

Conclusion: We found a significant difference in RV volume measurements between the two imaging sequences with SSFP yielding larger EDV and ESV and lower ejection fractions. It is therefore not possible to use the two techniques interchangeably for serial monitoring of a given patient.

The lower observer variability and the better agreement between the LV and RV stroke volume for the SSFP sequence

may be due to the improved image quality and better delineation of the endocardial border.

In our unit the SSFP sequence is also twice as fast as TGE which is of some significance for clinical practice in view of the cost of MRI time. However, normal ranges for the new technique will need to be established.

256. Cardiac Imaging with Steady-State Free Precession: Multi-shot Echo-Planar vs Conventional Single-Echo

Glenn Slavin,¹ Sandeep Gupta,¹ ¹GE Medical Systems, Johns Hopkins Hospital, Baltimore, Maryland, United States

Introduction: Due to its superior image quality, SNR, and contrast, steady-state free precession imaging (SSFP, True-FISP, FIESTA) seems poised to replace spoiled gradient-echo imaging for routine cine MRI of the heart. Nevertheless, a functional exam using cine MRI still requires roughly 12–15 imaged sections (and an equivalent number of breath-holds) to

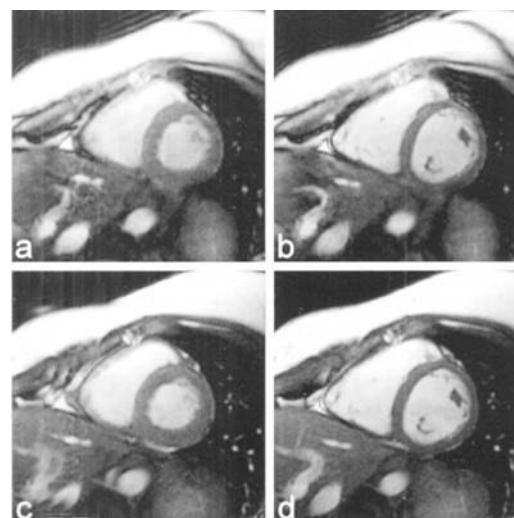


Figure 1. Short-axis images a0 Systolic and b0 diastolic phases from SSFP-EPI. C0 Systolic and d0 diastolic phases from conventional SSFP.

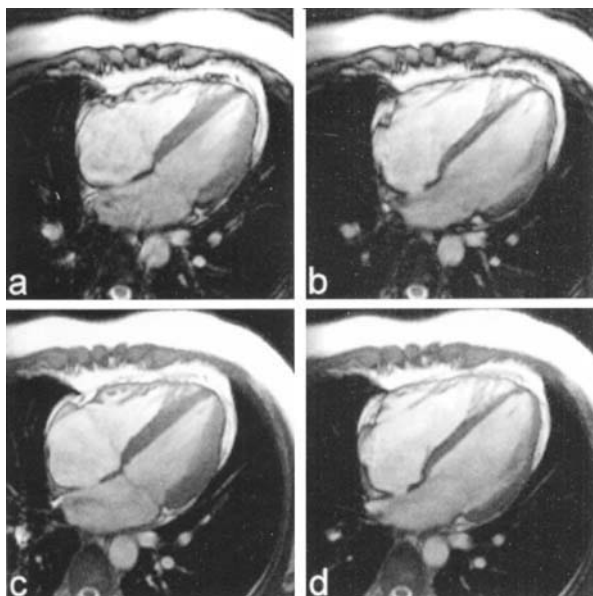


Figure 2. Long-axis images. a) Systolic and b) diastolic phases from SSFP-EPI. c) Systolic and d) diastolic phases from conventional SSFP.

cover the left ventricle from apex to base. For high-resolution imaging, each breath-hold can take up to 16 sec, depending on heart rate, and may be difficult for some patients.

Combining multi-shot echo-planar imaging (EPI) with SSFP can provide the ability to reduce both the breath-hold duration and the total exam time. The SSFP-EPI technique offers SSFP-like image quality with the increased imaging speed of EPI, while avoiding the SNR loss of standard gradient-echo EPI.

Purpose: The purpose of the study was to perform an initial quantitative comparison between a multi-shot EPI variant of SSFP and the conventional single-echo SSFP. Measured and calculated parameters include SNR, end-diastolic volume, end-systolic volume, stroke volume, and ejection fraction.

Methods: Cine MR imaging of the heart was performed on three healthy volunteers with the SSFP-EPI technique. An echo-train length (ETL) of 3 was used as a compromise between maximizing efficiency and minimizing TR. The effective echo time TE occurred on the second gradient echo. Imaging was done on a 1.5 T Signa CV/i scanner (GE Medical Systems,

Milwaukee, WI) with 40 mT/m peak gradients and 150 T/m/s maximum slew rate. For SSFP-EPI, imaging parameters were: ETL 3; ECG-triggering; 256 × 192 matrix; 24 views per segment (8 shots); TR 6.2–6.7 msec; TE 3.1 msec; 45° flip angle; 34 × 26 cm field-of-view; 7 mm section thickness; 11 contiguous sections; 250 kHz bandwidth; 50 msec temporal resolution; 20 reconstructed cardiac phases. Conventional single-echo SSFP was performed with identical parameters, except: 12 views per segment; TR 3.7–4.2 msec; TE 1.4 msec. Acquisition times were 7 heartbeats for SSFP-EPI and 13 heartbeats for conventional SSFP.

Quantitative volumetric measurements were performed using MASS Analysis Software (Medis Medical Systems, Netherlands) running on a GE Advanced Development Workstation. Left-ventricular contours were traced semi-automatically on short-axis images, and end-diastolic and end-systolic volumes were measured. Stroke volume and ejection fractions were calculated and compared for the two approaches for all three subjects.

SNR measurements of the myocardium were made in short-axis images from both the SSFP-EPI and conventional SSFP acquisitions. Measurements were performed in a mid-ventricular slice at both end-systole and end-diastole.

Results: All volunteer studies demonstrated very good image quality for SSFP-EPI, which was qualitatively similar to that of conventional SSFP. Figures 1 and 2 show representative short- and long-axis systolic and diastolic images acquired with both techniques. In general, the SSFP-EPI images exhibited more banding artifacts (in the chest wall) and flow-related ghosting artifacts (in the most basal slices) than did the conventional SSFP images. However, these artifacts did not hinder image analysis.

Quantitatively, the initial studies demonstrate excellent correlation between the SSFP-EPI and SSFP images. The ventricular volume results are presented in Table 1. The average SNR values were 60.0 for SSFP-EPI and 54.9 for SSFP at end-systole and 48.7 for SSFP-EPI and 43.8 for SSFP at end-diastole.

Conclusion: SSFP-EPI has demonstrated the ability to provide image quality similar to conventional SSFP in roughly half the acquisition time, without a loss of SNR. The scan time reduction can be used either to shorten each breath-hold (as well as the required recovery time between them) or reduce the number of scans by acquiring more than one slice per breath-hold.

Additional studies are necessary to determine if the higher SNR of SSFP-EPI is statistically significant. Further work is

Table 1

Volumetric Measurements. EDV=End-diastolic volume, ESV = End-systolic volume, SV = Stroke volume

	Subj 1 SSFP-EPI	Subj 1 SSFP	Subj 2 SSFP-EPI	Subj 2 SSFP	Subj 3 SSFP-EPI	Subj 3 SSFP
EDV (ml)	148.1	153.4	125.5	130.5	118.7	120.6
ESV (ml)	75.5	79.0	53.3	52.8	45.0	50.4
SV (ml)	72.5	74.4	72.2	77.7	73.7	70.2
Eject. Frac.	48.9%	48.5%	57.5%	59.5%	62.1%	58.9%

also required to optimize image contrast. Because of its higher TR, SSFP-EPI can utilize higher flip angles than can conventional SSFP without exceeding SAR limitations. This would be expected to slightly decrease myocardial SNR but increase blood-to-myocardium contrast.

257. Improved Uniformity Of Myocardial Perfusion Measurements Using Sensitivity Encoding (SENSE)

John Ridgway,¹ Sven Plein,² Andrea Kassner,³ Mohan Sivanathan.² ¹Leeds Teaching Hospitals, Department of Medical Physics, Leeds, West Yorkshire, United Kingdom; ²Leeds General Infirmary, Gt. George Street, Leeds, West Yorkshire, United Kingdom; ³Philips Medical Systems, The Observatory, Reigate, Surrey, UK

Introduction: The assessment of myocardial perfusion during the first pass of contrast agent through the heart requires rapid dynamic acquisition of multiple slices throughout the heart, typically once per heart beat. The number of slices that can be acquired each heart beat is limited by the heart rate and the chosen data acquisition scheme. Fast imaging techniques such as segmented EPI have been used to minimise the data acquisition time per slice. However, such techniques are prone to poor signal to noise ratio, ghosting and susceptibility artefacts and exhibit poor signal uniformity across the myocardium, mainly caused by the non-uniformity of the receiver coil. This can make image interpretation difficult and some form of uniformity correction is required before quantitative or semi-quantitative analysis can be performed. Parallel imaging methods such as SENSE offer an alternative way to reduce data acquisition times per slice without some of the limitations of EPI-based methods and additionally apply a correction for coil related image uniformities by using a low resolution reference scan [1].

Purpose: We describe the use of SENSE to acquire dynamic, multislice myocardial perfusion images in 10 clinical patients and compare the signal uniformity of the myocardium with that obtained using a segmented-EPI based method in 10 further subjects.

Methods: Myocardial perfusion imaging at rest has been performed in clinical patients using (i) a segmented EPI pulse sequence (TFE-EPI) and (ii) a segmented k-space gradient echo pulse sequence (TFE) with SENSE. All imaging was performed on a 1.5 T Philips Intera CV equipped with Master gradients (30 mT/m; 150 mT/m/ms). Imaging parameters were as follows: For the TFE-EPI method six short axis slices were acquired over two heartbeats. The total acquisition time for each slice was 90 ms (9 RF pulses TR 8.7 ms, TE 3.7 ms,

FA = 30°, 5 EPI readouts, 'halfscan' factor = 0.71, 128 × 96 matrix, 6 mm slice thickness, 288 mm × 193 mm FOV). For the SENSE-TFE method four short axis slices were acquired in a single heart beat. The total acquisition time for each slice was 116ms (35 rf pulses, TR 3.3 ms, TE = 1.6 ms, FA = 15°, halfscan factor = 0.625, 160 × 111 matrix, 8mm slices, 400 mm × 360 mm FOV). For both methods T1 contrast is achieved by the use of a saturation pulse applied after the R wave. Gd-DTPA was administered intravenously by a bolus injection (0.05 mmol/kg) followed by a saline flush. Signal uniformity from within the myocardium at baseline was assessed by comparison of the mean signal intensities obtained from 12 equally-spaced different myocardial segments in 2 slices for each technique, averaged over the series of images acquired prior to contrast injection. The results were expressed as the %range, (difference of the maximum and minimum segments as a percentage of the mean for all the segments), and the %StDev (standard deviation of all segments expressed as a percentage of the mean). The mean of these values for the TFE-SENSE method was then compared with the mean results for the TFE-EPI method. A qualitative comparison was also made by comparing the dispersion of the perfusion curves obtained for the two methods before any normalisation was applied.

Results: The results of the mean values for %range and %StDev are given in table 1. Both values were significantly smaller for the TFE-SENSE technique, compared to those for the TFE-EPI method. Visual inspection of the perfusion curves for the SENSE-TFE technique also showed significantly less dispersion between different myocardial segments than for the TFE-EPI method at baseline, 1st pass and washout phases, making qualitative comparison between segments easier.

Conclusion: The use of SENSE combined with myocardial perfusion imaging improves the signal uniformity from within the myocardium, thus making qualitative comparison of perfusion curves easier, and reduces the need for normalisation of the dynamic data prior to semi-quantitative analysis.

258. Blood Oxygen Level Dependent (BOLD) Cardiac Imaging Using T2-Prepared TrueFISP

David Fieno,¹ Steven Shea,¹ Richard Tang,¹ Yongzhong Li,¹ Debiao Li,¹ J. Paul Finn.¹ ¹Northwestern University, 448 E. Ontario St., Chicago, Illinois, United States

Introduction: The blood oxygen level dependent (BOLD) effect is a potential mechanism for myocardial perfusion reserve measurement. During vasodilation, increases in blood flow to the myocardium cause increases in venous blood oxygen saturation and T2* and T2 relaxation times of the myocardium. Previously, a T2-prepared FLASH (fast low angle shot) sequence was used to demonstrate regional myocardial signal increases with local adenosine infusion. (1) The major drawback of the technique is the relatively low signal-to-noise ratio. TrueFISP (2) (fast imaging with steady-state precession) has recently found various applications in cardiac imaging. It can provide substantial SNR improvement over FLASH.

Table 1

Myocardial Signal Uniformity

	TFE-SENSE	TFE-EPI	p value
% range	36.4	83.6	<0.0001
% st dev	12.2	27.2	<0.0001

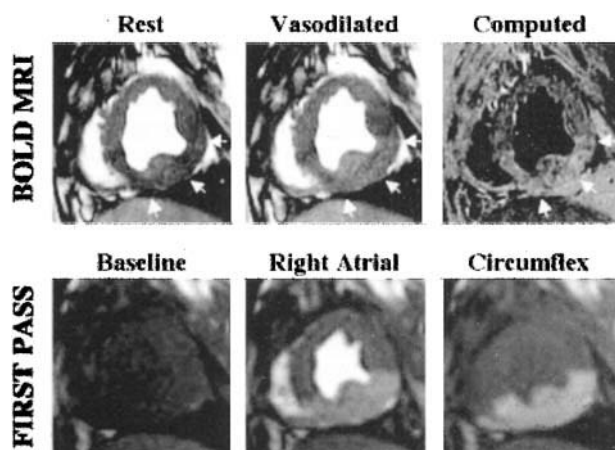


Figure 1. (Top, from left to right) Examples of BOLD images at rest, at maximum vasodilation, and the calculated image, which highlights the region of increased signal intensity. (Bottom, from left to right) First-pass images were acquired at the same slice location at baseline, during right atrial, and during left circumflex injection of contrast. For an animated version, see <http://165.124.58.100/mriweb/bold/fig3>

Purpose: The goal of this work was to evaluate the utility of a recently developed T2-prepared TrueFISP technique for myocardial perfusion assessment in a canine model.

Methods: We imaged dogs ($n = 4$) on a clinical 1.5-T clinical scanner using a novel T2-prepared TrueFISP BOLD MRI pulse sequence. In all animals, segmented k-space T2-prepared TrueFISP BOLD images were acquired from base to apex during repeated breath-holds using the following parameters: TR/TE = 3.0/1.5 msec, T2 preparation time (determines the T2-weighting the MR signal) 40 msec, FOV 250 mm, slice thickness 5 mm, number of averages 3, breath-hold duration 29 sec. Images were acquired at rest and during graded levels of selective left circumflex adenosine vasodilation (rest, 0.01, 0.05, and 0.30 mg/min). To determine actual perfusion, fluorescent microspheres were injected at baseline and during each adenosine dose. Relative perfusion was determined by dividing the image and fluorescence intensities by that of remote myocardium.

Results: Comparison of the perfusion index using T2-prepared TrueFISP BOLD MRI to that determined from microsphere analysis showed good correlation for analysis of both left ($y = 0.12x + 0.93$, $R = 0.78$) and right ventricular myocardium ($y = 0.10x + 0.85$, $R = 0.71$). BOLD images were of high quality, demonstrated transmural changes in signal intensity, and revealed signal increases of $24 \pm 3.1\%$ compared to baseline ($P < 0.01$), which made possible visual assessment of relative perfusion. (See Figure.)

Conclusion: We conclude that T2-prepared TrueFISP BOLD MRI is a sensitive method to assess local myocardial perfusion changes in this animal model. Its potential advantage over contrast-enhanced perfusion measurement is that high spatial resolution imaging in the steady state with entire heart coverage is possible. Further investigations of this technique are warranted.

259. Three Dimensional Breath-Held Imaging of Myocardial Infarction Using Variable Sampling in Time (VAST)

Thomas Foo,¹ Ernesto Castillo,² Dara Kraitchman,² Katherine Wu,² David Bluemke,² Joao Lima.² ¹G. E. Medical Systems, 600 N Wolfe St, Baltimore, MD, United States; ²Johns Hopkins University, 600 N. Wolfe Street, Baltimore, Maryland, United States

Introduction: Current technique used to visualize the myocardial delayed enhancement (MDE) is a single-slice 2D breath-held gradient echo pulse sequence preceded by an inversion recovery (IR) magnetization preparation segment. In order to cover the entire heart in the short axis plane, between 10–14 sections are required. With each section acquired in a single 10–16 sec breath-hold, whole heart coverage is possible but with an overall acquisition time of between 30–50 sec per section. This additional period of time accounts for the fact that the patient must be allowed to rest between breath-holds. As the overall scan time for all sections takes between 7–12 minutes, there is substantial contrast variation between the first and last acquired image.

Purpose: A 3D breath-held acquisition using variable sampling in time (VAST) is proposed to acquire images of

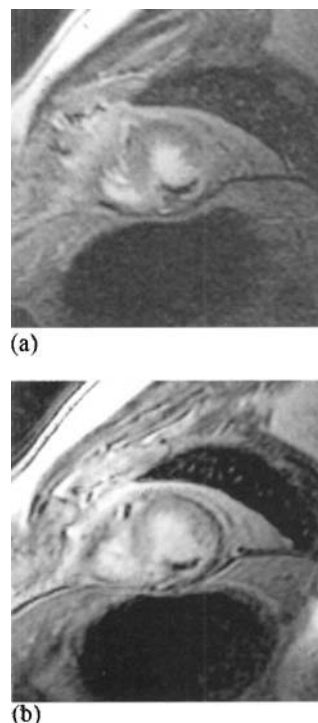


Figure 1. Comparison between a 2D (a) and 3D (b) acquisition in a 54 year-old male patient with a known myocardial infarct. Note that a core region of hypo-enhancement illustrative of micro-vascular obstruction with a peripheral hyper-enhanced rim is well visualized in both the 2D and 3D acquisition.

delayed hyper-enhancement in a single breath-hold. The 3D technique will allow all images to be acquired at a single time point. A study comparing 2D and 3D techniques in patients with known myocardial infarction is proposed. The image contrast and overall image quality between the 2D and 3D techniques are to be assessed.

Methods: Seven patients with known myocardial infarction were studied using both the standard 2D multiple breath-hold technique and the 3D MDE sequence using VAST. With the 3D technique, an interleaved view acquisition order was used such that the low spatial frequencies were acquired in 32 views per R-R interval while the high spatial frequency views were acquired in 48 or more views per R-R interval, depending on the acquisition matrix chosen. In all cases, 24 heart-beats were required to acquire a 12 partition 256×160 matrix volume. The 3D acquisition had parameters of twelve 8.0 mm partitions (interpolated to twenty-four 4.0 mm partitions), 256×160 matrix in 32 cm FOV, 0.5 NEX, TE/TR/flip = 1.4/3.8 msec/20. In comparison, the 2D acquisition had parameters of 8.0 mm sections/0.0 mm gap, 256×160 matrix, 24 views per segment, NEX = 2, TE/TR/flip = 3.2/7.2/20. In both the 2D and 3D acquisitions, images were acquired at a delay time of 300 msec after the R-wave and an inversion time (TI) of 200 msec were used. Scan time for the 2D acquisition was 12 heart-beats while that for the 3D acquisition was 24 heart-beats.

Results: Of the seven patients studied, respiratory motion artifacts were noted in 2 of 7 3D acquisitions and in 2 of 7 2D acquisitions. In all cases, the area of the myocardial infarction was well visualized in both the 2D and 3D acquisitions. The contrast between the infarcted and the normal myocardium averaged over all patients as measured in a single slice location for each patient was 77 ± 8 for the 2D MDE images, while that for the 3D MDE images were 79 ± 14 . An analysis of variance (ANOVA) between the two data samples indicated that there was no significant difference in the contrast between the 2D and 3D images ($p < 0.92$).

Conclusion: Although the scan times for the 3D acquisition were longer than that of the 2D acquisition, patients appeared to be more tolerant of a single long breath-hold rather than several short breath-holds. Moreover, the 3D acquisition could be repeated at different time points. Since the image quality was at least equivalent to the 2D acquisition, the proposed 3D MDE technique allows a much shorter overall examination time, and perhaps better patient compliance. The latter could be borne out in a study of a larger patient population.

260. BOLD-MRI of Endothelial Function at 3 T

Wolfgang Utz,¹ Jaro Hubacek,² Neil Filipchuk,³ Richard Frayne,⁴ Hamid Benjamali,³ Rainer Dietz,⁵ Todd Anderson,² Matthias Friedrich.¹ ¹Franz-Volhard-Klinik, Charite, Wiltbergstr. 50, Berlin, Germany; ²Dept. of Cardiology, University of Calgary, Calgary, AL, Canada; ³Dept. of Nuclear Medicine, University of Calgary, Foothills Hospital, Calgary, AB, Canada; ⁴Seaman Family MR Center, Foothills Hospital, Calgary, AB, Canada; ⁵Franz-Volhard-Klinik, Charite Campus Buch, Wiltbergstr. 50, Berlin, Germany

Introduction: Vascular endothelial dysfunction is a hallmark of atherosclerosis or its risk factors. BOLD-MRI is known to

reflect changes of tissue perfusion due to the relation of the signal intensity to the ratio of oxy-hemoglobin to deoxy-hemoglobine. Since this phenomenon, the BOLD effect, is positively correlated to the magnetic field strength, measurements at high field strength seem to be advantageous.

Purpose: We addressed the question whether BOLD-MRI in a high-field system provides accurate and reproducible data on alterations of endothelial function.

Methods: 17 volunteers (34 ± 4 years) were studied using a 3 T MRI system (Signa, GE Medical Systems, Milwaukee, USA). The subjects were placed in a supine position with one of the forearms lifted and put into the head coil. Using a gradient echo sequence with variable echo times, $T2^*$ of the muscular tissue was calculated. A two-shot gradient-echo/EPI sequence was applied (TE 20 ms, effective TR 2000 ms, slice thickness 10 mm, field of view 160×160 mm, matrix 256×256) to generate $T2^*$ -sensitive images. The signal was continuously obtained before drug and after interventions on tissue perfusion (reactive hypremia/RH and infusion of Acetylcholine/ACh with different dosages). RH measurements were repeated and then compared to the same set of measurements as performed by strain gauge plethysmography within 4 hours. In the BOLD-MRI images, the signal difference between baseline and maximum was calculated. Plethysmography data were used to estimate blood flow increase.

Results: Image quality was good to excellent in all cases. No visible artefacts occurred. Mean $T2^*$ of the muscular tissue was 24 ± 0.5 ms. There was a good reproducibility of RH protocol data for both, BOLD-MRI and plethysmography, with no significant difference of the mean variance. Results of BOLD-MRI correlated very well with plethysmography ($p < 0.05$) except in two cases with a complete lack of response to ACh in BOLD-MRI. We observed an inhomogeneous response to ACh, but not to RH in the muscular tissue.

Conclusion: We conclude that BOLD-MRI at 3 T can be used to assess endothelial function in the forearm. It correlates well with plethysmography and thus may serve as an alternative approach, especially when questions related to regional tissue perfusion itself are to be addressed.

261. 2-D Breath-Hold Spiral Spoiled Gradient Echo for the Non Invasive Detection of Coronary Artery Disease: A Magnetic Resonance Imaging Study

Martha Morelos,¹ Alessandro Pingitore,¹ Alessandro Vittore,¹ Piero Ghedin,¹ Massimo Lombardi.¹ ¹National Research Council, Via Moruzzi 1, Pisa, Italy

Introduction: Magnetic Resonance Coronary angiography (MRCA) is a noninvasive developing method for detecting coronary artery disease (CAD). 2-D breath-hold Spiral Spoiled Gradient Echo (SSGE) is a high resolution technique with short time consumption that permits to freeze cardiac motion.

Purpose: To assess diagnostic accuracy of Magnetic Resonance Coronary Angiography (MRCA) by using 2-D breath-hold Spiral Spoiled Gradient Echo (SSGE) sequence, for the detection of coronary artery disease (CAD).

Methods: 36 consecutive pts (22 males, 59 ± 10 years) with suspected CAD underwent MRCA and conventional X-ray coronary angiography in random order, within 7 days of each

other. 2-D multiphase SSGE sequences were acquired with ECG triggering and breath-hold technique. The sequence parameters were: TR/TE 1071/5.6 msec, flip angle 60°, bandwidth 125 KHz, FOV 24 cm, slice thickness 5 mm, NEX 1, Arms 16 Points 4096. Effective resolution was 0.86 mm.

Results: Signal-to-noise ratio and contrast-to noise ratio were, respectively, 8.05 ± 4.2 and 7.95 ± 1.6 . for right coronary artery (RCA) and 7.88 ± 4.1 and 6.1 ± 2.6 for left coronary artery (LAD), 50 ± 14 mm for circumflex (CX) and 112 ± 10 mm for RCA. A total of 44 significant (>50%) coronary stenosis were detected with conventional angiography. Of these, 34 (78%) were identified by MRCA. K agreement was 0.66. Of the 260 coronary artery segments, 229 (91%) were analyzed by MRCA. Sensitivity, specificity and diagnostic accuracy were, respectively, 82% 87% and 83% for LAD. 51% 70% and 63% for CX and 84.6% 82% and 83% for RCA.

Conclusion: 2D SSGE sequence with breath hold technique is an effective in the detection CAD; particularly in the left descending and right coronary arteries. However, further technique implementations is needed to improve global diagnostic accuracy of the MRCA.

262. Definition of an Optimal Image Analysis Protocol for the Assessment of Left Ventricular Function from Short-Axis Cardiac MR Data Sets

Emmanuelle Angelie,¹ Jos Westenberg,¹ Rob Van Der Geest,¹ Gerhard Koning,¹ Johan Reiber.¹ ¹Leiden University, Albinusdreef 2, Leiden, Holland, The Netherlands

Introduction: To quantitatively analyze global and regional left ventricular volume and function from short-axis cardiac MR images, the contours of the endocardium (ENDO) and epicardium (EPI) need to be defined. Towards that goal we used the MASS analytical software package (1). To apply this

technique in clinical practice requires that these analyses be carried out in an accurate manner and an acceptable time period.

Purpose: The goal of this study was to derive an optimal image analysis protocol within the clinical constraints using the MASS analytical software.

Methods: MASS package was developed to automatically quantify the volume and function of the heart from the short-axis MR-images. MASS provides an automatic image segmentation method that can be improved by manual corrections. Four different protocols for image segmentation based on the available automatic contour detection within MASS (version 5.0) were analyzed:

1. a fully-automatic contour detection (A) without any manual correction
2. a semi-automatic contour detection (AS) defined as the fully-automatic detection with manual correction
3. a constraint segmentation (C) defined as an automatic contour detection with an initialization (i.e. manual EPI and ENDO contours in the middle slice of the exam were used as seed contours for the automatic contour detection in the other slices)
4. a semi-constraint contour detection (CS) defined as a constraint segmentation with manual corrections.

The results of these protocols were compared to the manual expert contour (M) considered as the gold standard. All the corrections carried out manually have to be realized considering a time constraint (<10 min per exam).

The protocol will be optimal when the segmentation time will be shortest and the accuracy of the segmentation the highest. The accuracy was characterized by two parameters, being the signed difference in area between the manual contour and the corresponding contour detected by one of the four segmentation protocols (resulting in four comparisons: manual-automatic (MA), manual-semiautomatic (MAS), manual-constraint (MC), manual-constraint corrected (MCS)), and the degree of similarity. The signed differences in area must be normalized (NDSA) for comparison purposes, since the areas of the contours

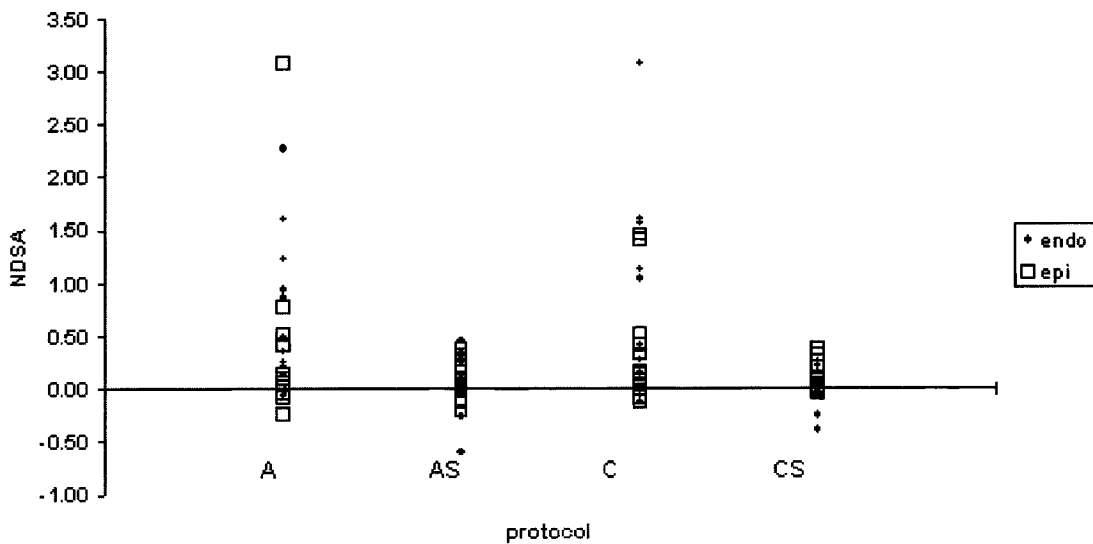


Figure 1. Mean NSDA between contours defined by four protocols with respect of the manual expert contours.

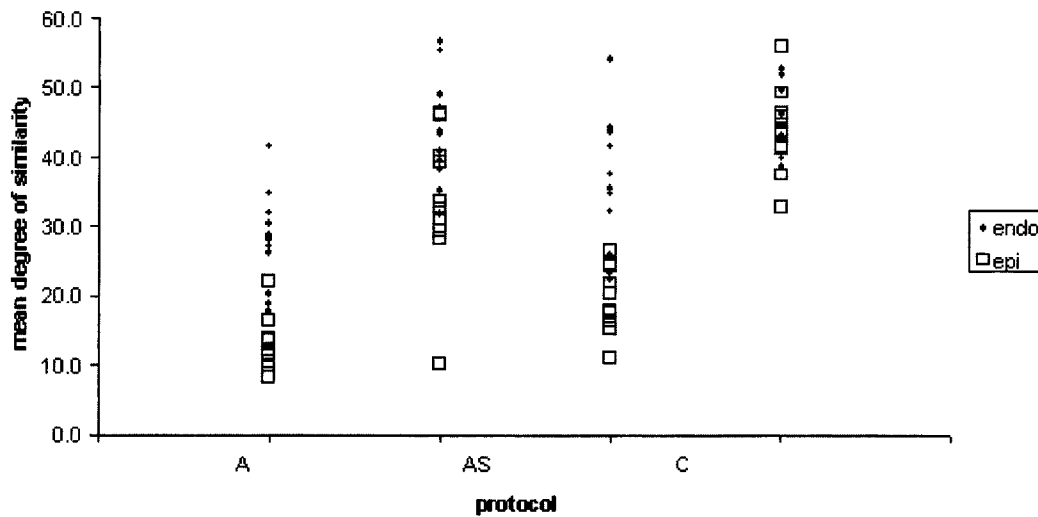


Figure 2. Mean degree of similarity for the for protocols with respect of the manual expert contours.

within a single exam can vary by a factor 2 from apex to base (NSDA's range was $[0,1]$). The degree of similarity is defined by the percentage of number of points of the contours that are in common; in other words two contours match better when the degree of similarity is larger. Two contour points were considered to be in common if and only if the distance between these was smaller than a threshold value (TH). The TH was the mean NSDA between two sets of manual contours drawn twice by a single observer on the same set of data.

The analysis was performed on a data set of 12 patient exams with 8–13 slices and two phases (end-systolic and end-diastolic). Two contours (EPI and ENDO) per slice were detected in each exam. The NSDA between the two contours were evaluated on a set of 100 points per slice. If the distance between the center of the detected set of contours and the manual set of contours exceeded a value of $0.5 \times \text{radius}$, the exam was excluded.

The comparison between the different protocols was studied using repeated measurement ANOVA tests.

Results: One exam was excluded following the previous criteria. Statistically significant differences in the NSDA and the degree of similarity were found between the four protocols of segmentation ($p < 0.00$).

In table 1, the mean values of the NSDA and the degree of similarity are given for the four protocols. The comparison between the mean degree of similarity of A and C protocols showed significant results ($p < 0.05$). It appears that AS and CS have a significant lower mean NSDA and significant higher mean degree of similarity compared to C and A for ENDO contours, whereas in the EPI contours only the degree of similarity appears to be significantly different. Except for the mean NSDA in the EPI contours, CS showed the highest mean degree of similarity and the lowest mean NSDA.

Conclusion: The goal of this study was to establish the optimal protocol for contour segmentation in short axis cardiac MR images analyzed with the MASS analytical package. The optimal protocol will be a compromise between the time spent on an exam and the accuracy achieved. The non-significant differences ($p > 0.05$) between the mean NSDA of A and AS protocols, A and C protocols and C and CS protocols in the EPI contours can be explained by the use of the signed difference instead of the absolute one.

Since the CS protocol showed the highest mean degree of similarity and the lowest mean NSDA, the CS protocol has the higher accuracy. Based on the quantitative anatomical data the optimal protocol is the CS protocol, although this one requires the

Table 1

Mean Degree of Similarity and Mean NSDA SD Between the Protocols

		A	A vs AS	AS	C	C vs CS	CS
ENDO	degree of similarity	27.7 ± 7.1	*	43.7 ± 7.8	35.9 ± 9.7	*	48.8 ± 5.1
ENDO	NSDA	0.7 ± 0.7	*	0.05 ± 0.3	0.8 ± 1.0	*	-0.01 ± 0.2
EPI	degree of similarity	13.6 ± 4.8	*	33.6 ± 1.0	19.4 ± 4.6	*	43.7 ± 6.0
EPI	NSDA	0.5 ± 0.9		0.07 ± 0.2	0.4 ± 0.5		0.01 ± 0.1

*shows significant difference ($p < 0.05$) between the protocols.

Table 2
Compromise in the Choice of the Protocol

	M	A	C	S	CS
>15 min	X				
10 < 15 min					X
<10 min				X	

longest processing time (around 15 min per exam). This study also shows that for a fully automatic protocol of segmentation (A) the accuracy can be significantly improved adding some manual corrections (protocol AS), and that in less than 10 min per exam. Also the same conclusion was drawn from the result between constraint contours (C) and constraint manually corrected (CS). As a consequence the clinician should choose a protocol following a certain number of criteria shown in the table 2.

263. Interactive Cardiac Modeling for Ventricular Volume and Mass Measurement

Robert Merrifield,¹ Dudley Pennel,² Guang-Zhong Yang.³
¹Royal Society/Wolfson Foundation MIC Laboratory, Imperial College, 180 Queen's Gate, London, England, United Kingdom; ²Royal Brompton CMR Unit, London, England, United Kingdom; ³Imperial College of Science, Technology and Medicine, University of London, London, England, United Kingdom

Introduction: Recent advances in cardiac imaging have allowed the complex dynamics of the endocardial border, papillary muscles and trabeculations of the left ventricle to be observed in-vivo. Despite this, the majority of semi-automatic techniques designed for clinical volume and mass measurement approximate the endocardial border as single smooth surface, thereby limiting the accuracy of measurements. We introduce in this study an Interactive Cardiac Modeling (ICM) method for the construction of complex dynamic 3D models of the left and right ventricles with minimal human interaction.

Methods: The uniqueness of the ICM encompasses the following two aspects. Firstly, segmentation and modeling is performed directly in four dimensions rather than from conventional 2D images. This allows subtle temporal and spatial characteristics of the ventricles to be captured. Secondly, Constructive Solid Geometry [1] is used to allow models to be described as the Boolean union, intersection and difference of a set of interactively deformable 4D geometric primitives. As there is no limit on the number of primitives that may be used, models of an arbitrary complexity may be constructed. This provides a unique platform for modeling the entire cardiac structure including inflow and outflow tracts, papillary muscles, trabeculations and valves. The technique has been validated with single breathhold cine multislice studies from 10 asymptomatic subjects acquired using Dual RF Flip Angle TrueFISP Imaging [2,3] using a Siemens Sonata 1.5T system (40 mT/m, 200 mT/m/ms). A phased array coil with two anterior and two posterior elements was used. For each subject,

7 short axis slices covering the left ventricle over 9–13 cine phases were acquired. The human interaction time and the intra-observer variability of the blood and myocardium volumes were measured for both ICM and conventional manual contour delineation. The epi- and endo-cardial borders and all visible papillary muscles and trabeculations of the left ventricle were delineated using both techniques. The intra-observer variability was calculated as the single determination standard deviation of the absolute difference between pairs of measurements.

Results: The human interaction time for ICM of (mean \pm sd) 723 ± 107 seconds was considerably lower than that for manual delineation of 1232 ± 169 seconds. In spite of this, the intra-observer variability for ICM of 41.2 mm^3 , lay within that for manual delineation of 44.5 mm^3 .

Conclusion: It is expected that when used with high-resolution navigated images, the level of detail that can be modeled with ICM will be greatly increased. The resultant models will aid the analysis of regional wall thickening and valve dynamics as well as increasing the reproducibility of ventricular volume and mass measurements. It is anticipated that its ease of use and flexibility will enable ICM to be used both as a valuable clinical and research tool.

264. Adaptive Free-Form Registration for First Pass MR Myocardial Perfusion Imaging

Nick Ablitt,¹ Jianxin Gao,¹ Peter Gatehouse,² David Firmin,² Dudley Pennel,² Guang-Zhong Yang.¹
¹Royal Society Wolfson Foundation MIC Laboratory, Imperial College, 180 Queen's Gate, London, England, United Kingdom; ²Royal Brompton CMR Unit, London, England, United Kingdom

Introduction: The assessment of regional myocardial perfusion requires an accurate tracking of the signal time course such that a detailed perfusion map can be derived. To obtain such a map in practice, however, is not trivial, as respiratory and cardiac motion has to be corrected for such that different segments of the myocardium are correctly aligned. This typically requires the manual location of ROI within each image frame, which is both time consuming and error prone. These problems are further amplified when the data set consists of multiple slices. This study describes a new way of adaptive free-form image registration for automatic image alignment for myocardial perfusion analysis.

Methods: The registration technique was adapted from our previous work on 2D electrophoresis image analysis[1]. The method uses multi-resolution free-form deformation correction based on a localized cross-correlation measure. It exploits the derivatives of the similarity function and uses the Broyden-Fletcher-Goldfarb-Shanno (BFGS) algorithm for parameter optimization with 512 degrees of freedom. The reference image was chosen to be at the end of the image series as all cardiac structures were clearly identifiable. Each image of the perfusion sequence was then registered to the reference image and the frame-by-frame registration time was about 5 seconds. In order to speed up the registration process, the repeatability of the respiration cycle and its induced cardiac motion was exploited. In this case, the user was required to identify retrospective navigator traces either through the chest or the

diaphragm. A Partial Least Squares Regression (PLSR) algorithm was used to recover the intrinsic pattern of the respiratory motion and the associated deformation of the left ventricle. This represents a learning cycle of the algorithm and when free-registration is applied, we only need to use the above free-form registration to a limited number of image frames (30 ~ 40%) within the series. The motion distribution for other frames can be derived through PLSR prediction. The advantage of this self-learning approach is that it not only doubles the computational speed but also improves the consistency of the recovered motion distribution. This is because in early perfusion image frames the original registration algorithm can give erroneous results due to the very low signal intensity within the myocardium. The NIPALS [2] algorithm was used for PLSR, in which the iteration stops when at least 90% of the variation of the covariant matrix is obtained.

The proposed technique was validated both on synthetic and 8 patient data sets acquired from a Siemens Sonata 1.5 T system (40mT/m, 200mT/m/ms). The FLASH sequence ($T_r = 3.7\text{ms}$) consists of three saturation-recovery short-axis slices per cardiac cycle, for 50 cycles during the first-pass of Gd-DTPA

(cubital vein, 0.1 mmol/kg, 3 ml/s) with a field of view of 400 mm (128 pixels) by 300mm (64 pixels). For each perfusion image sequence, four perfusion signal time curves were measured at the Anterior, Posterior, Septal, and Lateral segments. Spline curve fitting was applied to each of these curves and the mean dispersion was used as an objective measure of the accuracy of the registration method.

Results: With the simulation data set the mean dispersion is reduced to about 85% of its original value by using the free-form registration procedure. With PLSR training, this error is further reduced (77%) while the actual computation time is halved. For the 8 patient data sets analyzed, the mean dispersion was reduced to 81% and 68%, respectively, by using the free-form registration method and the PLSR approach.

Conclusion: It has been shown that the proposed techniques provide a correctly aligned image sequence from which the perfusion indices can be derived without frame-by-frame manual correction. This greatly simplifies the analysis procedure and makes the subsequent perfusion quantification much more accurate.